UNIVERSITY OF OKLAHOMA

GRADUATE COLLEGE

CO-SPATIAL UV-OPTICAL HST/STIS SPECTRA OF SEVEN GALACTIC PLANETARY NEBULAE: NEBULAR AND STELLAR PROPERTIES

A DISSERTATION

SUBMITTED TO THE GRADUATE FACULTY

in partial fulfillment of the requirements for the

Degree of

DOCTOR OF PHILOSOPHY

By

TIMOTHY MILLER
Norman, Oklahoma
2017

CO-SPATIAL UV-OPTICAL HST/STIS SPECTRA OF SEVEN GALACTIC PLANETARY NEBULAE: NEBULAR AND STELLAR PROPERTIES

A DISSERTATION APPROVED FOR THE
HOMER L. DODGE DEPARTMENT OF PHYSICS AND ASTRONOMY

BY

Dr. Richard Henry, Chair

Dr. Karen Leighly

Dr. Xinyu Dai

Dr. Mukremin Kilic

Dr. J. R. Cruz

Acknowledgements

This dissertation would not have been possible with the support of so many individuals.

I would like to thank first my advisor, Dr. Richard Henry, for his infinite patience and guidance throughout this entire project. Without it, I would have been lost.

To Dr. Leighly, thank you for helping me make a strong entrance into the AGN field as I start my first postdoc.

To Brent McCoy, thank you so much for helping me get my tables to work.

To my wife, Jenna, thank you for your support, encouragement, faith and love. They were absolutely vital to my success.

To all my other friends and family, thank you all for being there whenever I was in need.

Lastly, I would like to thank the people who operate the OU Supercomputing Center for Education and Research (OSCER) at the University of Oklahoma, where the majority of the modeling for this project occurred.

Table of Contents

List of Tables

List of Figures

Abstract

This project had two main goals: (1) to investigate to what extent planetary nebulae (PNe) are chemically homogeneous; and (2) to provide physical constraints on the central star properties of each PN. The first goal was accomplished by using HST/STIS spectra to measure the abundances of up to seven elements in numerous spatial regions within each of seven PNe (IC 2165, IC 3568, NGC 2440, NGC 3242, NGC 5315, NGC 5882, and NGC 7662). The second goal was achieved by computing a photoionization model of each nebula, using the observed emission line strengths as constraints. The major finding of this study is that the nebular abundances of He, C, N, O, Ne, S, and Ar are consistent with a chemically homogeneous picture for each PN. Additionally, it was found through experimenting with three different density profiles (constant, Gaussian, and Gaussian with a power-law) that the determination of the central star's temperature and luminosity is only slightly sensitive to the profile choice. Lastly, post-AGB evolutionary model predictions of temperature and luminosity available in the literature were plotted along with the values inferred from the photoionization model analysis to yield initial and final mass estimates of each central star.

Chapter 1

Introduction

All stars begin their lives fusing hydrogen-1 into helium-4. Fusion of any element requires very high temperatures such that the Coulomb repulsion force felt between two nuclei is overcome. This commonly occurs in the cores of stars, and while the star is fusing hydrogen in its core, it is said to be on the main sequence. The main sequence spans a specific region of the Hertzsprung-Russell (H-R) diagram, a plot of stellar luminosity vs. temperature (see Figure 1.1). The end products of hydrogen fusion are a helium-4 nucleus and energy in the form of light. This released energy heats the star's interior, increasing its outward pressure to the point where it counters the inward gravitational pressure. This stabilizes the size and temperature of the star.

Hydrogen fusion occurs in two main channels: the proton-proton (PP) chain reaction and the carbon-nitrogen-oxygen (CNO) cycle. The PP chain is dominant for stars of mass < 1.3 $M_{\odot}$, while the CNO cycle is dominant for stars with masses above 1.3 $M_{\odot}$ (Salaris & Cassisi [52]). Only hydrogen-1 and its fusion products (deuterium and helium-3) are needed for the production of helium-4. The CNO cycle, however, requires carbon to act as a catalyst for the conversion of hydrogen-1 into helium-4. The CNO cycle starts with carbon-12, fuses it with hydrogen-1, and produces nitrogen-13. Nitrogen-13 is an unstable isotope and will decay to carbon-13 in a matter of minutes. Then, hydrogen-1 will fuse with carbon-13 to create nitrogen-14. Nitrogen-14 has the smallest fusion cross-section in the CNO cycle, making its fusion rate with hydrogen-1 very small. This creates a bottle-neck in the CNO cycle, resulting in an overall increase of this isotope in the core. Also due to this bottleneck, carbon-13 increases in the core.

Fig. 1.1.— The Hertzsprung-Russell diagram showing the regions of stellar evolution that stars reside in for long periods of time. Each region is a different evolutionary stage, and each point is a star.

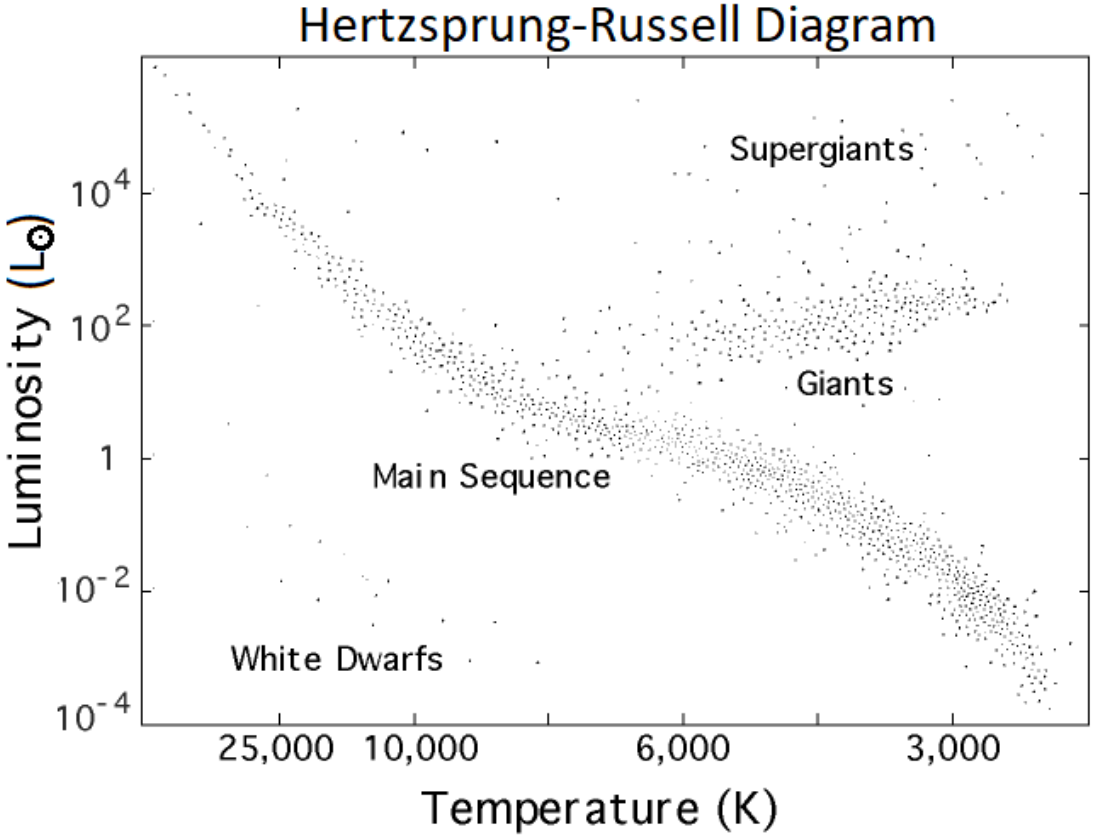

The star will be on the main sequence for the majority of its life (millions to billions of years, depending on its mass), leaving once all hydrogen in the core has been fused into helium. At this point, the core will collapse until either the force of gravity is balanced by the force associated with electron degeneracy pressure[a] (the core is not hot enough to fuse helium, stellar mass $< 2\ M_{\odot}$), or the core becomes hot enough to fuse helium (stellar mass $> 2\ M_{\odot}$, Karakas & Lattanzio [27]).

While the core is collapsing, it is also getting hotter as the gravitational energy is being converted to thermal energy. This causes a shell of hydrogen surrounding the core to become hot enough to begin fusing. With the now hotter core and shell fusion occurring just outside the core (closer to the surface of the star), the star will expand to return to equilibrium. The net result is an increase in luminosity and decrease in temperature, as the star enters the giant region of the H-R diagram (see Figure 1.1).

During the ascent to the giant region, convection within the star's envelope will extend downward and mix with the hydrogen fusing shell. The envelope will therefore become enriched with hydrogen fusion products in what is called the first dredge-up. For PP chain dominated shells, the primary product is helium-4, but for CNO cycle dominated shells, the products are helium-4, nitrogen-14 and carbon-13. Also, the envelope will be so extended after the equilibrium between gravity and the hotter internal conditions is re-established that mass loss occurs via stellar winds. These stellar winds are generated by turbulence within the envelope (possibly associated with Alfvén waves; Schröder & Cuntz [55]) that has enough mechanical energy to escape the gravitational potential well of the star. Depending on the mass of the star, this may result in as much as 30% of the star's original mass to be lost (Karakas & Lattanzio [27]). This mass loss enriches the

[a]Electron degeneracy pressure occurs because the Pauli exclusion principle doesn't allow electrons to simultaneously occupy the same quantum state. This restricts how compressed the matter within the core can be.

interstellar medium in the vicinity of the star with these nuclear products.

Eventually, the cores of stars with masses < 2 $M_\odot$ will become hot enough from helium deposition from the hydrogen fusing shell that helium will begin to fuse. Since the core is initially in a degenerate state, the core will not increase in size in response to an increase in temperature, resulting in a runaway of helium fusion within the core. This results in what is called a helium flash, where a large amount of helium is fused in a matter of seconds. The flash is short because the core becomes non-degenerate again and expands until equilibrium is restored and quiescent helium-4 fusion ensues. This restructuring will affect the surface where the temperature will increase and the luminosity will slightly decrease, but the star remains in the giant region. While it is fusing helium-4 in its core, it is said to be on the horizontal branch and will remain there for millions to hundreds of millions of years, depending on its mass.

Helium fusion follows the triple-alpha process, where three helium-4 nuclei are combined to make carbon-12. Occasionally, carbon-12 will fuse with helium-4 to produce oxygen-16 as well. This builds up a core of carbon and oxygen.

After all of the helium-4 in the core is fused, the core will collapse in all cases to a degenerate state. Now there will be a shell of hydrogen fusion making helium and a shell of helium fusion making carbon and oxygen for stars with masses < 2 $M_\odot$. For all others, the hydrogen fusion shell is extinguished first and reignited once the helium fusion shell is exhausted. For stars above 4 $M_\odot$, a second dredge-up will occur, enriching the surface with more helium and nitrogen-14 (Karakas & Lattanzio [27]). Again, the star will become more luminous and cooler, entering the supergiant region of the H-R diagram (see Figure 1.1).

As the star remains in the supergiant region, the helium shell is replenished with helium-4 by the hydrogen fusion shell. While the helium shell is building up, the small region closest to the core will be degenerate. Eventually, the helium

shell will become hot enough to begin fusing. Like before, the degenerate portion of the helium shell will fuse in a matter of seconds in what is called a helium shell flash. This causes the star to expand and the hydrogen shell to cease fusion, and is known as a thermal pulse. Also, convection in the form of the third dredge-up mixes helium and hydrogen fusion products (i.e. carbon-12, oxygen-16, and helium-4) to the surface. After this thermal pulse, the star will contract again until the hydrogen fusion shell is re-ignited. The hydrogen shell begins building up the helium shell until it reaches a high enough temperature again and the process repeats. It will continue these pulsations for upwards of hundreds of thousands of years, depending on the mass.

If the star has a mass above 5 $M_{\odot}$, a phase known as hot bottom burning may occur (Karakas & Lattanzio [27]). For stars of this mass, the hydrogen-rich convective envelope may reach all the way to the hydrogen burning shell in between dredge-up events. In this case, the bottom of the hydrogen-rich convection envelope will reach temperatures hot enough for the CNO cycle to occur and, due to the convection, carbon-12 will be converted to nitrogen-14 and mixed throughout the envelope as the nitrogen is produced. This reduces the total abundance of carbon as the total nitrogen abundance is increased. However, after hot bottom burning ceases, there may be more dredge-up episodes to mix in more carbon from the helium fusion shell.

With each thermal pulse, the surface of the star will expand, cool, and lose mass to stellar winds. If the pulsation occurs such that shock waves propagate through the stellar atmosphere and drive the upper layers out far enough, the gas will cool enough for heavy elements to condense into grains (Villaver et al. [62]). Then radiation pressure and the coupling of the grains and gas will drive off the outer layers of the star with a speed of approximately 20-30 km/s. Eventually, the entire envelope is thrown off, exposing internal layers that are on the order of

10^5 K. These hot layers emit copious amounts of radiation with photon energies high enough to ionize hydrogen.

The previously expelled gas, which is composed of mostly hydrogen but now enriched with fusion products and s-process elements, absorbs the ionizing photons, causing the gas temperature to increase from scattering between the ions (protons, electrons, etc.) in the gas. The free electrons become thermalized quickly from scattering with hydrogen and helium (H and He e^--scattering cross section $\gg$ photoionization cross section). Cooling of the gas happens in the form of electron free-free, free-bound, and bound-bound emission of photons. Electron free-free photon emission, or Bremsstrahlung emission, occurs when a free election is decelerated by an atomic ion, emitting a photon. Electron free-bound emission, or recombination emission, is the result of a free electron recombining with an atomic ion and emitting a photon. The last emission, electron bound-bound emission, happens after a collision between ions excites a bound electron to a higher energy level. The excited electron eventually transitions to lower levels, emitting photons. This last emission process is the dominant cooling mechanism in the gas. Metals within the gas, such as oxygen and carbon, cool the gas by this collisional process, emitting photons whose energies are below the ionizing threshold of hydrogen and escape the gas. At steady-state, the absorption of ionizing photons and the emission of photons that escape the gas become equal, resulting in the fairly constant emission nebula known as the planetary nebula.

Thus, a planetary nebula, the subject of this dissertation, is a low density, light emitting gas that has recently been ejected from a 0.8 - 8 $M_\odot$ star as it nears the end of its life. After thousands to a few tens of thousands of years, the nebula will become diffuse enough that it no longer radiates and the gas will become part of the interstellar medium. Typically, planetary nebulae have masses in the range

of 0.1-1.0 $M_{\odot}$, densities of order 10^2-10^4 cm^{-3}, and temperatures between 8000 and 20,000 K. They are concentrated on the sky along the Galactic plane and toward the Galactic center. The emission lines commonly used to identify these objects while they are still radiating are the strong forbidden lines of oxygen at wavelengths 4959 and 5007 Å. When these emission lines were first observed, they were erroneously thought to originate from a mysterious element called "nebulium" that only existed in extra-terrestrial conditions. In 1928, the physicist and astronomer Ira Bowen determined they were in fact electronic transitions of O^{+2}.

Throughout the lives of these progenitor stars, there are two main times when a large amount of material is returned to the interstellar medium. The first is during the ascent to the giant region of the H-R diagram. The second, the focus of this dissertation, is during the formation of planetary nebulae. Both of these events enrich the interstellar medium, affecting the chemical composition of galaxies and the formation of new stars. For planetary nebulae, this enrichment or stellar yield is primarily in the form of carbon, nitrogen, and helium. The carbon will especially influence the effectiveness of the CNO cycle and subsequent lifespans of the next generation of stars that form from the enriched material. Also, since all known life uses carbon and nitrogen, understanding the production and distribution of these elements is important to astrobiology research as well. However, more massive stars also enrich the interstellar medium with these elements. Whether planetary nebula forming stars or more massive stars are the dominant contributors of carbon and nitrogen is uncertain and an active area of research. Therefore, a complete and accurate model of the evolution of stars occupying the mass range between 0.8 and 8 $M_{\odot}$ is particularly important for understanding the contribution that these stars make to the buildup of carbon and nitrogen in the interstellar medium.

One requirement for a good model is the proper understanding of the mass ejection process, where some of the details of this process should be revealed by studying the spatial variations in the matter that comprises a planetary nebula (PN). If PNe are chemically inhomogeneous, it would raise questions as to the validity of the current formation theory for planetary nebulae where the nebulae are assumed to be homogeneous. This would impact the stellar yield by adding a directional dependence that would need to be accounted for in chemical evolution modeling of the Galaxy. Seven PNe (IC 2165, IC 3568, NGC 2440, NGC 3242, NGC 5315, NGC 5882, and NGC 7662) are analyzed here with the purpose of addressing chemical homogeneity in planetary nebulae.

The planetary nebulae in this study were first presented in Dufour et al. [13] (hereafter Paper I), where the main goal was to measure critical emission lines of carbon and nitrogen for accurate abundance calculations of these elements. Among the selection criteria for the planetary nebulae were a high surface brightness and, where practical, large angular size. These criteria make them ideal candidates for studying the chemical distribution of their matter.

Each of the seven planetary nebulae can be seen in Figures 1.2 & 1.3. IC 2165 is a slightly elliptical planetary nebula with shells detected at $2''$, $4''$, and $20''$ (not visible in Figure 1.2) from the central star (Corradi et al. [10]). IC 3568 has only two detected shells at radii of $4''$ and $9''$ (not visible in Figure 1.2) and is very circular in appearance (Balick et al. [5] and Corradi et al. [10]). The shape of NGC 2440 is more complicated, with three bipolar structures emanating at various angles from the central star (López et al. [35]), while NGC 3242 exhibits a multi-shell structure. The brightest features for NGC 3242 include an inner $28''$x$20''$ shell surrounded by a $46''$x$40''$ halo (not visible in Figure 1.2; Ruiz et al. [49]). NGC 5315 is an irregularly shaped, compact PN of radius $3''$ (Acker et al. [1]). An elliptical shell with radial dimensions of $5.5''$ x $3''$, a more circular shell of radius

7.5″, and a halo (not visible in Figure 1.3) that extends to 90″ are observed for NGC 5882 (Corradi et al. [9] and Weller & Heathcote [64]). NGC 7662 is another triple-shell PN with two elliptical shells of radii 9″ x 6.2″ (only visible part in Figure 1.3) and 15.4″ x 13.7″ encompassed by a 67″ circular shell (Guerrero et al. [17]).

Given these morphologies, the central star of each PN has experienced mass ejections which may have been inhomogeneous in their elemental composition, either from shell to shell or at different positions within one ejection. Each shell could have a unique composition if each ejection occurred with a different core temperature, resulting in a change in fusion rates around the core and convection rates to the surface. If the convection process was naturally asymmetrical or influenced by a companion star (stripping material), an ejection may result in an uneven distribution of elements. *Therefore, the main goal of this project is to look for spatial differences in the abundances of carbon, nitrogen, helium, oxygen, neon, sulfur, and argon relative to hydrogen across each planetary nebula, using the spectroscopic data presented in Paper I.*

Turning to the problem of determining the central star properties, many authors have inferred the stellar temperature and luminosity using techniques such as photoionization modeling of the nebula (see e.g. Henry et al. [21], hereafter Paper II) and the Zanstra method[a] (see e.g. Shaw and Kaler [57], [58]; Zhang & Kwok [65]). Consequently, there is often a large range in the derived stellar parameters for any one object. In particular, the Zanstra method gives very different temperatures for the same star depending on if hydrogen or helium lines are used in the method. Since the mass of a star is the primary factor that determines its luminosity and temperature, having uncertain measurements of these stellar parameters results in unreliable initial/final mass calculations.

Fig. 1.2.— The locations of the extracted spectra where all seven gratings spatially overlap one another from STIS. In addition to the individual regions, a Full region for each object was extracted over all the regions shown. From left to right, top to bottom: IC2165, IC 3568, NGC2440, NGC 3242. The double slits in NGC 2440 are the result of a pointing error discussed in the text.

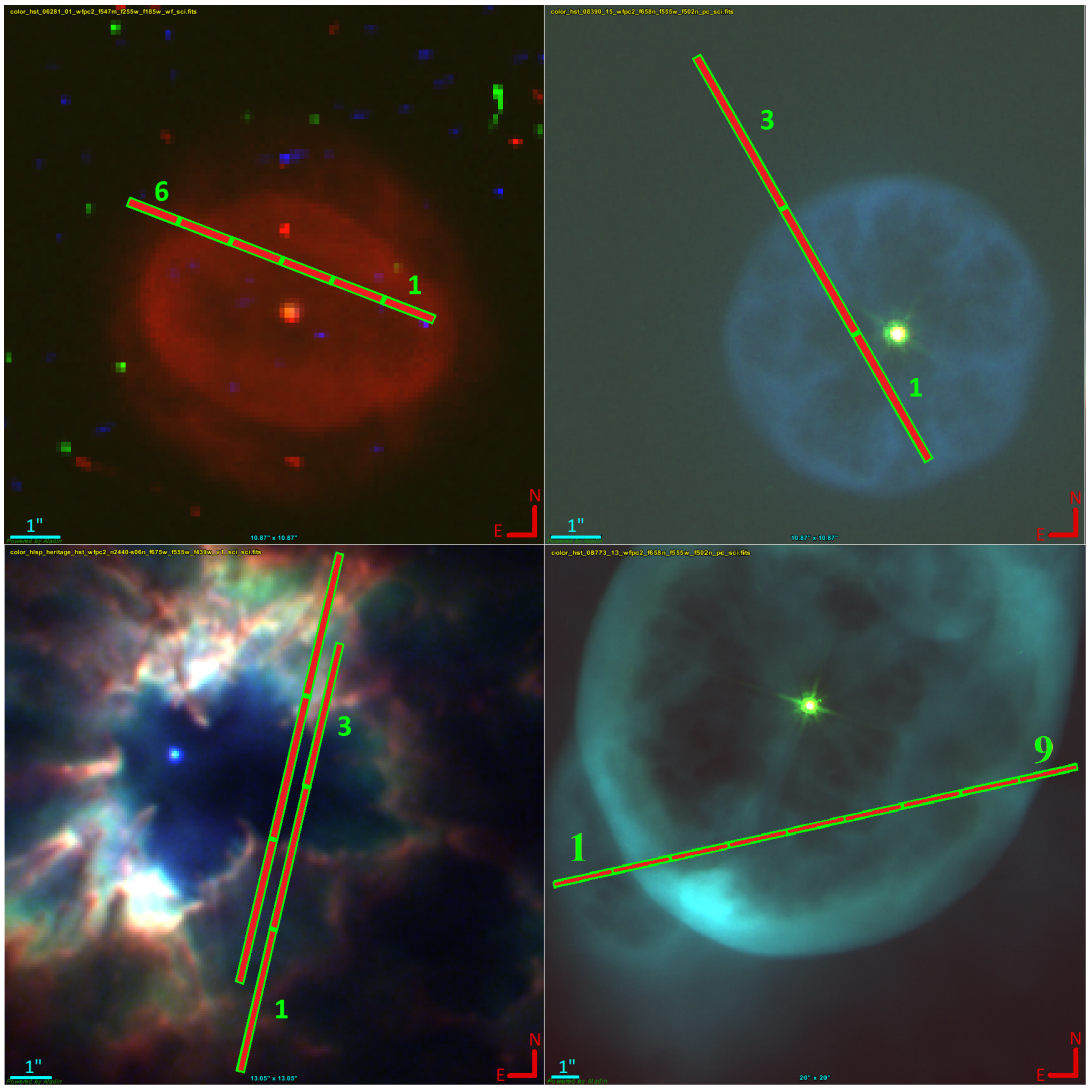

Fig. 1.3.— The same as Figure 1.2. From left to right, top to bottom: NGC 5315, NGC 5882, NGC 7662.

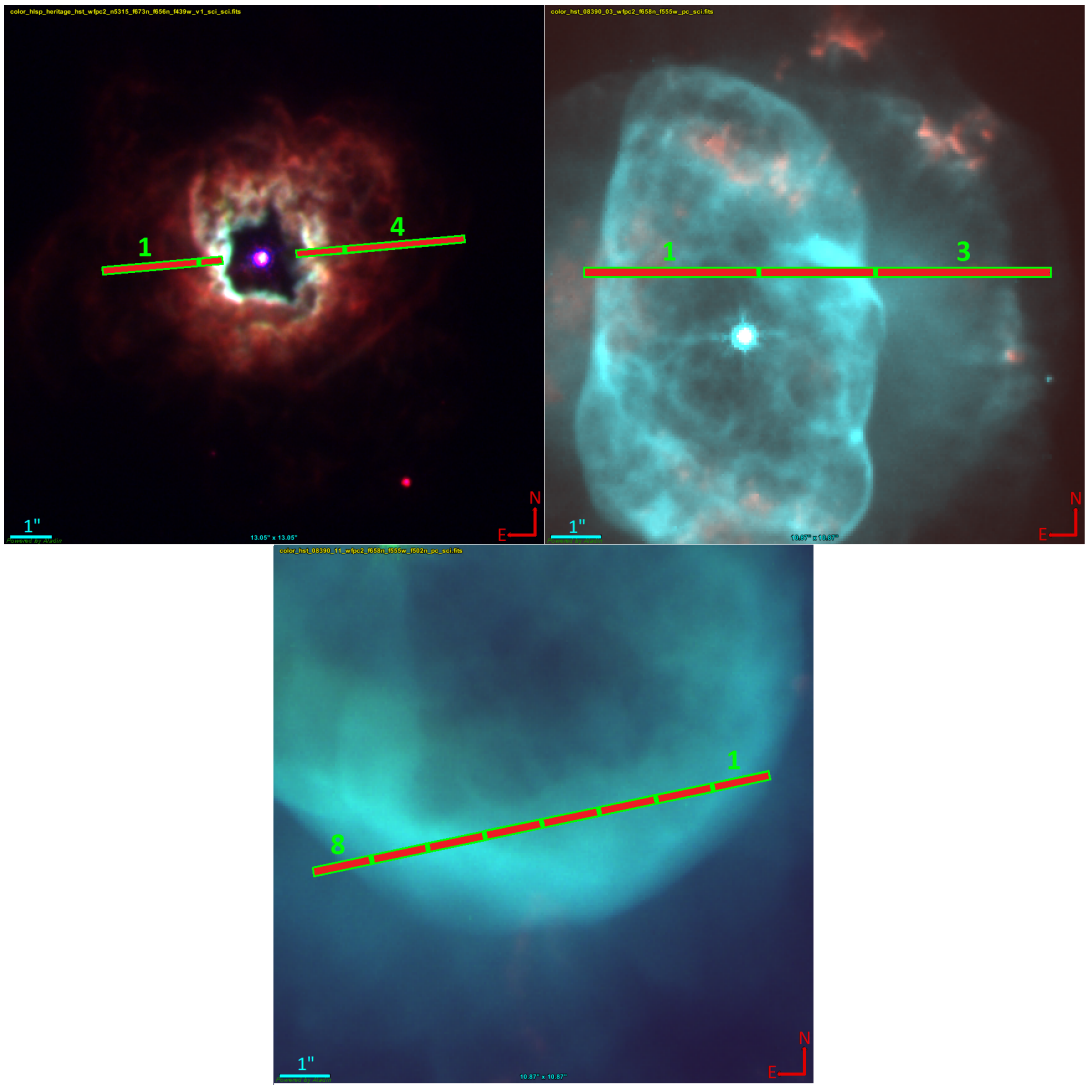

This leads to the second goal of this dissertation: to constrain the stellar temperature and luminosity of each planetary nebula by modeling each with the photoionization code Cloudy, using the observations as constraints. However, unlike previous photoionization modeling work extant in the literature, a physically motivated spectral energy distribution is used here for the central star, and the modeled emission lines are calculated as seen through the slit instead of over the entire nebula.

The observations and analysis are presented in Chapter 2 followed by results in Chapters 3 and 4. Chapter 5 contains the summary and conclusions while Chapter 6 addresses improvements and future work.

[a]The Zanstra method assumes all ionizing photons from the Lyman continuum are absorbed by the nebula, which makes it possible to determine the stellar temperature from a nebular line such as Hβ.

Chapter 2

Data Acquisition and Analysis

Co-spatial HST/STIS spectra, with 0.05″ resolution and spanning the wavelength range of 1150-10,270 Å, were obtained during the GO12600 spectra cycle 19 program and presented in Paper I. An example of the data quality is shown in Figures 2.1 & 2.2 for NGC 3242. Numerous lines are identified and the insets highlight certain line complexes that contain important lines for nebular diagnostics discussed later. A Python script was used to extract spectra for numerous regions in each PN, allowing for a comparison of abundances among different regions. Each region's location was chosen to correspond with different structures within each nebula. The size of each region was chosen by looking at the signal-to-noise of the weakest lines and reducing the size until those lines were still able to be reliably measured. This maximized the total number of emission lines that could be used for analysis.

Fig. 2.1.— The spectrum for NGC 3242 spanning the UV portion of the wavelength range. The inset shows the closely spaced [C III] λ 1907 and C III] λ 1909 emission lines. Numerous other emission lines are identified as well.

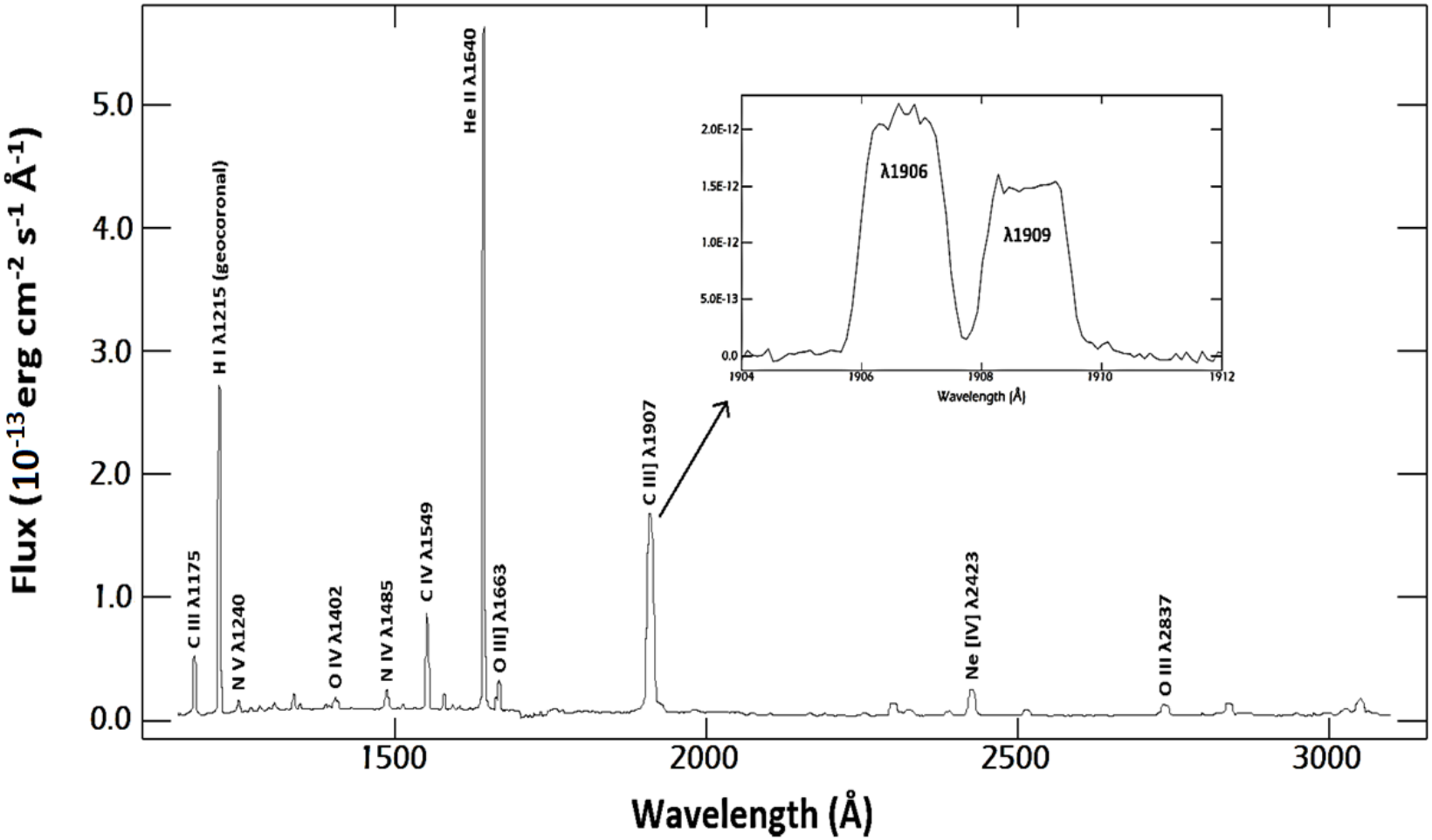

Fig. 2.2.— The spectrum for NGC 3242 spanning the optical portion of the wavelength range. The inset shows the closely spaced emission lines of Hγ and [O III] λ 4363. Numerous other emission lines are identified as well.

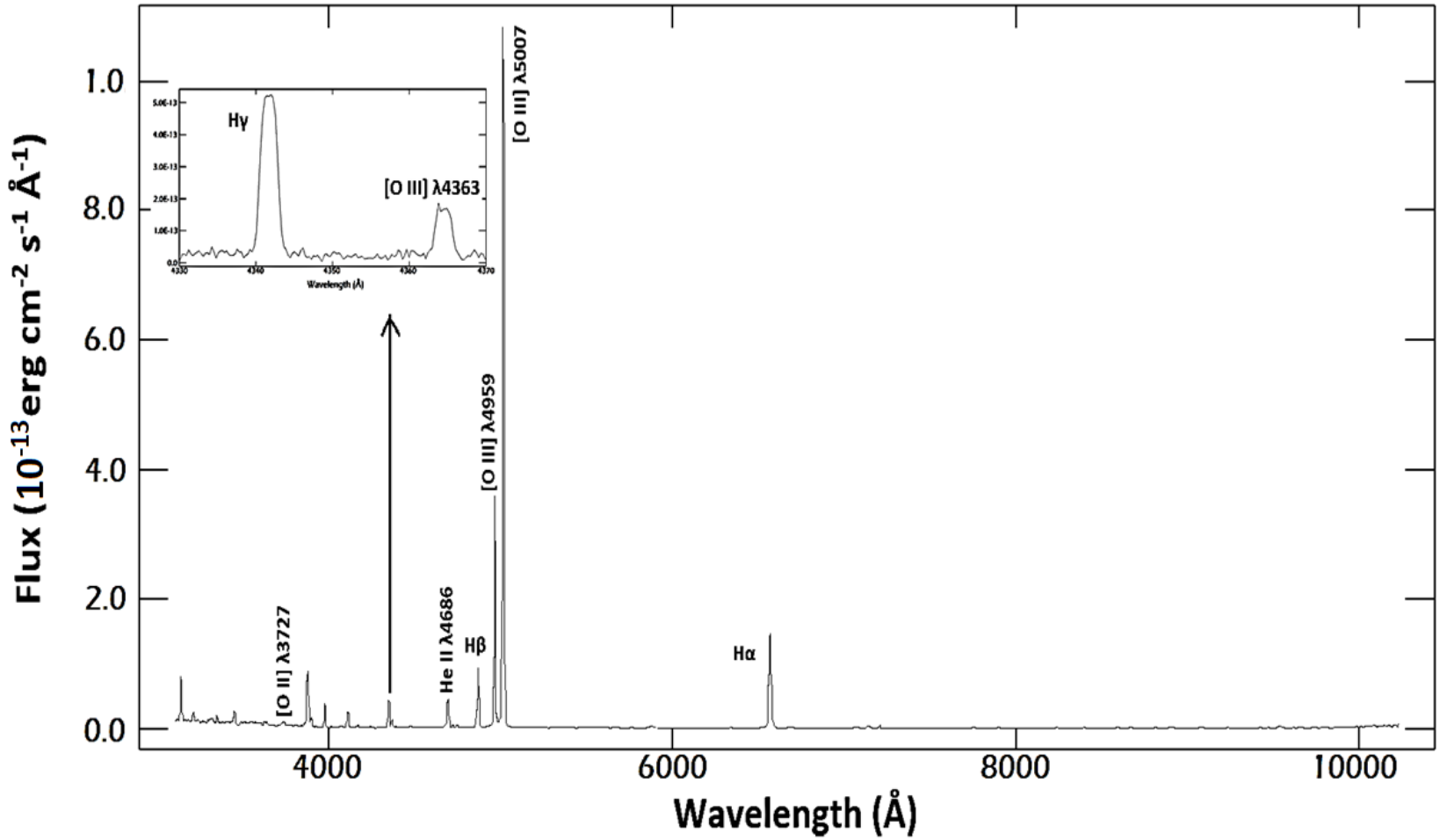

All regions can be seen in Figures 1.2 & 1.3, where the numbers identify each of the smaller regions, and the full region encompasses all of the numbered regions. The two slits shown for NGC 2440 were the result of a pointing error where the central star, which was going to be used as the guide star, was originally not within the field of view. Each slit shows the final UV (right) and optical (left) positions, so that the observations as a whole are not co-spatial for this one object.

Emission line fluxes were measured with IRAF[a] using the task *splot* by fitting Gaussian profiles. Special treatment was needed for lines originating from the higher resolution gratings of STIS, namely summing the observed flux instead of fitting Gaussian profiles. This last operation corrected for the flat-top features of the emission lines exhibited in the higher resolution gratings, inherent to the instrument. Any over-estimation of line strengths from the smaller regions was prevented by requiring the sum of the smaller regions' line strengths to equal the full region's value. The uncertainty estimates for the flux of each emission line were calculated by taking twice the FWHM of each emission line and multiplying it by the average of the continuum rms noise measured on either side of the line.

The observed and dereddened line intensities for each region are shown in Table 2.1. The first column specifies the wavelength measured in Å, while the second column lists the ion responsible for the emission line. Each wavelength's value for the reddening function, f(λ), can be found in the third column. The following pairs of columns contain the observed and dereddened line strengths under F(λ) and I(λ), respectively. All line strengths are normalized to F(Hβ) or I(Hβ) = 100.

The dereddened values and accompanying errors were calculated using the program ELSA (Johnson et al. [26]). ELSA corrects the emission lines for interstellar

[a]IRAF is distributed by the National Optical Astronomy Observatory, which is operated by the Association of Universities for Research in Astronomy (AURA) under cooperative agreement with the National Science Foundation.

extinction (using the function prescribed by Savage & Mathis [50] and Seaton [56] for optical and ultraviolet wavelengths, respectively) and contamination from He^+ recombination lines (Pickering series) to the first four hydrogen Balmer lines while propagating the observed uncertainties. ELSA propagates uncertainties by adding the contributing uncertainties in quadrature and iteratively calculating the partial derivatives of the dependence each output value has on the input data. Following the last emission line of each region is the logarithmic reddening parameter, c, the theoretical ratio of F(Hα/Hβ), and the observed, uncorrected flux of Hβ. Calculations for F(Hα/Hβ) occur in an iterative loop as well within ELSA since the value of c, which is used to determine the ratio, depends on the nebular temperature and density. The lines that determine these nebular properties, typically [O III] lines for the temperature and C III]/[C III] lines for the density, also depend on the value of c, which necessitates an iterative loop in order to obtain a stable solution.

Table 2.1. Fluxes and Intensities

Fluxes and Intensities												
Wave			IC2165 Full		IC2165 1		IC2165 2		IC2165 3		IC2165 4	
(Å)	ID	f(λ)	F(λ)	I(λ)	F(λ)	I(λ)	F(λ)	I(λ)	F(λ)	I(λ)	F(λ)	I(λ)
1485	N IV]	1.231	13.7	47.9±5.20	10.4	34.5±5.10	19.4	76.7±11.59	17.2	55.2±7.43	18.6	53.4±6.95
1907	[C III]	1.226	112	387±41	123	404±53	108	426±62	101	323±42	100	286±36
1909	C III]	1.229	86.4	301±32	93.0	306±40	93.8	370±55	75.0	240±32	76.2	218±28
3869	[Ne III]	0.224	59.4	76.8±5.40	65.8	84.1±6.29	48.3	64.0±7.00	47.7	60.5±7.18	44.6	55.3±6.24
4363	[O III]	0.118	16.0	18.0±1.94	20.0	22.4±3.96	15.0	17.1±2.34	14.1	15.7±3.16	13.8	15.2±3.35
4686	He II	0.036	60.0	62.2±2.97	58.4	60.5±3.59	80.5	83.8±4.75	68.3	70.7±4.14	78.7	81.2±3.70
4861	Hβ	0.000	100	100±0	100	100±0	100	100±0	100	100±0	100	100±0
4959	[O III]	-0.030	396	384±10	448	435±12	322	312±11	346	336±10	301	293±8
5007	[O III]	-0.042	1229	1178±26	1415	1359±36	980	936±28	1035	995±27	938	905±24
5876	He I	-0.231	10.6	8.41±1.18	11.2	8.92±2.53	9.48	7.32±2.99	8.29	6.66±2.13	6.37	5.23±1.91
7136	[Ar III]	-0.453	13.0	8.20±1.15	15.7	10.1±1.49	10.3	6.24±1.87	10.4	6.79±1.01	8.60	5.83±1.31
9532	[S III]	-0.632	50.5	26.6±1.57	45.9	24.9±2.92	45.8	22.6±2.22	47.1	25.9±3.01	36.6	21.3±2.92
c[a]			0.44		0.42		0.48		0.41		0.37	
Hα/Hβ[b]			2.80		2.79		2.78		2.80		2.79	
log F$_{H\beta}$[c]			-12.43		-13.11		-13.20		-13.21		-13.15	

Wave			IC2165 5		IC2165 6		IC3568 Full		IC3568 1		IC3568 2	
(Å)			F(λ)	I(λ)	F(λ)	I(λ)	F(λ)	I(λ)	F(λ)	I(λ)	F(λ)	I(λ)
1485	N IV]	1.231	8.95	29.9±4.83	0.715	4.51±2.51	···	···	···	···	···	···
1549	C IV	1.184	···	···	···	···	23.0	43.2±5.50	25.9	43.0±8.00	19.7	37.9±6.62
1907	[C III]	1.226	130	431±59	100	629±209	41.4	79.5±7.77	38.9	65.8±9.39	42.2	83.0±12.89
1909	C III]	1.229	94.3	315±43	85.7	539±182	31.1	59.9±6.39	30.3	51.2±9.38	29.8	58.7±9.72
3869	[Ne III]	0.252	81.5	104±8	79.7	116±21	68.4	78.2±4.35	71.0	79.0±4.12	68.2	78.4±4.45
4363	[O III]	0.118	19.4	21.8±3.57	7.08	8.45±6.13	7.22	7.69±2.37	9.69	10.2±2.14	6.23	6.65±2.74
4686	He II	0.036	37.8	39.2±3.03	···	···	···	···	···	···	···	···
4861	Hβ	0.000	100	100±0	100	100±0	100	100±0	100	100±0	100	100±0
4959	[O III]	-0.030	516	501±16	499	477±34	350	344±8	350	346±9	336	330±10
5007	[O III]	-0.042	1542	1480±41	1747	1642±108	1182	1156±21	1174	1153±29	1135	1109±31

Table 2.1—Continued

Fluxes and Intensities												
Wave			IC2165 5		IC2165 6		IC3568 Full		IC3568 1		IC3568 2	
(Å)	ID	f(λ)	F(λ)	I(λ)	F(λ)	I(λ)	F(λ)	I(λ)	F(λ)	I(λ)	F(λ)	I(λ)
5876	He I	-0.231	14.0	11.2±1.62	20.9	14.8±4.08	15.4	13.6±1.93	16.2	14.7±3.50	14.1	12.4±3.60
7136	[Ar III]	-0.453	15.7	10.1±1.36	22.9	11.6±2.73	9.29	7.29±1.55	8.94	7.36±2.99	8.36	6.51±2.05
9532	[S III]	-0.632	68.7	36.9±2.55	75.3	29.2±5.38	···	···	···	···	···	···
c[a]			0.43		0.65		0.23		0.19		0.24	
Hα/Hβ[b]			2.80		2.86		2.85		2.83		2.86	
log $F_{H\beta}$[c]			-13.16		-13.61		-12.55		-12.90		-12.88	

Wave			IC3568 3		NGC2440 Full		NGC2440 1		NGC2440 2		NGC2440 3	
(Å)			F(λ)	I(λ)	F(λ)	I(λ)	F(λ)	I(λ)	F(λ)	I(λ)	F(λ)	I(λ)
1485	N IV]	1.231	···	···	73.3	229±27	37.2	122±13	138	326±69	74.5	264±30
1549	C IV	1.184	25.1	72.8±31.66	···	···	···	···	···	···	···	···
1907	[C III]	1.226	51.1	154±73	135	420±49	99.5	324±33	154	362±77	159	561±64
1909	C III]	1.229	40.2	121±57	103	321±37	65.8	215±23	129	303±65	123	434±49
3727	[O II]	0.292	···	···	71.7	93.9±5.50	119	157±9	9.18	11.3±9.78	60.1	81.1±6.45
3869	[Ne III]	0.252	57.9	72.6±21.22	73.6	92.9±4.74	92.5	118±7	24.9	29.7±7.90	73.4	95.1±6.12
4363	[O III]	0.118	5.40	6.00±5.77	21.3	23.8±2.41	23.7	26.5±2.22	14.5	15.8±8.19	25.5	28.8±2.45
4686	He II	0.036	···	···	80.8	83.5±2.93	54.6	56.5±2.43	113	116±8	87.2	90.5±3.98
4861	Hβ	0.000	100	100±0	100	100±0	100	100±0	100	100±0	100	100±0
4959	[O III]	-0.030	414	403±37	454	441±11	520	505±11	216	211±11	510	495±12
5007	[O III]	-0.042	1459	1405±120	1402	1349±32	1578	1516±31	731	710±31	1520	1456±34
5876	He I	-0.231	18.0	14.6±10.75	9.92	8.01±0.80	13.5	10.8±1.78	···	···	10.2	8.02±1.33
6584	[N II]	-364	···	···	819	585±2	1293	911±4	147	114±2	752	518±2
7136	[Ar III]	-0.453	15.3	10.2±7.13	28.1	18.5±0.73	33.2	21.5±1.21	13.6	9.94±1.87	31.4	19.7±0.84
9532	[S III]	-0.632	···	···	50.5	28.2±1.23	50.6	27.5±2.36	17.4	11.2±3.07	56.2	29.3±1.81
c[a]			0.39		0.40		0.42		0.30		0.45	
Hα/Hβ[b]			2.87		2.79		2.79		2.77		2.78	
log $F_{H\beta}$[c]			-13.58		-12.43		-12.90		-13.16		-12.76	

Table 2.1—Continued

Fluxes and Intensities												
Wave			NGC3242 Full		NGC3242 1		NGC3242 2		NGC3242 3		NGC3242 4	
(Å)	ID	f(λ)	F(λ)	I(λ)	F(λ)	I(λ)	F(λ)	I(λ)	F(λ)	I(λ)	F(λ)	I(λ)
1485	N IV]	1.231	8.47	10.1±0.86	2.24	2.66±0.92	7.06	8.41±1.43	11.2	12.3±1.89	7.73	9.80±1.88
1907	[C III]	1.226	121	144±5	117	138±27	118	141±12	130	143±15	129	163±21
1909	C III]	1.229	88.8	106±4	80.8	95.6±19.07	91.3	109±9	92.7	102±11	92.5	117±16
3727	[O II]	0.292	4.38	4.57±1.85	...	...	...	...	...	...	...	...
3869	[Ne III]	0.252	96.6	100±2	106	110±9	101	105±7	90.8	92.7±5.26	105	110±7
4363	[O III]	0.118	12.8	13.0±0.96	12.8	13.0±4.58	14.1	14.4±1.33	12.7	12.9±2.20	15.2	15.6±2.97
4686	He II	0.036	47.4	47.6±0.73	18.6	18.7±3.90	41.1	41.3±2.99	55.8	56.0±2.49	36.6	36.9±3.97
4861	Hβ	0.000	100	100±0	100	100±0	100	100±0	100	100±0	100	100±0
4959	[O III]	-0.030	414	412±3	459	457±19	441	439±8	369	368±8	448	446±12
5007	[O III]	-0.042	1233	1225±8	1367	1359±53	1313	1305±22	1098	1095±22	1336	1326±34
5876	He I	-0.231	9.71	9.39±0.66	15.3	14.8±3.44	13.0	12.6±2.41	9.15	8.98±3.38	10.4	9.98±3.82
7136	[Ar III]	-0.453	6.83	6.39±0.68	...	...	...	...	...	...	...	...
9532	[S III]	-0.632	10.6	9.67±1.91	...	...	...	...	...	...	...	...
c[a]			0.06		0.06		0.06		0.03		0.08	
Hα/Hβ[b]			2.82		2.83		2.82		2.82		2.82	
log $F_{H\beta}$[c]			-12.00		-13.03		-12.79		-12.84		-13.00	

Wave			NGC3242 5		NGC3242 6		NGC3242 7		NGC3242 8		NGC3242 9	
(Å)			F(λ)	I(λ)	F(λ)	I(λ)	F(λ)	I(λ)	F(λ)	I(λ)	F(λ)	I(λ)
1485	N IV]	1.231	8.22	10.2±2.04	8.85	11.1±2.23	9.31	11.6±1.77	11.6	13.4±1.82	7.47	9.18±2.88
1907	[C III]	1.226	121	150±18	123	154±17	114	141±18	122	141±15	120	147±20
1909	C III]	1.229	88.5	110±14	90.0	113±13	91.7	114±14	88.7	102±11	82.3	101±14
3869	[Ne III]	0.252	96.2	101±6	103	108±6	92.0	96.2±6.20	93.9	96.8±4.97	103	108±7
4363	[O III]	0.118	12.7	12.9±3.23	13.3	13.6±3.61	12.5	12.8±3.17	14.2	14.4±2.19	14.2	14.5±2.08
4686	He II	0.036	47.6	47.9±3.26	47.5	47.9±4.24	52.4	52.7±4.33	68.5	68.8±2.44	47.0	47.3±4.78
4861	Hβ	0.000	100	100±0	100	100±0	100	100±0	100	100±0	100	100±0
4959	[O III]	-0.030	420	418±10	422	420±9	396	394±10	364	363±8	439	437±12
5007	[O III]	-0.042	1251	1242±29	1258	1248±27	1179	1171±29	1086	1080±23	1309	1300±34

Table 2.1—Continued

Fluxes and Intensities												
Wave			NGC3242 5		NGC3242 6		NGC3242 7		NGC3242 8		NGC3242 9	
(Å)	ID	f(λ)	F(λ)	I(λ)	F(λ)	I(λ)	F(λ)	I(λ)	F(λ)	I(λ)	F(λ)	I(λ)
5876	He I	-0.231	8.03	7.71±2.37	7.64	7.32±2.51	7.75	7.44±2.01	5.66	5.50±1.46	10.6	10.2±3.55
c[a]			0.08		0.08		0.08		0.05		0.07	
Hα/Hβ[b]			2.82		2.82		2.82		2.81		2.82	
log $F_{H\beta}$[c]			-13.03		-12.99		-12.98		-12.86		-13.17	
Wave			NGC5315 Full		NGC5315 1		NGC5315 2		NGC5315 3		NGC5315 4	
(Å)			F(λ)	I(λ)	F(λ)	I(λ)	F(λ)	I(λ)	F(λ)	I(λ)	F(λ)	I(λ)
1549	C IV	1.184	6.96	31.2±1.30	21.4	135±15	4.47	17.8±1.07	6.54	34.8±2.13	13.3	76.4±13.45
1907	[C III]	1.226	2.27	10.7±0.73	3.20	21.6±4.92	2.31	9.66±0.58	1.83	10.3±1.22	3.17	19.4±5.81
1909	C III]	1.229	4.17	19.8±1.01	6.30	42.7±10.63	4.22	17.7±0.61	3.32	18.8±1.76	4.98	30.6±7.51
3869	[Ne III]	0.252	54.9	75.5±0.86	40.2	59.5±4.62	63.6	85.3±0.56	45.6	65.1±1.10	40.8	30.4±11.51
4363	[O III]	0.118	3.23	3.75±0.23	4.25	5.11±1.86	3.56	4.09±0.10	2.74	3.24±0.45	1.45	1.73±1.14
4861	Hβ	0.000	100	100±0	100	100±0	100	100±0	100	100±0	100	100±0
4959	[O III]	-0.030	288	277±2	237	226±6	310	300±2	275	264±2	225	215±6
5007	[O III]	-0.042	896	850±4	938	879±16	926	882±3	897	846±5	825	776±20
5876	He I	-0.231	23.4	17.5±0.21	16.6	11.6±1.55	23.7	18.1±0.19	25.0	18.0±0.24	23.5	16.7±0.85
7136	[Ar III]	-0.453	53.1	29.9±0.13	57.4	28.4±0.70	52.6	31.0±0.07	55.2	29.1±0.16	47.5	24.3±1.00
9532	[S III]	-0.632	286	128±1	292	109±2	285	136±0	300	123±1	220	86.4±2.88
c[a]			0.55		0.68		0.51		0.61		0.64	
Hα/Hβ[b]			2.87		2.86		2.86		2.87		2.91	
log $F_{H\beta}$[c]			-11.76		-12.87		-12.02		-12.29		-12.96	
Wave			NGC5882 Full		NGC5882 1		NGC5882 2		NGC5882 3			
(Å)			F(λ)	I(λ)	F(λ)	I(λ)	F(λ)	I(λ)	F(λ)	I(λ)		
1549	C IV	1.184	1.39	3.27±0.78	1.74	3.78±1.32	1.70	3.92±0.75	0.337	0.926±1.02		
1907	[C III]	1.226	4.08	9.88±1.40	...	...	...	...	...	...		
1909	C III]	1.229	4.83	11.7±1.34	7.13[d]	16.0±4.11[d]	10.0[d]	23.9±3.48[d]	9.61[d]	27.4±7.25[d]		
3869	[Ne III]	0.252	70.8	84.9±3.21	70.4	83.1±4.17	75.1	89.8±2.76	64.0	79.3±7.04		

Table 2.1—Continued

Fluxes and Intensities										
Wave			NGC5882 Full		NGC5882 1		NGC5882 2		NGC5882 3	
(Å)	ID	f(λ)	F(λ)	I(λ)	F(λ)	I(λ)	F(λ)	I(λ)	F(λ)	I(λ)
4363	[O III]	0.118	3.92	4.27±0.87	4.42	4.78±1.68	3.87	4.21±0.97	3.16	3.50±3.00
4686	He II	0.036	3.60	3.69±0.88	5.31	5.44±1.17	4.25	4.36±0.79	···	···
4861	Hβ	0.000	100	100±0	100	100±0	100	100±0	100	100±0
4959	[O III]	-0.030	338	331±6	343	336±7	337	330±3	335	327±9
5007	[O III]	-0.042	1218	1182±18	1229	1196±25	1193	1158±9	1223	1180±30
5876	He I	-0.231	18.8	15.9±0.80	18.5	15.9±1.89	19.0	16.1±0.88	19.1	15.6±1.47
6584	[N II]	-0.364	13.6	10.5±0.34	23.2	18.3±0.38	6.15	4.75±0.18	11.2	8.22±0.37
7136	[Ar III]	-0.453	20.0	14.4±0.76	20.9	15.5±1.11	18.1	13.2±0.43	21.9	14.8±1.28
9532	[S III]	-0.632	64.2	40.7±1.29	73.7	48.6±1.72	54.0	34.6±1.01	67.4	39.3±2.94
c[a]			0.31		0.29		0.31		0.37	
Hα/Hβ[b]			2.89		2.89		2.88		2.90	
log $F_{H\beta}$[c]			-12.15		-12.61		-12.54		-12.77	

Wave			NGC7662 Full		NGC7662 1		NGC7662 2		NGC7662 3		NGC7662 4	
(Å)			F(λ)	I(λ)	F(λ)	I(λ)	F(λ)	I(λ)	F(λ)	I(λ)	F(λ)	I(λ)
1485	N IV]	1.231	12.1	19.8±1.13	7.14	13.1±2.46	11.3	16.4±1.63	12.8	18.8±2.62	13.7	23.8±2.46
1549	C IV	1.184	346	555±24	221	396±37	307	439±22	334	483±50	339	578±41
1750	N III]	1.119	7.54	11.8±2.81	15.7	27.2±13.01	7.24	10.1±6.66	9.06	12.8±4.7	6.73	11.2±6.07
1907	[C III]	1.226	166	271±12	162	296±28	179	259±13	162	237±25	171	297±22
1909	C III]	1.229	118	192±9	117	215±21	134	194±10	119	174±19	117	203±15
3727	[O II]	0.292	6.35	7.13±2.17	10.1	11.6±5.23	6.12	6.68±4.02	4.09	4.48±2.49	6.27	7.16±4.94
3869	[Ne III]	0.252	98.2	109±3	127	144±7	100	108±4	86.3	93.3±5.27	92.9	104±3
4363	[O III]	0.118	17.6	18.5±1.02	19.6	20.8±2.91	17.9	18.6±1.91	15.2	15.8±1.21	17.4	18.3±0.75
4686	He II	0.036	52.5	53.3±0.97	48.5	49.4±2.27	63.4	64.1±1.51	58.6	59.3±2.14	68.0	69.1±1.56
4861	Hβ	0.000	100	100±0	100	100±0	100	100±0	100	100±0	100	100±0
4959	[O III]	-0.030	432	427±6	534	526±11	449	445±5	373	370±9	381	376±6
5007	[O III]	-0.042	1431	1408±13	1771	1735±33	1447	1429±15	1312	1295±28	1258	1234±19
5876	He I	-0.231	8.57	7.81±1.11	12.1	10.8±4.11	7.83	7.30±3.54	6.58	6.12±2.32	5.06	4.56±1.40

Table 2.1—Continued

Fluxes and Intensities												
Wave			NGC7662 Full		NGC7662 1		NGC7662 2		NGC7662 3		NGC7662 4	
(Å)	ID	f(λ)	F(λ)	I(λ)	F(λ)	I(λ)	F(λ)	I(λ)	F(λ)	I(λ)	F(λ)	I(λ)
7136	[Ar III]	-0.453	9.25	7.72±0.90	11.3	9.02±1.29	10.5	9.12±1.11	9.72	8.44±0.74	9.07	7.39±0.92
9532	[S III]	-0.632	24.6	19.1±1.81	28.0	20.5±3.18	36.0	29.7±4.89	23.7	19.5±3.71	24.6	18.5±2.70
c[a]			0.17		0.21		0.13		0.13		0.20	
Hα/Hβ[b]			2.81		2.81		2.81		2.81		2.80	
log $F_{H\beta}$[c]			-12.21		-13.25		-13.16		-13.08		-13.06	

Wave			NGC7662 5		NGC7662 6		NGC7662 7		NGC7662 8	
(Å)			F(λ)	I(λ)	F(λ)	I(λ)	F(λ)	I(λ)	F(λ)	I(λ)
1485	N IV]	1.231	15.9	26.4±2.86	12.2	22.0±2.28	9.80	14.8±1.76	13.6	28.3±4.92
1549	C IV	1.184	357	581±30	340	598±21	374	557±42	575	1165±95
1750	N III]	1.119	8.75	13.9±4.02	6.22	10.6±4.74	5.91	8.61±5.01	5.93	11.6±13.64
1907	[C III]	1.226	173	287±15	172	309±11	151	228±18	159	331±28
1909	C III]	1.229	121	200±11	124	223±8	105	158±13	117	243±22
3727	[O II]	0.292	7.22	8.15±4.76	6.89	7.93±3.31	5.37	5.93±1.76	5.09	6.06±2.95
3869	[Ne III]	0.252	90.8	101±3	94.5	107±2	100	109±4	115	133±5
4363	[O III]	0.118	16.8	17.6±2.91	19.8	20.9±1.64	16.9	17.6±1.48	19.6	21.0±4.04
4686	He II	0.036	70.4	71.5±1.52	55.7	56.7±1.14	37.5	37.9±1.40	46.4	47.5±2.98
4861	Hβ	0.000	100	100±0	100	100±0	100	100±0	100	100±0
4959	[O III]	-0.030	393	388±4	473	466±4	421	417±7	531	522±10
5007	[O III]	-0.042	1247	1225±13	1568	1537±11	1472	1452±23	1623	1583±26
5876	He I	-0.231	6.77	6.16±1.53	9.42	8.44±0.97	13.0	12.0±2.76	9.67	8.42±3.34
7136	[Ar III]	-0.453	9.25	7.67±1.41	9.25	7.44±1.27	8.32	7.14±0.77	6.75	5.15±3.88
9532	[S III]	-0.632	24.9	19.2±2.74	23.8	17.5±2.33	18.4	14.9±2.46	19.4	13.3±10.61

Table 2.1—Continued

Fluxes and Intensities				
	NGC7662 5	NGC7662 6	NGC7662 7	NGC7662 8
c[a]	0.18	0.21	0.15	0.26
Hα/Hβ[b]	2.80	2.81	2.82	2.81
log $F_{H\beta}$[c]	-13.06	-13.01	-13.07	-13.37

[a]Logarithmic extinction at Hβ

[b]Expected intrinsic Hα/Hβ ratio at nebular temperature and density

[c]ergs cm^{-2} s^{-1} in the extracted spectra

[d]Blended 1907 and 1909

The nebular properties were also calculated using ELSA. To summarize the process, ELSA used the corrected line strengths and a 5-level atom scheme to calculate the abundances of all observable ions. The 5-level atom scheme is an approximation of each ion as consisting of only five energy levels for the electrons to occupy. The highest level is ≈5 eV above the ground state for each ion, which is about the maximum available energy for collisional excitations in the gas. ELSA also propagates uncertainties in the same manner as described before for each ionic state. These 1 σ uncertainties account for the errors from the line strengths as well as the temperature, density and logarithmic extinction. Then, for elements with unseen ionization states, ionization correction factors (ICFs) were calculated by ELSA and then applied to the sum of the observed ionic states to determine elemental abundances. These ICFs are calculated using the prescriptions outlined in Paper I and Kwitter & Henry [31]. For carbon and nitrogen, Paper I showed that the direct sum of the observed ionic states was more accurate than an ICF-derived total abundance, so the total abundances for carbon and nitrogen are the result of summing the observed ionic states.

Table 2.2 lists the ionic abundances for every observed element. The ionic species and wavelength (in Ångstroms) of the specific emission line used to derive the ionic abundance are provided in the first column. Each column to the right of column 1 contains the ionic abundances for each region identified in the column head. Additionally, an ICF value is listed below the observed ions for each element (except for carbon and nitrogen, since those ICFs were not used to determine the total abundance). Each region follows in the remaining columns with its associated ionic abundances and ICFs. Finally, at the bottom of each object column are the inferred values for the [O III] temperature and the C III] or [S II] density of the nebula.

Table 2.2. Ionic Abundances[a] , Temperatures and Densities

Ionic Abundances[a] , Temperatures and Densities							
Ion	IC2165 Full	IC2165 1	IC2165 2	IC2165 3	IC2165 4	IC2165 5	IC2165 6
He^{+}(5876)	5.67±1.62(-2)	5.12±1.50(-2)	3.87±1.60(-2)	3.95±1.30(-2)	2.97±1.12(-2)	6.86±1.07(-2)	1.00±0.28(-1)
He^{+2}(4686)	5.65±0.27(-2)	5.47±0.33(-2)	7.52±0.43(-2)	6.42±0.39(-2)	7.33±0.36(-2)	3.58±0.28(-2)	···
icf(He)	1.00	1.00	1.00	1.00	1.00	1.00	1.00
O^{+}(3727)	7.44±4.06(-6)	7.91±3.45(-6)	9.00±2.89(-6)	5.80±3.51(-6)	2.11±1.72(-6)	1.24±0.33(-5)	1.48±0.77(-4)
O^{+}(7325)	2.31±2.24(-5)	8.55±4.08(-6)	3.66±2.16(-6)	9.65±8.20(-6)	5.91±7.13(-6)	2.02±0.79(-5)	6.68±5.23(-5)
O^{+}(adopt)	1.14±0.41(-5)	8.06±2.76(-6)	7.94±2.54(-6)	6.90±3.60(-6)	3.74±4.18(-6)	1.44±0.33(-5)	1.29±0.69(-4)
O^{+2}(5007)	1.60±0.21(-4)	1.71±0.37(-4)	1.08±0.18(-4)	1.31±0.32(-4)	1.11±0.30(-4)	2.13±0.41(-4)	7.61±5.41(-4)
O^{+2}(4959)	1.55±0.20(-4)	1.64±0.35(-4)	1.08±0.18(-4)	1.32±0.32(-4)	1.08±0.29(-4)	2.15±0.42(-4)	6.60±4.69(-4)
O^{+2}(4363)	1.56±0.21(-4)	1.71±0.37(-4)	1.08±0.18(-4)	1.31±0.32(-4)	1.11±0.30(-4)	2.13±0.41(-4)	7.61±5.41(-4)
O^{+2}(adopt)	1.59±0.20(-4)	1.70±0.37(-4)	1.08±0.18(-4)	1.32±0.32(-4)	1.10±0.30(-4)	2.13±0.41(-4)	7.39±5.25(-4)
icf(O)	2.00±0.29	2.07±0.31	2.94±0.80	2.63±0.54	3.47±0.92	1.52±0.09	1.00
Ar^{+2}(7135)	3.93±0.67(-7)	4.59±1.01(-7)	2.65±0.86(-7)	3.20±0.75(-7)	2.61±0.79(-7)	5.04±1.00(-7)	1.30±0.72(-6)
Ar^{+2}(7751)	6.94±3.54(-7)	8.61±5.81(-7)	3.40±4.71(-7)	5.37±5.92(-7)	6.76±3.36(-7)	8.87±3.35(-7)	1.70±1.58(-6)
Ar^{+2}(adopt)	4.88±1.52(-7)	5.91±2.63(-7)	2.84±1.53(-7)	3.86±2.39(-7)	4.27±1.90(-7)	6.25±1.60(-7)	1.41±0.84(-6)
icf(Ar)	2.07±0.28	2.11±0.32	3.02±0.81	2.68±0.54	3.50±0.92	1.59±0.09	1.18±0.05
C^{+}(2325)	1.00±0.16(-6)	7.56±1.81(-7)	8.29±2.71(-7)	5.24±2.48(-7)	4.09±1.56(-7)	1.17±0.26(-6)	1.08±0.40(-5)
C^{+2}(1909)	2.14±0.58(-5)	1.91±0.84(-4)	1.77±0.61(-4)	1.66±0.83(-4)	1.29±0.71(-4)	2.63±1.07(-4)	5.69±9.45(-5)
C^{+2}(1907)	2.14±0.58(-5)	1.90±0.84(-4)	1.76±0.61(-4)	1.66±0.83(-4)	1.29±0.71(-4)	2.63±1.06(-4)	5.69±9.44(-5)
C^{+2}(adopt)	2.14±0.58(-5)	1.90±0.84(-4)	1.76±0.61(-4)	1.66±0.83(-4)	1.29±0.71(-4)	2.63±1.07(-4)	5.69±9.44(-4)
C^{+3}(1549)	2.00±0.65(-5)	1.19±0.63(-4)	2.05±0.83(-4)	2.17±1.30(-4)	1.62±1.07(-4)	1.60±0.78(-4)	3.21±6.54(-3)
N^{+}(6584)	3.80±0.28(-5)	1.91±0.19(-6)	1.66±0.15(-6)	1.95±0.22(-6)	9.01±1.28(-7)	4.84±0.40(-6)	3.60±1.25(-5)
N^{+}(6548)	3.46±0.33(-5)	1.65±0.28(-6)	1.26±0.28(-6)	1.85±0.32(-6)	1.12±0.28(-6)	4.75±0.49(-6)	3.14±1.10(-5)
N^{+}(adopt)	3.72±0.28(-5)	1.85±0.19(-6)	1.58±0.14(-6)	1.93±0.22(-6)	9.67±1.48(-7)	4.82±0.40(-6)	3.49±1.21(-5)
N^{+3}(1485)	6.80±2.28(-5)	4.07±2.26(-5)	7.08±3.00(-5)	7.38±4.61(-5)	5.92±4.08(-5)	4.99±2.56(-5)	2.09±4.54(-4)
N^{+4}(1240)	4.62±1.84(-5)	1.04±0.75(-5)	4.81±2.40(-5)	7.30±5.36(-5)	4.45±3.60(-5)	1.18±0.82(-5)	···
Ne^{+2}(3869)	2.57±0.41(-5)	2.59±0.65(-6)	1.77±0.37(-5)	1.97±0.59(-5)	1.66±0.54(-5)	3.75±0.85(-5)	1.64±1.40(-4)
Ne^{+3}(1602)	6.59±2.27(-5)	···	···	···	···	···	···
Ne^{+4}(1575)	1.04±0.37(-5)	···	···	···	···	···	···
icf(Ne)	2.09±0.35	2.16±0.34	3.19±0.88	2.74±0.57	3.53±0.95	1.61±0.10	1.20±0.07

Table 2.2—Continued

Ionic Abundances[a] , Temperatures and Densities							
Ion	IC2165 Full	IC2165 1	IC2165 2	IC2165 3	IC2165 4	IC2165 5	IC2165 6
S^{+}(6716)	1.04±0.62(-7)	···	···	···	···	···	···
S^{+}(6731)	1.01±0.63(-7)	···	···	···	···	···	···
S^{+}(adopt)	1.02±0.62(-7)	···	···	···	···	···	···
S^{+2}(9069)	···	7.33±2.33(-7)	···	···	···	···	···
S^{+2}(9532)	8.13±0.86(-7)	···	6.25±0.94(-7)	7.8±1.58(-7)	6.14±1.41(-7)	1.18±0.18(-6)	1.85±0.85(-6)
icf(S)	1.97±0.34	1.98±0.35	1.84±0.26	2.26±0.66	4.42±2.94	1.66±0.14	1.22±0.05
[O III] T_e(K)	13600±600	13900±1000	14300±800	13700±1100	14000±1300	13300±900	9300±1900
[S II] $N_e(cm^{-3})$	1500^{+3800}_{-1500}	···	···	···	···	···	···
C III] $N_e(cm^{-3})$	7700±1200	6600±1800	14200±2300	5400±1800	6800±1600	4500±1200	10800±3400

Ion	IC3568 Full	IC3568 1	IC3568 2	IC3568 3	NGC2440 Full	NGC2440 1	NGC2440 2
He^{+}(5876)	9.39±1.36(-2)	9.79±2.38(-2)	8.80±2.59(-2)	1.00±0.74(-1)	5.13±0.77(-2)	7.05±2.32(-2)	1.02±0.08(-1)
He^{+2}(4686)	1.49±1.05(-3)	2.21±1.70(-3)	1.09±1.17(-3)	···	7.49±0.27(-2)	5.08±0.22(-2)	···
icf(He)	1.00	1.00	1.00	1.00	1.00	1.00	1.00
O^{0}(6300)	···	···	···	···	1.63±0.32(-5)	3.08±0.77(-5)	5.04±3.96(-6)
O^{0}(6363)	···	···	···	···	1.32±0.31(-5)	2.40±0.92(-5)	···
O^{0}(adopt)	···	···	···	···	1.56±0.31(-5)	2.94±0.74(-5)	···
O^{+}(3727)	7.16±4.15(-6)	1.05±0.55(-5)	4.55±2.06(-6)	···	1.93±0.71(-5)	4.59±3.46(-5)	1.25±1.49(-6)
O^{+}(7325)	···	···	···	···	3.63±1.36(-5)	8.94±5.86(-5)	···
O^{+}(adopt)	···	···	···	···	2.25±0.63(-5)	5.29±2.32(-5)	···
O^{+2}(5007)	4.02±1.27(-4)	3.01±0.68(-4)	4.24±1.76(-4)	7.67±7.14 (-4)	1.53±0.19(-4)	1.74±0.18(-4)	6.33±4.15(-5)
O^{+2}(4959)	3.58±1.13(-4)	2.69±0.61(-4)	3.77±1.57(-4)	6.56±6.10 (-4)	1.49±0.18(-4)	1.73±0.18(-4)	5.62±3.69(-5)
O^{+2}(4363)	4.02±1.27(-4)	3.01±0.68(-4)	4.24±1.76(-4)	7.67±7.14 (-4)	1.50±0.18(-4)	1.75±0.19(-4)	6.33±4.15(-5)
O^{+2}(adopt)	3.92±1.24(-4)	2.94±0.66(-4)	4.13±1.72(-4)	7.42±6.91 (-4)	1.52±0.18(-4)	1.74±0.18(-4)	6.17±4.05(-5)
icf(O)	1.02±0.01	1.02±0.02	1.01±0.01	1.00	2.46±0.22	1.72±0.24	1.00
Ar^{+2}(7135)	6.79±2.09(-7)	5.61±2.45(-7)	6.47±2.79(-7)	1.29±1.23(-6)	7.79±0.78(-7)	9.13±0.87(-7)	3.50±1.84(-7)
Ar^{+2}(7751)	···	···	···	···	9.24±1.28(-7)	7.81±2.20(-7)	7.08±3.82(-7)
Ar^{+2}(adopt)	···	···	···	···	8.13±0.82(-7)	8.89±0.87(-7)	4.71±2.45(-7)
Ar^{+3}(4740)	···	···	···	···	7.05±1.01(-7)	1.09±0.14(-6)	3.99±2.92(-7)

Table 2.2—Continued

Ionic Abundances[a] , Temperatures and Densities							
Ion	IC3568 Full	IC3568 1	IC3568 2	IC3568 3	NGC2440 Full	NGC2440 1	NGC2440 2
Ar^{+4}(7005)	···	···	···	···	3.30±0.66(-7)	1.49±1.30(-7)	5.44±3.48(-7)
icf(Ar)	1.87	1.87	1.87	1.87	2.60±0.24	1.99±0.32	1.02±0.03
C^{+}(2325)	2.02±0.85(-7)	2.6±3.76(-7)	1.40±2.65(-7)	···	2.04±0.27(-6)	2.01±0.31(-6)	9.33±3.44(-7)
C^{+2}(1909)	3.49±2.50(-4)	1.51±0.77(-4)	4.41±4.19(-4)	2.00±4.38 (-3)	1.60±0.40(-4)	1.17±0.25(-4)	8.72±11.30(-5)
C^{+2}(1907)	3.49±2.50(-4)	1.51±0.77(-4)	4.40±4.19(-4)	1.99±4.38 (-3)	1.60±0.40(-4)	1.17±0.25(-4)	8.71±11.30(-5)
C^{+2}(adopt)	3.49±2.50(-4)	1.51±0.77(-4)	4.40±4.19(-4)	1.99±4.38 (-3)	1.60±0.40(-4)	1.17±0.25(-4)	8.72±11.30(-5)
C^{+3}(1549)	1.17±1.04(-4)	5.17±3.22(-5)	1.34±1.58(-4)	7.26±19.60 (-3)	5.75±1.72(-4)	3.47±0.87(-5)	5.99±9.43(-5)
N^{+}(6584)	···	···	···	···	6.52±0.87(-5)	1.23±0.24(-4)	6.60±3.15(-6)
N^{+}(6548)	···	···	···	···	6.22±0.83(-5)	1.17±0.23(-4)	6.44±3.07(-6)
N^{+}(5755)	···	···	···	···	6.52±0.87(-5)	1.23±0.24(-4)	6.6±3.15(-6)
N^{+}(adopt)	···	···	···	···	6.45±0.86(-5)	1.22±0.23(-4)	6.56±3.13(-6)
N^{+2}(1751)	···	···	···	···	1.32±0.36(-4)	9.19±2.67(-5)	6.96±9.87(-5)
N^{+3}(1485)	···	···	···	···	2.06±0.64(-4)	1.12±0.29(-4)	1.56±2.54(-4)
N^{+4}(1240)	···	···	···	···	5.95±2.17(-5)	1.59±0.51(-5)	5.67±10.80(-5)
Ne^{+2}(3869)	7.89±2.95(-5)	5.65±1.48(-5)	8.85±4.35(-5)	1.25±1.43(-4)	2.54±0.36(-5)	3.26±0.40(-5)	6.12±4.75(-6)
Ne^{+3}(1602)	···	···	···	···	4.71±1.55(-5)	2.85±1.51(-5)	2.83±4.36(-5)
Ne^{+4}(1575)	···	···	···	···	1.07±0.32(-5)	···	1.23±1.18(-5)
icf(Ne)	1.03±0.02	1.06±0.03	1.02±0.02	1.00	2.77±0.33	2.17±0.61	1.02±0.03
S^{+}(6716)	···	···	···	···	2.11±0.76(-7)	2.89±2.06(-7)	···
S^{+}(6731)	···	···	···	···	2.07±0.74(-7)	2.80±2.07(-7)	···
S^{+}(adopt)	···	···	···	···	2.08±0.75(-7)	2.84±2.12(-7)	···
S^{+2}(9069)	···	···	···	···	···	···	3.25±2.04(-7)
S^{+2}(9532)	···	···	···	···	7.69±0.73(-7)	7.70±0.88(-7)	···
icf(S)	···	···	···	···	1.56±0.12	1.28±0.11	2.05±1.06
[O III] T_e(K)	10100±900	11000±800	9800±1200	8800±2300	14400±600	14400±500	15700±3800
[S II] $N_e(cm^{-3})$	···	···	···	···	1700±1700	1500^{+3700}_{-1500}	···
C III] $N_e(cm^{-3})$	5300±3100	7000±6500	2600±3200	6800±10400	7100±500	100^{+1300}_{-100}	12600±2200

Table 2.2—Continued

Ionic Abundances[a] , Temperatures and Densities							
Ion	NGC2440 3	NGC3242 Full	NGC3242 1	NGC3242 2	NGC3242 3	NGC3242 4	NGC3242 5
He^{+}(5876)	4.39±0.87(-2)	6.25±0.45(-2)	0.106±0.026	8.10±1.56(-2)	5.99±2.27(-2)	6.61±2.55(-2)	5.15±1.60(-2)
He^{+2}(4686)	8.03±0.35(-2)	4.40±0.07(-2)	1.73±0.36(-2)	3.82±0.28(-2)	5.16±0.23(-2)	3.40±0.37(-2)	4.43±0.30(-2)
icf(He)	1.00	1.00	1.00	1.00	1.00	1.00	1.00
O^{0}(6300)	1.14±0.29(-5)	···	···	···	···	···	···
O^{0}(6363)	1.12±0.34(-5)	···	···	···	···	···	···
O^{0}(adopt)	1.14±0.29(-5)	···	···	···	···	···	···
O^{+}(3727)	1.77±1.21(-5)	2.23±0.90(-6)	···	···	···	···	···
O^{+}(7325)	1.88±0.44(-5)	···	···	···	···	···	···
O^{+}(adopt)	1.80±0.95(-5)	···	···	···	···	···	···
O^{+2}(5007)	1.44±0.15(-4)	2.58±0.21(-4)	3.17±1.21(-4)	2.67±0.27(-4)	2.04±0.40(-4)	2.48±0.53(-4)	2.67±0.74(-4)
O^{+2}(4959)	1.46±0.15(-4)	2.59±0.21(-4)	3.18±1.22(-4)	2.68±0.27(-4)	2.05±0.40(-4)	2.48±0.54(-4)	2.67±0.74(-4)
O^{+2}(4363)	1.43±0.16(-4)	2.58±0.21(-4)	3.17±1.21(-4)	2.67±0.27(-4)	2.04±0.40(-4)	2.48±0.53(-4)	2.67±0.74(-4)
O^{+2}(adopt)	1.45±0.15(-4)	2.59±0.21(-4)	3.17±1.21(-4)	2.67±0.27(-4)	2.04±0.40(-4)	2.48±0.53(-4)	2.67±0.74(-4)
icf(O)	2.83±0.37	1.70±0.05	1.16±0.05	1.47±0.10	1.86±0.33	1.52±0.2	1.86±0.27
Ar^{+2}(7135)	7.54±0.67(-7)	···	···	···	···	···	···
Ar^{+2}(7751)	7.95±2.10(-7)	···	···	···	···	···	···
Ar^{+2}(adopt)	7.63±0.79(-7)	···	···	···	···	···	···
Ar^{+3}(4740)	5.57±1.67(-7)	···	···	···	···	···	···
Ar^{+4}(7005)	3.10±0.64(-7)	···	···	···	···	···	···
icf(Ar)	2.94±0.40	···	···	···	···	···	···
C^{+}(2325)	2.64±0.34(-6)	3.72±0.28(-7)	3.20±1.09(-7)	3.43±0.66(-7)	3.50±0.70(-7)	4.26±1.19(-7)	3.46±0.72(-7)
C^{+2}(1909)	1.63±0.36(-4)	2.01±0.35(-4)	2.35±1.96(-4)	1.87±0.42(-4)	1.51±0.62(-4)	1.73±0.80(-4)	2.18±1.30(-4)
C^{+2}(1907)	1.63±0.36(-4)	2.01±0.35(-4)	2.35±1.96(-4)	1.87±0.42(-4)	1.51±0.62(-4)	1.73±0.80(-4)	2.17±1.30(-4)
C^{+2}(adopt)	1.63±0.36(-4)	2.01±0.35(-4)	2.35±1.96(-4)	1.87±0.42(-4)	1.51±0.62(-4)	1.73±0.80(-4)	2.67±0.74(-4)
C^{+3}(1549)	3.40±0.87(-4)	3.12±0.67(-5)	3.08±3.14(-5)	3.36±0.90(-5)	2.54±1.27(-5)	2.09±1.17(-5)	2.88±2.10(-5)
N^{+}(6584)	5.12±1.01(-5)	···	···	···	···	···	···
N^{+}(6548)	4.93±0.97(-5)	···	···	···	···	···	···
N^{+}(5755)	5.12±1.01(-5)	···	···	···	···	···	···
N^{+}(adopt)	5.07±1.00(-5)	···	···	···	···	···	···

Table 2.2—Continued

Ionic Abundances[a] , Temperatures and Densities							
Ion	NGC2440 3	NGC3242 Full	NGC3242 1	NGC3242 2	NGC3242 3	NGC3242 4	NGC3242 5
N^{+2}(1751)	1.38±0.33(-4)	···	···	···	···	···	···
N^{+3}(1485)	1.68±0.45(-4)	···	···	···	···	···	···
N^{+4}(1240)	3.79±1.19(-4)	···	···	···	···	···	···
Ne^{+2}(3869)	2.23±0.28(-5)	5.60±0.53(-5)	6.89±3.06(-5)	5.65±0.75(-5)	4.50±1.02(-5)	5.36±1.34(-5)	5.74±1.85(-5)
Ne^{+3}(1602)	4.40±1.58(-5)	···	···	···	···	···	···
Ne^{+4}(1575)	1.12±0.41(-5)	3.52±0.45(-5)	2.66±1.61(-5)	4.23±0.99(-5)	2.40±0.75(-5)	2.63±1.20(-5)	3.46±1.74(-5)
icf(Ne)	3.18±0.57	1.72±0.05	1.16±0.05	1.47±0.10	1.86±0.33	1.52±0.20	1.86±0.27
S^{+}(6716)	3.21±2.04(-7)	···	···	···	···	···	···
S^{+}(6731)	3.17±2.03(-7)	···	···	···	···	···	···
S^{+}(adopt)	3.18±2.03(-7)	···	···	···	···	···	···
S^{+2}(9532)	7.34±0.70(-7)	···	···	···	···	···	···
icf(S)	1.63±0.26	···	···	···	···	···	···
[O III] T_e(K)	15100±600	11700±300	11400±1400	11900±400	12200±800	12200±800	11700±1000
[S II] $N_e(cm^{-3})$	4700^{+4900}_{-4700}	···	···	···	···	···	···
C III] $N_e(cm^{-3})$	7800±500	4500±300	1800±1700	7000±900	3300±1000	3700±1400	4400±1300

Ion	NGC3242 6	NGC3242 7	NGC3242 8	NGC3242 9	NGC5315 Full	NGC5315 1	···
He^{+}(5876)	4.84±1.68(-2)	4.75±1.31(-2)	3.60±0.96(-2)	7.26±2.62(-2)	1.19±0.02(-1)	7.95±1.07(-2)	···
He^{+2}(4686)	4.42±0.39(-2)	4.87±0.40(-2)	6.34±0.22(-2)	4.36±0.44(-2)	···	···	···
icf(He)	1.00	1.00	1.00	1.00	1.00	1.00	···
O^{0}(6300)	···	···	···	···	2.74±0.50(-6)	4.14±1.31(-6)	···
O^{0}(6363)	···	···	···	···	4.63±0.95(-6)	9.43±4.97(-6)	···
O^{0}(adopt)	···	···	···	···	3.41±0.64(-6)	6.39±2.90(-6)	···
O^{+}(3727)	···	···	···	···	1.03±0.46(-5)	2.45±0.91(-5)	···
O^{+}(7325)	···	···	···	···	1.31±0.20(-5)	1.69±0.44(-5)	···
O^{+}(adopt)	···	···	···	···	1.17±0.32(-5)	2.22±0.71(-5)	···
O^{+2}(5007)	2.54±0.76(-4)	2.45±0.68(-4)	1.96±0.35(-4)	2.55±0.40(-4)	4.95±0.32(-4)	3.87±1.42(-4)	···
O^{+2}(4959)	2.55±0.76(-4)	2.46±0.68(-4)	1.96±0.35(-4)	2.55±0.40(-4)	4.82±0.31(-4)	2.97±1.09(-4)	···
O^{+2}(4363)	2.54±0.76(-4)	2.45±0.68(-4)	1.96±0.35(-4)	2.55±0.40(-4)	4.04±0.30(-4)	3.01±1.13(-4)	···

Table 2.2—Continued

Ionic Abundances[a] , Temperatures and Densities						
Ion	NGC3242 6	NGC3242 7	NGC3242 8	NGC3242 9	NGC5315 Full	NGC5315 1
O^{+2}(adopt)	2.55±0.76(-4)	2.45±0.68(-4)	1.96±0.35(-4)	2.55±0.40(-4)	4.92±0.31(-4)	3.69±1.35(-4)
icf(O)	1.91±0.33	2.02±0.29	2.76±0.47	1.60±0.23	1.00	1.00
Ar^{+2}(7135)	···	···	···	···	3.70±0.16(-6)	2.88±0.74(-6)
Ar^{+2}(7751)	···	···	···	···	3.67±0.20(-6)	3.47±1.10(-6)
Ar^{+2}(adopt)	···	···	···	···	3.69±0.16(-6)	3.03±0.80(-6)
icf(Ar)	···	···	···	···	1.02±0.01	1.06±0.03
C^{+}(2325)	4.51±1.05(-7)	3.78±1.34(-7)	3.76±1.20(-7)	3.13±1.69(-7)	4.65±0.36(-7)	8.45±4.01(-7)
C^{+2}(1909)	1.99±1.26(-4)	2.01±1.19(-4)	1.40±0.53(-4)	1.69±0.59(-4)	2.22±0.34(-4)	2.35±2.01(-4)
C^{+2}(1907)	1.99±1.26(-4)	2.01±1.19(-4)	1.40±0.53(-4)	1.69±0.59(-4)	2.22±0.34(-4)	2.34±2.00(-4)
C^{+2}(adopt)	1.99±1.26(-4)	2.01±1.19(-4)	1.40±0.53(-4)	1.69±0.59(-4)	2.22±0.34(-4)	2.35±2.01(-4)
C^{+3}(1549)	2.49±1.93(-5)	2.06±1.49(-5)	1.88±0.86(-5)	4.57±1.90(-5)	2.98±0.56(-4)	5.51±5.71(-4)
N^{+}(6584)	···	···	···	···	1.82±0.25(-5)	3.14±0.46(-5)
N^{+}(6548)	···	···	···	···	1.85±0.26(-5)	3.35±0.49(-5)
N^{+}(5755)	···	···	···	···	1.82±0.25(-5)	3.14±0.46(-5)
N^{+}(adopt)	···	···	···	···	1.83±0.25(-5)	3.19±0.47(-5)
Ne^{+2}(3869)	5.81±2.00(-5)	5.30±1.70(-5)	4.53±0.93(-5)	5.52±1.04(-5)	1.27±0.10(-4)	7.04±3.07(-5)
Ne^{+4}(1575)	3.60±1.59(-5)	4.64±1.92(-5)	2.83±0.86(-5)	2.66±1.20(-5)	···	···
icf(Ne)	1.91±0.33	2.02±0.29	2.76±0.47	1.60±0.23	1.02±0.01	1.06±0.03
S^{+}(6716)	···	···	···	···	4.85±1.81(-7)	9.74±2.96(-7)
S^{+}(6731)	···	···	···	···	4.88±1.78(-7)	9.86±2.92(-7)
S^{+}(adopt)	···	···	···	···	4.87±1.79(-7)	9.82±2.94(-7)
S^{+2}(9532)	···	···	···	···	9.76±0.38(-6)	7.19±1.61(-6)
icf(S)	···	···	···	···	2.02±0.35	1.44±0.14
[O III] T_e(K)	11900±1100	11800±1000	12300±700	12000±600	8900±200	9600±1000
[S II] $N_e(cm^{-3})$	···	···	···	···	10800±4700	6500±2800
C III] $N_e(cm^{-3})$	4500±1200	9000±1200	4000±1300	1500^{+2000}_{-1500}	63600±7900	74000±34900

Table 2.2—Continued

Ionic Abundances[a] , Temperatures and Densities						
Ion	NGC5315 2	NGC5315 3	NGC5315 4	NGC5882 Full	NGC5882 1	NGC5882 2
He^{+}(5876)	1.22±0.13(-1)	1.21±0.02(-1)	1.11±0.07(-1)	1.12±0.07(-1)	1.14±0.14(-1)	1.10±0.09(-1)
He^{+2}(4686)	···	···	···	3.22±0.77(-3)	4.78±1.04(-3)	3.80±0.69(-3)
icf(He)	1.00	1.00	1.00	1.00	1.00	1.00
O^{0}(6300)	1.55±0.08(-6)	4.41±1.25(-6)	1.51±0.45(-5)	···	···	···
O^{0}(6363)	2.23±0.17(-6)	6.97±2.10(-6)	2.77±1.16(-5)	···	···	···
O^{0}(adopt)	1.76±0.10(-6)	5.28±1.50(-6)	1.98±0.68(-5)	···	···	···
O^{+}(3727)	6.29±0.35(-6)	2.43±1.59(-5)	6.77±4.72(-5)	5.13±2.14(-6)	8.61±1.81(-6)	3.13±5.00(-6)
O^{+}(7325)	7.20±0.47(-6)	2.49±0.90(-5)	6.71±1.73(-5)	1.55±1.25(-5)	2.92±1.22(-5)	5.38±5.33(-6)
O^{+}(adopt)	6.86±0.41(-6)	2.46±1.22(-5)	6.75±3.61(-5)	7.19±2.05(-6)	1.22±0.34(-5)	3.77±2.16(-6)
O^{+2}(5007)	5.07±0.13(-4)	5.79±0.82(-4)	8.36±5.19(-4)	7.62±1.50(-4)	6.79±2.33(-4)	7.38±1.81(-4)
O^{+2}(4959)	5.14±0.14(-4)	5.39±0.76(-4)	6.90±4.29(-4)	6.37±1.25(-4)	5.70±1.95(-4)	6.27±1.54(-4)
O^{+2}(4363)	4.31±0.12(-4)	4.89±0.77(-4)	7.12±4.49(-4)	6.81±1.36(-4)	6.79±2.33(-4)	7.38±1.82(-4)
O^{+2}(adopt)	5.09±0.13(-4)	5.69±0.80(-4)	8.04±5.00(-4)	7.35±1.45(-4)	6.56±2.24(-4)	7.14±1.75(-4)
icf(O)	1.00	1.00	1.00	1.03±0.01	1.04±0.01	1.03±0.01
Ar^{+2}(7135)	3.80±0.06(-6)	4.01±0.39(-6)	4.62±2.01(-6)	1.98±0.29(-6)	2.02±0.50(-6)	1.84±0.30(-6)
Ar^{+2}(7751)	3.61±0.10(-6)	4.00±0.40(-6)	4.54±2.54(-6)	1.98±0.44(-6)	1.86±0.63(-6)	1.95±0.40(-6)
Ar^{+2}(adopt)	3.76±0.07(-6)	4.01±0.39(-6)	4.60±2.03(-6)	1.98±0.29(-6)	1.99±0.50(-6)	1.87±0.31(-6)
Ar^{+3}(4740)	···	···	···	7.56±3.32(-7)	6.72±3.39(-7)	1.19±0.51(-6)
icf(Ar)	1.01±0.01	1.04±0.02	1.08±0.06	1.04±0.01	1.06±0.01	1.04±0.01
C^{+}(2325)	3.62±0.37(-7)	4.89±0.61(-7)	1.51±0.57(-6)	6.09±3.53(-8)	6.87±5.03(-8)	6.87±3.83(-8)
C^{+2}(1909)	1.94±0.12(-4)	3.15±1.07(-4)	1.71±2.57(-3)	2.23±1.05(-4)	1.26±1.05(-4)	2.52±1.50(-4)
C^{+2}(1907)	1.93±0.12(-4)	3.15±1.07(-4)	1.71±2.57(-3)	2.23±1.05(-4)	···	···
C^{+2}(adopt)	1.94±0.12(-4)	3.15±1.07(-4)	1.71±2.57(-3)	2.23±1.05(-4)	···	···
C^{+3}(1549)	1.64±0.15(-4)	5.41±2.23(-4)	4.93±9.13(-3)	4.91±3.03(-5)	4.22±4.40(-5)	6.19±4.49(-5)
N^{+}(6584)	1.05±0.03(-5)	2.74±0.67(-5)	7.33±1.70(-5)	2.27±0.14(-6)	3.86±0.29(-6)	1.09±0.27(-6)
N^{+}(6548)	1.10±0.03(-5)	2.74±0.67(-5)	7.32±1.70(-5)	1.99±0.23(-6)	3.42±0.33(-6)	7.93±2.21(-7)
N^{+}(5755)	1.05±0.03(-5)	2.74±0.67(-5)	7.33±1.70(-5)	···	···	···
N^{+}(adopt)	1.07±0.03(-5)	2.74±0.67(-5)	7.33±1.70(-5)	2.21±0.13(-6)	3.76±0.28(-6)	1.04±0.25(-6)
Ne^{+2}(3869)	1.41±0.04(-4)	1.33±0.22(-4)	2.16±1.64(-4)	1.72±0.41(-4)	1.51±0.62(-4)	1.87±0.53(-4)

Table 2.2—Continued

Ionic Abundances[a] , Temperatures and Densities						
Ion	NGC5315 2	NGC5315 3	NGC5315 4	NGC5882 Full	NGC5882 1	NGC5882 2
Ne^{+4}(1575)	···	···	···	4.91±2.61(-5)	···	···
icf(Ne)	1.01±0.01	1.04±0.03	1.08±0.07	1.04±0.01	1.06±0.01	1.04±0.01
S^{+}(6716)	2.39±0.21(-7)	8.87±4.54(-7)	2.14±1.25(-6)	7.98±3.84(-8)	1.28±0.12(-7)	6.48±10.40(-8)
S^{+}(6731)	2.44±0.11(-7)	8.86±4.50(-7)	2.16±1.24(-6)	8.11±3.80(-8)	1.30±0.13(-7)	6.51±10.50(-8)
S^{+}(adopt)	2.43±0.10(-7)	8.86±4.52(-7)	2.15±1.24(-6)	8.06±3.84(-8)	1.29±0.12(-7)	6.50±10.40(-8)
S^{+2}(9069)	···	1.02±1.87(-5)	9.23±3.34(-6)	···	···	···
S^{+2}(9532)	1.03±0.02(-5)	···	···	3.13±0.37(-6)	3.53±0.73(-6)	2.61±0.35(-6)
icf(S)	2.58±0.08	1.60±0.27	1.38±0.22	3.72±1.14	2.56±0.47	5.34±6.86
[O III] T_e(K)	8900±100	8500±300	7500±1100	8500±400	8700±800	8500±500
[S II] $N_e(cm^{-3})$	···	17600±8300	7600±3300	1400^{+2800}_{-1400}	900±300	6700^{+20500}_{-6700}
C III] $N_e(cm^{-3})$	62900±6700	61200±14000	45300±26700	27700±9200	···	···

Ion	NGC5882 3	NGC7662 Full	NGC7662 1	NGC7662 2	NGC7662 3	···
He^{+}(5876)	1.08±0.12(-1)	5.11±0.75(-2)	7.05±2.71(-2)	4.58±2.22(-2)	3.96±1.50(-2)	···
He^{+2}(4686)	···	4.90±0.09(-2)	4.55±0.21(-2)	5.90±0.14(-2)	5.47±0.20(-2)	···
icf(He)	1.00	1.00	1.00	1.00	1.00	···
O^{+}(3727)	5.51±5.21(-6)	2.80±0.92(-6)	5.15±2.38(-6)	3.33±2.02(-6)	2.07±1.15(-6)	···
O^{+}(7325)	1.33±1.47(-5)	···	···	···	···	···
O^{+}(adopt)	6.99±5.53(-6)	···	···	···	···	···
O^{+2}(5007)	8.95±7.35(-4)	2.30±0.15(-4)	3.18±0.51(-4)	2.40±0.29(-4)	2.32±0.19(-4)	···
O^{+2}(4959)	7.39±6.07(-4)	2.09±0.13(-4)	2.88±0.46(-4)	2.23±0.27(-4)	1.98±0.16(-4)	···
O^{+2}(4363)	8.95±7.35(-4)	2.30±0.15(-4)	3.18±0.51(-4)	2.40±0.29(-4)	2.32±0.19(-4)	···
O^{+2}(adopt)	8.62±7.07(-4)	2.25±0.14(-4)	3.11±0.50(-4)	2.36±0.28(-4)	2.25±0.18(-4)	···
icf(O)	1.00	1.96±0.14	1.65±0.25	2.29±0.63	2.38±0.53	···
Ar^{+2}(7135)	2.35±1.36(-6)	4.26±0.54(-7)	5.38±0.99(-7)	5.12±0.77(-7)	4.96±0.53(-7)	···
Ar^{+2}(7751)	2.39±1.90(-6)	···	···	···	···	···
Ar^{+2}(adopt)	2.35±1.39(-6)	···	···	···	···	···
Ar^{+3}(4740)	1.01±0.97(-6)	4.40±0.72(-7)	3.31±2.30(-7)	3.32±1.20(-7)	3.67±1.96(-7)	···
icf(Ar)	1.01±0.01	1.97±0.14	1.66±0.25	2.30±0.63	2.39±0.53	···

Table 2.2—Continued

Ionic Abundances[a] , Temperatures and Densities					
Ion	NGC5882 3	NGC7662 Full	NGC7662 1	NGC7662 2	NGC7662 3
C^{+}(2325)	3.09±3.34(-8)	5.37±0.43(-7)	6.77±1.50(-7)	5.20±0.99(-7)	4.65±1.24(-7)
C^{+2}(1909)	4.40±8.61(-4)	2.15±0.29(-4)	3.03±1.03(-4)	2.23±0.56(-4)	2.32±0.43(-4)
C^{+2}(1907)	···	2.15±0.29(-4)	3.03±1.03(-4)	2.22±0.56(-4)	2.32±0.43(-4)
C^{+2}(adopt)	···	2.15±0.29(-4)	3.03±1.03(-4)	2.23±0.56(-4)	2.32±0.43(-4)
C^{+3}(1549)	2.47±6.53(-5)	1.93±0.31(-4)	1.85±0.76(-4)	1.63±0.50(-4)	2.13±0.46(-4)
N^{+}(6584)	2.01±0.78(-6)	5.21±0.72(-7)	7.00±2.14(-7)	5.28±1.61(-7)	5.51±0.86(-7)
N^{+}(6548)	2.00±0.82(-6)	···	···	···	···
N^{+}(adopt)	2.01±0.78(-6)	···	···	···	···
N^{+2}(1751)	···	2.54±0.70(-5)	7.63±4.55(-5)	2.32±1.64(-5)	3.42±1.38(-5)
N^{+3}(1485)	···	4.69±0.81(-5)	4.21±1.92(-5)	4.14±1.36(-5)	5.69±1.38(-5)
N^{+4}(1240)	···	4.45±1.00(-6)	···	···	···
Ne^{+2}(3869)	2.05±2.03(-4)	4.53±0.34(-5)	6.84±1.26(-5)	4.64±0.66(-5)	4.32±0.45(-5)
Ne^{+3}(1602)	···	4.78±1.23(-5)	5.66±4.89(-5)	2.86±1.91(-5)	5.38±2.52(-5)
Ne^{+4}(1575)	···	1.38±2.22(-5)	1.54±2.78(-5)	1.44±1.69(-5)	1.69±1.13(-5)
icf(Ne)	1.01±0.01	1.98±0.14	1.67±0.25	2.32±0.63	2.40±0.53
S^{+}(6716)	7.41±4.00(-8)	···	···	···	···
S^{+}(6731)	7.53±4.07(-8)	···	···	···	···
S^{+}(adopt)	7.48±4.05(-8)	···	···	···	···
S^{+2}(9069)	···	···	9.79±4.44(-7)	···	9.46±2.11(-7)
S^{+2}(9532)	3.32±1.62(-6)	6.63±0.69(-7)	···	1.04±0.19(-6)	···
icf(S)	3.87±2.21	3.91±0.92	2.90±0.83	3.99±1.92	5.80±3.06
[O III] T_e(K)	8100±1700	12700±300	12300±600	12600±500	12400±300
[S II] $N_e(cm^{-3})$	1800^{+2500}_{-1800}	···	···	···	···
C III] $N_e(cm^{-3})$	···	3200±1200	4000±1000	5700±700	4500±500

Ion	NGC7662 4	NGC7662 5	NGC7662 6	NGC7662 7	NGC7662 8
He^{+}(5876)	3.09±0.96(-2)	4.03±1.02(-2)	5.37±0.63(-2)	8.23±1.91(-2)	5.32±2.14(-2)
He^{+2}(4686)	6.30±0.14(-2)	6.53±0.15(-2)	5.20±0.11(-2)	3.49±0.13(-2)	4.36±0.28(-2)
icf(He)	1.00	1.00	1.00	1.00	1.00

Table 2.2—Continued

Ionic Abundances[a] , Temperatures and Densities					
Ion	NGC7662 4	NGC7662 5	NGC7662 6	NGC7662 7	NGC7662 8
O^{+}(3727)	2.20±1.53(-6)	2.83±1.67(-6)	3.31±1.39(-6)	2.16±0.68(-6)	2.75±1.40(-6)
O^{+2}(5007)	1.73±0.07(-4)	1.79±0.36(-4)	2.42±0.23(-4)	2.59±0.24(-4)	2.58±0.58(-4)
O^{+2}(4959)	1.57±0.07(-4)	1.69±0.34(-4)	2.19±0.20(-4)	2.22±0.21(-4)	2.53±0.57(-4)
O^{+2}(4363)	1.73±0.07(-4)	1.79±0.36(-4)	2.42±0.23(-4)	2.59±0.24(-4)	2.58±0.58(-4)
O^{+2}(adopt)	1.69±0.07(-4)	1.77±0.35(-4)	2.37±0.22(-4)	2.51±0.24(-4)	2.57±0.58(-4)
icf(O)	3.04±0.63	2.62±0.41	1.97±0.12	1.42±0.10	1.82±0.33
Ar^{+2}(7135)	3.65±0.47(-7)	3.90±0.92(-7)	3.99±0.73(-7)	4.19±0.54(-7)	2.82±2.18(-7)
Ar^{+3}(4740)	4.80±0.88(-7)	6.25±1.81(-7)	3.39±0.84(-7)	5.35±1.28(-7)	3.76±1.59(-7)
icf(Ar)	3.05±0.63	2.64±0.41	1.98±0.12	1.43±0.10	1.83±0.33
C^{+}(2325)	5.67±0.96(-7)	5.32±1.11(-7)	6.44±0.96(-7)	4.53±0.97(-7)	5.29±2.19(-7)
C^{+2}(1909)	1.67±0.17(-4)	1.78±0.72(-4)	2.28±0.44(-4)	2.15±0.44(-4)	2.63±1.24(-4)
C^{+2}(1907)	1.67±0.17(-4)	1.78±0.72(-4)	2.28±0.44(-4)	2.15±0.44(-4)	2.63±1.23(-4)
C^{+2}(adopt)	1.67±0.17(-4)	1.78±0.72(-4)	2.28±0.44(-4)	2.15±0.44(-4)	2.63±1.23(-4)
C^{+3}(1549)	1.35±0.16(-4)	1.52±0.75(-4)	1.89±0.44(-4)	2.43±0.59(-4)	3.99±2.28(-4)
N^{+}(6584)	5.32±0.47(-7)	5.14±0.96(-7)	5.95±1.11(-7)	5.77±1.01(-7)	4.34±0.58(-7)
N^{+2}(1751)	1.69±0.93(-5)	2.32±1.22(-5)	2.10±1.03(-5)	2.27±1.40(-5)	2.46±3.15(-5)
N^{+3}(1485)	3.72±0.52(-5)	4.63±2.42(-5)	4.70±1.23(-5)	4.42±1.19(-5)	6.57±4.02(-5)
Ne^{+2}(3869)	3.64±0.20(-5)	3.70±0.84(-5)	4.26±0.46(-5)	5.03±0.56(-5)	5.52±1.43(-5)
Ne^{+3}(1602)	5.97±2.58(-5)	6.22±3.72(-5)	3.60±2.47(-5)	2.98±2.16(-5)	3.80±2.40(-5)
Ne^{+4}(1575)	6.53±7.55(-6)	1.27±0.78(-5)	1.86±1.12(-5)	1.37±1.43(-5)	2.34±4.19(-5)
icf(Ne)	3.08±0.64	2.66±0.42	2.00±0.12	1.44±0.10	1.84±0.34
S^{+2}(9069)	7.13±1.12(-7)	···	···	···	···
S^{+2}(9532)	···	6.20±1.21(-7)	5.92±0.87(-7)	5.47±0.97(-7)	4.57±3.71(-7)
icf(S)	5.34±3.25	4.03±1.80	3.61±1.05	4.04±0.95	4.12±1.68
[O III] T_e(K)	13400±200	13200±900	12900±400	12400±400	12800±900
C III] $N_e(cm^{-3})$	1600±500	2400±500	3900±500	2200±900	4700±1600

[a]Abundances relative to H^{+}; n.nn±n.nn(-k) == (n.nn±n.nn) x 10^{-k}

The final abundances for each of the seven elements measured in each region are presented in Table 2.3. The abundances relative to hydrogen or oxygen are given in columns 2-7, while the solar values from Asplund et al. [4] are provided in column 8.

Table 2.3. Total Elemental Abundances

Total Elemental Abundances								
Parameter	IC2165 Full	IC2165 1	IC2165 2	IC2165 3	IC2165 4	IC2165 5	IC2165 6	Solar[a]
He/H (10^{-2})	$11.30^{+1.65}_{-1.65}$	$10.60^{+1.56}_{-1.56}$	$11.40^{+1.67}_{-1.67}$	$10.40^{+1.38}_{-1.38}$	$10.30^{+1.21}_{-1.21}$	$10.40^{+1.13}_{-1.13}$	$10.00^{+2.78}_{-2.78}$	8.51
C/H (10^{-4})	$4.14^{+0.87}_{-0.87}$	$3.09^{+1.05}_{-1.05}$	$3.81^{+1.03}_{-1.03}$	$3.83^{+1.54}_{-1.54}$	$2.91^{+1.28}_{-1.28}$	$4.23^{+1.32}_{-1.32}$	$89.00^{+114.84}_{-89.00}$	2.69
C/O	$1.221^{+0.343}_{-0.343}$	$0.842^{+0.348}_{-0.348}$	$1.117^{+0.453}_{-0.453}$	$1.052^{+0.519}_{-0.519}$	$0.735^{+0.409}_{-0.409}$	$1.223^{+0.443}_{-0.443}$	$10.253^{+14.954}_{-10.253}$	0.550
N/H (10^{-4})	$1.18^{+0.29}_{-0.29}$	$0.53^{+0.24}_{-0.24}$	$1.21^{+0.38}_{-0.38}$	$1.49^{+0.71}_{-0.71}$	$1.05^{+0.54}_{-0.54}$	$0.67^{+0.27}_{-0.27}$	$2.44^{+4.54}_{-2.44}$	0.68
N/O	$0.348^{+0.108}_{-0.108}$	$0.144^{+0.073}_{-0.073}$	$0.353^{+0.155}_{-0.155}$	$0.409^{+0.227}_{-0.227}$	$0.264^{+0.164}_{-0.164}$	$0.192^{+0.085}_{-0.085}$	$0.281^{+0.557}_{-0.281}$	0.138
O/H (10^{-4})	$3.39^{+0.64}_{-0.64}$	$3.67^{+0.87}_{-0.87}$	$3.41^{+1.03}_{-1.03}$	$3.64^{+1.04}_{-1.04}$	$3.96^{+1.35}_{-1.35}$	$3.46^{+0.63}_{-0.63}$	$8.68^{+5.90}_{-5.90}$	4.90
Ne/H (10^{-5})	$5.36^{+1.26}_{-1.26}$	$5.61^{+1.49}_{-1.49}$	$5.63^{+1.84}_{-1.84}$	$5.41^{+1.78}_{-1.78}$	$5.86^{+2.22}_{-2.22}$	$6.03^{+1.31}_{-1.31}$	$19.50^{+16.00}_{-16.00}$	8.51
Ne/O	$0.158^{+0.048}_{-0.048}$	$0.153^{+0.054}_{-0.054}$	$0.165^{+0.073}_{-0.073}$	$0.149^{+0.065}_{-0.065}$	$0.148^{+0.075}_{-0.075}$	$0.174^{+0.049}_{-0.049}$	$0.225^{+0.239}_{-0.225}$	0.174
S/H (10^{-6})	$1.80^{+0.31}_{-0.31}$	$1.45^{+0.56}_{-0.56}$	$1.15^{+0.25}_{-0.25}$	$1.76^{+0.67}_{-0.67}$	$2.71^{+1.98}_{-1.98}$	$1.95^{+0.38}_{-0.38}$	$2.26^{+1.10}_{-1.10}$	13.2
S/O	$0.005^{+0.001}_{-0.001}$	$0.004^{+0.002}_{-0.002}$	$0.003^{+0.001}_{-0.001}$	$0.005^{+0.002}_{-0.002}$	$0.007^{+0.006}_{-0.006}$	$0.006^{+0.002}_{-0.002}$	$0.003^{+0.002}_{-0.002}$	0.027
Ar/H (10^{-7})	$10.10^{+3.42}_{-3.42}$	$12.50^{+5.73}_{-5.73}$	$8.55^{+5.08}_{-5.08}$	$10.30^{+6.62}_{-6.62}$	$14.90^{+7.39}_{-7.39}$	$9.91^{+2.48}_{-2.48}$	$16.60^{+9.47}_{-9.47}$	25.12
Ar/O	$0.003^{+0.001}_{-0.001}$	$0.003^{+0.002}_{-0.002}$	$0.003^{+0.002}_{-0.002}$	$0.003^{+0.002}_{-0.002}$	$0.004^{+0.002}_{-0.002}$	$0.003^{+0.001}_{-0.001}$	$0.002^{+0.002}_{-0.002}$	0.005
	IC3568 Full	IC3568 1	IC3568 2	IC3568 3	NGC2440 Full	NGC2440 1	NGC2440 2	
He/H (10^{-2})	$9.53^{+1.36}_{-1.36}$	$10.00^{+2.39}_{-2.39}$	$8.91^{+2.59}_{-2.59}$	$10.00^{+7.38}_{-7.38}$	$12.60^{+0.84}_{-0.84}$	$12.10^{+2.33}_{-2.33}$	$10.20^{+0.80}_{-0.80}$	8.51
C/H (10^{-4})	$4.66^{+2.71}_{-2.71}$	$2.03^{+0.83}_{-0.83}$	$5.74^{+4.48}_{-4.48}$	$27.16^{+47.99}_{-27.16}$	$2.18^{+0.44}_{-0.44}$	$1.52^{+0.27}_{-0.27}$	$1.47^{+1.47}_{-1.47}$	2.69
C/O	$1.148^{+0.756}_{-0.756}$	$0.652^{+0.304}_{-0.304}$	$1.357^{+1.197}_{-1.197}$	$3.660^{+7.310}_{-3.660}$	$0.506^{+0.127}_{-0.127}$	$0.388^{+0.119}_{-0.119}$	$2.339^{+2.787}_{-2.787}$	0.550
N/H (10^{-4})	···	···	···	···	$4.62^{+0.77}_{-0.77}$	$3.42^{+0.46}_{-0.46}$	$2.89^{+2.93}_{-2.93}$	0.68
N/O	···	···	···	···	$1.074^{+0.241}_{-0.241}$	$0.874^{+0.249}_{-0.249}$	$4.592^{+5.527}_{-5.527}$	0.138
O/H (10^{-4})	$4.06^{+1.26}_{-1.26}$	$3.11^{+0.69}_{-0.69}$	$4.23^{+1.74}_{-1.74}$	$7.42^{+6.91}_{-6.91}$	$4.30^{+0.65}_{-0.65}$	$3.91^{+0.98}_{-0.98}$	$0.63^{+0.41}_{-0.41}$	4.90
Ne/H (10^{-5})	$8.15^{+1.26}_{-1.26}$	$5.98^{+1.49}_{-1.49}$	$9.05^{+1.84}_{-1.84}$	$12.50^{+1.78}_{-1.78}$	$7.03^{+1.24}_{-1.24}$	$7.08^{+2.25}_{-2.25}$	$0.62^{+0.48}_{-0.48}$	8.51
Ne/O	$0.201^{+0.070}_{-0.070}$	$0.192^{+0.064}_{-0.064}$	$0.214^{+0.098}_{-0.098}$	$0.168^{+0.159}_{-0.159}$	$0.163^{+0.038}_{-0.038}$	$0.181^{+0.073}_{-0.073}$	$0.099^{+0.100}_{-0.100}$	0.174
S/H (10^{-6})	···	···	···	···	$1.52^{+0.16}_{-0.16}$	$1.35^{+0.23}_{-0.23}$	$0.67^{+0.61}_{-0.61}$	13.2
S/O	···	···	···	···	$0.004^{+0.001}_{-0.001}$	$0.003^{+0.001}_{-0.001}$	$0.011^{+0.012}_{-0.012}$	0.027
Ar/H (10^{-7})	$12.70^{+3.91}_{-3.91}$	$10.50^{+4.58}_{-4.58}$	$12.10^{+5.21}_{-5.21}$	$24.10^{+23.00}_{-23.00}$	$48.00^{+6.47}_{-6.47}$	$42.40^{+8.45}_{-8.45}$	$14.40^{+8.11}_{-8.11}$	25.12
Ar/O	$0.003^{+0.001}_{-0.001}$	$0.003^{+0.002}_{-0.002}$	$0.003^{+0.002}_{-0.002}$	$0.003^{+0.004}_{-0.003}$	$0.011^{+0.002}_{-0.002}$	$0.011^{+0.003}_{-0.003}$	$0.023^{+0.020}_{-0.020}$	0.005

Table 2.3—Continued

Total Elemental Abundances								
Parameter	NGC2440 3	NGC3242 Full	NGC3242 1	NGC3242 2	NGC3242 3	NGC3242 4	NGC3242 5	Solar[a]
He/H (10^{-2})	$12.40^{+0.95}_{-0.95}$	$10.60^{+0.50}_{-0.50}$	$12.30^{+2.60}_{-2.60}$	$11.90^{+1.60}_{-1.60}$	$11.1^{+2.3}_{-2.3}$	$10.0^{+2.58}_{-2.58}$	$9.57^{+1.63}_{-1.63}$	8.51
C/H (10^{-4})	$1.97^{+0.37}_{-0.37}$	$2.32^{+0.36}_{-0.36}$	$2.66^{+1.98}_{-1.98}$	$2.21^{+0.43}_{-0.43}$	$1.76^{+0.63}_{-0.63}$	$1.94^{+0.80}_{-0.80}$	$2.47^{+1.32}_{-1.32}$	2.69
C/O	$0.427^{+0.116}_{-0.116}$	$0.523^{+0.091}_{-0.091}$	$0.721^{+0.602}_{-0.602}$	$0.562^{+0.127}_{-0.127}$	$0.463^{+0.203}_{-0.203}$	$0.517^{+0.248}_{-0.248}$	$0.498^{+0.304}_{-0.304}$	0.550
N/H (10^{-4})	$3.95^{+0.58}_{-0.58}$	···	···	···	···	···	···	0.68
N/O	$0.856^{+0.211}_{-0.211}$	···	···	···	···	···	···	0.138
O/H (10^{-4})	$4.61^{+0.91}_{-0.91}$	$4.44^{+0.36}_{-0.36}$	$3.69^{+1.40}_{-1.40}$	$3.93^{+0.45}_{-0.45}$	$3.80^{+0.96}_{-0.96}$	$3.75^{+0.92}_{-0.92}$	$4.96^{+1.46}_{-1.46}$	4.90
Ne/H (10^{-5})	$7.08^{+1.60}_{-1.60}$	$9.62^{+0.91}_{-0.91}$	$8.02^{+3.55}_{-3.55}$	$8.31^{+1.20}_{-1.20}$	$8.37^{+2.31}_{-2.31}$	$8.12^{+2.23}_{-2.23}$	$10.70^{+3.60}_{-3.60}$	8.51
Ne/O	$0.154^{+0.046}_{-0.046}$	$0.217^{+0.004}_{-0.004}$	$0.217^{+0.016}_{-0.016}$	$0.211^{+0.014}_{-0.014}$	$0.220^{+0.012}_{-0.012}$	$0.216^{+0.011}_{-0.011}$	$0.215^{+0.013}_{-0.013}$	0.174
S/H (10^{-6})	$1.71^{+0.19}_{-0.19}$	···	···	···	···	···	···	13.2
S/O	$0.004^{+0.001}_{-0.001}$	···	···	···	···	···	···	0.027
Ar/H (10^{-7})	$48.00^{+9.19}_{-9.19}$	···	···	···	···	···	···	25.12
Ar/O	$0.010^{+0.003}_{-0.003}$	···	···	···	···	···	···	0.005
	NGC3242 6	NGC3242 7	NGC3242 8	NGC3242 9	NGC5315 Full	NGC5315 1	···	
He/H (10^{-2})	$9.26^{+1.74}_{-1.74}$	$9.62^{+1.38}_{-1.38}$	$9.93^{+1.00}_{-1.00}$	$11.6^{+2.70}_{-2.70}$	$11.90^{+0.17}_{-0.17}$	$7.95^{+1.07}_{-1.07}$	···	8.51
C/H (10^{-4})	$2.24^{+1.27}_{-1.27}$	$2.22^{+1.20}_{-1.20}$	$1.59^{+0.53}_{-0.53}$	$2.15^{+0.62}_{-0.62}$	$5.20^{+0.65}_{-0.65}$	$7.86^{+6.05}_{-6.05}$	···	2.69
C/O	$0.460^{+0.300}_{-0.300}$	$0.447^{+0.273}_{-0.273}$	$0.294^{+0.119}_{-0.119}$	$0.527^{+0.187}_{-0.187}$	$1.032^{+0.146}_{-0.146}$	$2.010^{+1.701}_{-1.701}$	···	0.550
N/H (10^{-4})	···	···	···	···	$7.86^{+1.01}_{-1.01}$	$5.63^{+2.29}_{-2.29}$	···	0.68
N/O	···	···	···	···	$1.560^{+0.224}_{-0.224}$	$1.440^{+0.773}_{-0.773}$	···	0.138
O/H (10^{-4})	$4.87^{+1.56}_{-1.56}$	$4.97^{+1.42}_{-1.42}$	$5.41^{+1.25}_{-1.25}$	$4.08^{+0.85}_{-0.85}$	$5.04^{+0.33}_{-0.33}$	$3.91^{+1.37}_{-1.37}$	···	4.90
Ne/H (10^{-5})	$11.1^{+4.00}_{-4.00}$	$10.7^{+3.50}_{-3.50}$	$12.5^{+3.20}_{-3.20}$	$8.83^{+2.06}_{-2.06}$	$12.90^{+1.01}_{-1.01}$	$7.48^{+3.15}_{-3.15}$	···	8.51
Ne/O	$0.228^{+0.014}_{-0.014}$	$0.216^{+0.014}_{-0.014}$	$0.231^{+0.010}_{-0.010}$	$0.216^{+0.012}_{-0.012}$	$0.256^{+0.026}_{-0.026}$	$0.191^{+0.105}_{-0.105}$	···	0.174
S/H (10^{-6})	···	···	···	···	$20.70^{+3.23}_{-3.23}$	$11.80^{+3.19}_{-3.19}$	···	13.2
S/O	···	···	···	···	$0.041^{+0.007}_{-0.007}$	$0.030^{+0.013}_{-0.013}$	···	0.027
Ar/H (10^{-7})	···	···	···	···	$37.80^{+1.70}_{-1.70}$	$32.00^{+7.96}_{-7.96}$	···	25.12
Ar/O	···	···	···	···	$0.008^{+0.001}_{-0.001}$	$0.008^{+0.004}_{-0.004}$	···	0.005

Table 2.3—Continued

Total Elemental Abundances								
Parameter	NGC5315 2	NGC5315 3	NGC5315 4	NGC5882 Full	NGC5882 1	NGC5882 2	···	Solar[a]
He/H (10^{-2})	$12.20^{+0.13}_{-0.13}$	$12.10^{+0.18}_{-0.18}$	$11.10^{+0.66}_{-0.66}$	$11.50^{+0.73}_{-0.73}$	$11.80^{+1.39}_{-1.39}$	$11.40^{+0.93}_{-0.93}$	···	8.51
C/H (10^{-4})	$3.58^{+0.20}_{-0.20}$	$8.56^{+2.47}_{-2.47}$	$66.40^{+94.85}_{-94.85}$	$2.72^{+1.09}_{-1.09}$	$1.66^{+1.14}_{-1.14}$	$3.14^{+1.57}_{-1.57}$	···	2.69
C/O	$0.694^{+0.042}_{-0.042}$	$1.441^{+0.464}_{-0.464}$	$7.615^{+11.747}_{-11.747}$	$0.357^{+0.159}_{-0.159}$	$0.239^{+0.182}_{-0.182}$	$0.423^{+0.235}_{-0.235}$	···	0.550
N/H (10^{-4})	$8.01^{+0.35}_{-0.35}$	$6.61^{+1.59}_{-1.59}$	$9.46^{+6.22}_{-6.22}$	$2.34^{+0.83}_{-0.83}$	$2.14^{+0.93}_{-0.93}$	$2.04^{+0.77}_{-0.77}$	···	0.68
N/O	$1.552^{+0.079}_{-0.079}$	$1.113^{+0.311}_{-0.311}$	$1.085^{+0.953}_{-0.953}$	$0.307^{+0.125}_{-0.125}$	$0.307^{+0.169}_{-0.169}$	$0.275^{+0.124}_{-0.124}$	···	0.138
O/H (10^{-4})	$5.16^{+0.13}_{-0.13}$	$5.94^{+0.84}_{-0.84}$	$8.72^{+5.08}_{-5.08}$	$7.63^{+1.49}_{-1.49}$	$6.96^{+2.35}_{-2.35}$	$7.42^{+1.83}_{-1.83}$	···	4.90
Ne/H (10^{-5})	$14.30^{+0.42}_{-0.42}$	$13.90^{+2.39}_{-2.39}$	$23.40^{+16.80}_{-16.80}$	$17.80^{+4.21}_{-4.21}$	$15.90^{+6.45}_{-6.45}$	$19.40^{+5.56}_{-5.56}$	···	8.51
Ne/O	$0.277^{+0.011}_{-0.011}$	$0.234^{+0.052}_{-0.052}$	$0.268^{+0.248}_{-0.248}$	$0.233^{+0.072}_{-0.072}$	$0.228^{+0.121}_{-0.121}$	$0.261^{+0.099}_{-0.099}$	···	0.174
S/H (10^{-6})	$27.20^{+1.13}_{-1.13}$	$17.70^{+2.76}_{-2.76}$	$15.70^{+6.40}_{-6.40}$	$11.90^{+4.29}_{-4.29}$	$9.36^{+3.43}_{-3.43}$	$14.30^{+17.80}_{-17.80}$	···	13.2
S/O	$0.053^{+0.003}_{-0.003}$	$0.030^{+0.006}_{-0.006}$	$0.018^{+0.013}_{-0.013}$	$0.016^{+0.006}_{-0.006}$	$0.013^{+0.007}_{-0.007}$	$0.019^{+0.024}_{-0.024}$	···	0.027
Ar/H (10^{-7})	$38.10^{+0.66}_{-0.66}$	$41.80^{+4.13}_{-4.13}$	$49.90^{+20.20}_{-20.20}$	$28.50^{+5.34}_{-5.34}$	$28.20^{+7.78}_{-7.78}$	$31.80^{+6.74}_{-6.74}$	···	25.12
Ar/O	$0.007^{+0.001}_{-0.001}$	$0.007^{+0.001}_{-0.001}$	$0.006^{+0.004}_{-0.004}$	$0.004^{+0.001}_{-0.001}$	$0.004^{+0.002}_{-0.002}$	$0.004^{+0.001}_{-0.001}$	···	0.005
	NGC5882 3	NGC7662 Full	NGC7662 1	NGC7662 2	NGC7662 3	···	···	
He/H (10^{-2})	$10.80^{+1.18}_{-1.18}$	$10.00^{+0.76}_{-0.76}$	$11.60^{+2.72}_{-2.72}$	$10.50^{+2.23}_{-2.23}$	$9.43^{+1.52}_{-1.52}$	···	···	8.51
C/H (10^{-4})	$4.65^{+8.63}_{-8.63}$	$4.08^{+0.43}_{-0.43}$	$4.88^{+1.28}_{-1.28}$	$3.86^{+0.75}_{-0.75}$	$4.45^{+0.63}_{-0.63}$	···	···	2.69
C/O	$0.535^{+1.086}_{-1.086}$	$0.913^{+0.129}_{-0.129}$	$0.938^{+0.316}_{-0.316}$	$0.704^{+0.247}_{-0.247}$	$0.824^{+0.224}_{-0.224}$	···	···	0.550
N/H (10^{-4})	$2.49^{+1.69}_{-1.69}$	$0.77^{+0.11}_{-0.11}$	$1.19^{+0.49}_{-0.49}$	$0.65^{+0.21}_{-0.21}$	$0.92^{+0.20}_{-0.20}$	···	···	0.68
N/O	$0.287^{+0.305}_{-0.305}$	$0.173^{+0.029}_{-0.029}$	$0.229^{+0.107}_{-0.107}$	$0.119^{+0.052}_{-0.052}$	$0.170^{+0.053}_{-0.053}$	···	···	0.138
O/H (10^{-4})	$8.69^{+7.12}_{-7.12}$	$4.47^{+0.42}_{-0.42}$	$5.20^{+1.10}_{-1.10}$	$5.48^{+1.60}_{-1.60}$	$5.40^{+1.25}_{-1.25}$	···	···	4.90
Ne/H (10^{-5})	$20.60^{+20.40}_{-20.40}$	$8.99^{+0.92}_{-0.92}$	$11.40^{+2.63}_{-2.63}$	$10.80^{+3.24}_{-3.24}$	$10.40^{+2.50}_{-2.50}$	···	···	8.51
Ne/O	$0.237^{+0.305}_{-0.305}$	$0.201^{+0.028}_{-0.028}$	$0.219^{+0.069}_{-0.069}$	$0.197^{+0.083}_{-0.083}$	$0.193^{+0.064}_{-0.064}$	···	···	0.174
S/H (10^{-6})	$13.10^{+11.30}_{-11.30}$	$2.59^{+0.68}_{-0.68}$	$2.84^{+1.55}_{-1.55}$	$4.17^{+2.18}_{-2.18}$	$5.49^{+3.17}_{-3.17}$	···	···	13.2
S/O	$0.015^{+0.018}_{-0.018}$	$0.006^{+0.002}_{-0.002}$	$0.005^{+0.003}_{-0.003}$	$0.008^{+0.005}_{-0.005}$	$0.010^{+0.006}_{-0.006}$	···	···	0.027
Ar/H (10^{-7})	$33.90^{+22.20}_{-22.20}$	$17.10^{+2.16}_{-2.16}$	$14.40^{+4.79}_{-4.79}$	$19.40^{+6.25}_{-6.25}$	$20.60^{+6.65}_{-6.65}$	···	···	25.12
Ar/O	$0.004^{+0.004}_{-0.004}$	$0.004^{+0.001}_{-0.001}$	$0.003^{+0.001}_{-0.001}$	$0.004^{+0.002}_{-0.002}$	$0.004^{+0.002}_{-0.002}$	···	···	0.005

Table 2.3—Continued

Total Elemental Abundances								
Parameter	NGC7662 4	NGC7662 5	NGC7662 6	NGC7662 7	NGC7662 8	···	···	Solar[a]
He/H (10^{-2})	$9.38^{+0.97}_{-0.97}$	$10.60^{+1.05}_{-1.05}$	$10.60^{+0.65}_{-0.65}$	$11.70^{+1.91}_{-1.91}$	$9.68^{+2.16}_{-2.16}$	···	···	8.51
C/H (10^{-4})	$3.02^{+0.23}_{-0.23}$	$3.30^{+1.04}_{-1.04}$	$4.17^{+0.62}_{-0.62}$	$4.58^{+0.74}_{-0.74}$	$6.62^{+2.59}_{-2.59}$	···	···	2.69
C/O	$0.579^{+0.131}_{-0.131}$	$0.701^{+0.275}_{-0.275}$	$0.882^{+0.159}_{-0.159}$	$1.272^{+0.252}_{-0.252}$	$1.403^{+0.669}_{-0.669}$	···	···	0.550
N/H (10^{-4})	$0.55^{+0.11}_{-0.11}$	$0.70^{+0.27}_{-0.27}$	$0.69^{+0.16}_{-0.16}$	$0.68^{+0.18}_{-0.18}$	$0.91^{+0.51}_{-0.51}$	···	···	0.68
N/O	$0.105^{+0.030}_{-0.030}$	$0.149^{+0.067}_{-0.067}$	$0.145^{+0.037}_{-0.037}$	$0.187^{+0.055}_{-0.055}$	$0.192^{+0.120}_{-0.120}$	···	···	0.138
O/H (10^{-4})	$5.22^{+1.11}_{-1.11}$	$4.71^{+1.10}_{-1.10}$	$4.73^{+0.48}_{-0.48}$	$3.60^{+0.41}_{-0.41}$	$4.72^{+1.29}_{-1.29}$	···	···	4.90
Ne/H (10^{-5})	$11.20^{+2.41}_{-2.41}$	$9.85^{+2.52}_{-2.52}$	$8.49^{+0.97}_{-0.97}$	$7.22^{+0.93}_{-0.93}$	$10.20^{+3.03}_{-3.03}$	···	···	8.51
Ne/O	$0.215^{+0.065}_{-0.065}$	$0.209^{+0.072}_{-0.072}$	$0.179^{+0.027}_{-0.027}$	$0.201^{+0.034}_{-0.034}$	$0.216^{+0.087}_{-0.087}$	···	···	0.174
S/H (10^{-6})	$3.81^{+2.40}_{-2.40}$	$2.50^{+1.27}_{-1.27}$	$2.14^{+0.71}_{-0.71}$	$2.21^{+0.68}_{-0.68}$	$1.88^{+1.74}_{-1.74}$	···	···	13.2
S/O	$0.007^{+0.005}_{-0.005}$	$0.005^{+0.003}_{-0.003}$	$0.005^{+0.002}_{-0.002}$	$0.006^{+0.002}_{-0.002}$	$0.004^{+0.004}_{-0.004}$	···	···	0.027
Ar/H (10^{-7})	$25.80^{+6.14}_{-6.14}$	$26.80^{+7.00}_{-7.00}$	$14.60^{+2.42}_{-2.42}$	$13.70^{+2.27}_{-2.27}$	$12.00^{+5.49}_{-5.49}$	···	···	25.12
Ar/O	$0.005^{+0.002}_{-0.002}$	$0.006^{+0.002}_{-0.002}$	$0.003^{+0.001}_{-0.001}$	$0.004^{+0.001}_{-0.001}$	$0.003^{+0.001}_{-0.001}$	···	···	0.005

[a]Asplund et al. [4]

Chapter 3

Are Planetary Nebulae Chemically Homogeneous?

With the abundances calculated from ELSA, a direct comparison between regions can be made to look for possible differences. Figures 3.1-3.3 compare the total abundances of each region with the values scaled to the abundance of the full region in each planetary nebula. The bottom two panels of Figure 3.3 also compare the [O III] temperature and C III] density of each region with each value scaled in the same manner as the abundances. Out of all the regions, only region 2 of NGC 2440 and region 1 of NGC 5315 show abundances that are significantly lower than the respective full regions. For region 2 of NGC 2440, this can likely be attributed to both the lack of co-spatiality between the UV and optical observations as well as NGC 2440's high ionization stratification (see e.g. López et al. [35] and Richer et al. [51]). Spurious abundances would result from combining areas where the distributions of the ionized states for a particular element are different. For region 1 of NGC 5315, a higher electron temperature is measured compared with the temperature of its full region, causing the inferred abundances to be lower. However, the temperature is consistent (given the errors) with the full region, and substituting the full region's temperature value in for the abundance calculations of Region 1 yields abundances consistent with the full region's values.

Fig. 3.1.— Helium, carbon, and nitrogen abundances for each region listed in Table 2.3 scaled to the full region of each PN. The abundances at nearly all positions in each object are consistent within errors, with outliers discussed in the text.

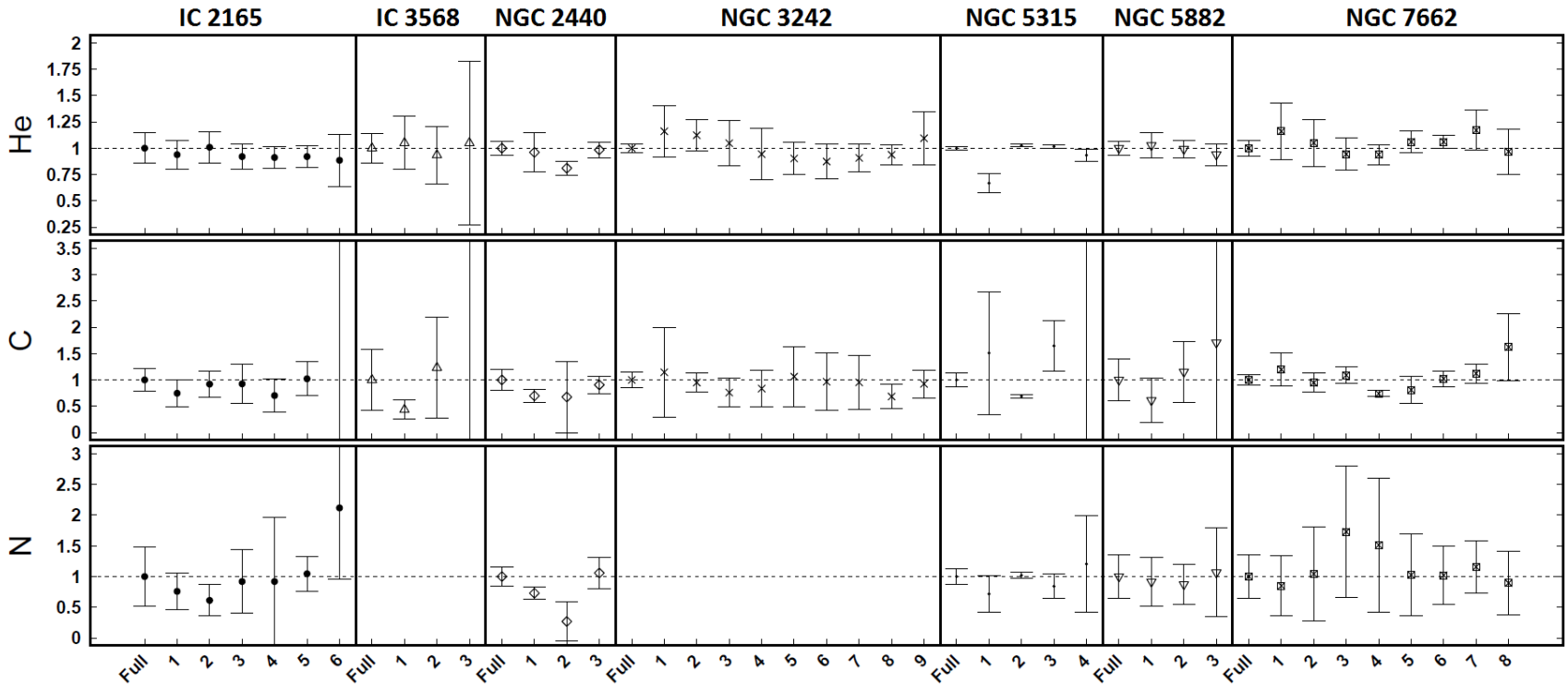

Fig. 3.2.— Same as Figure 3.1 but for oxygen, neon and argon.

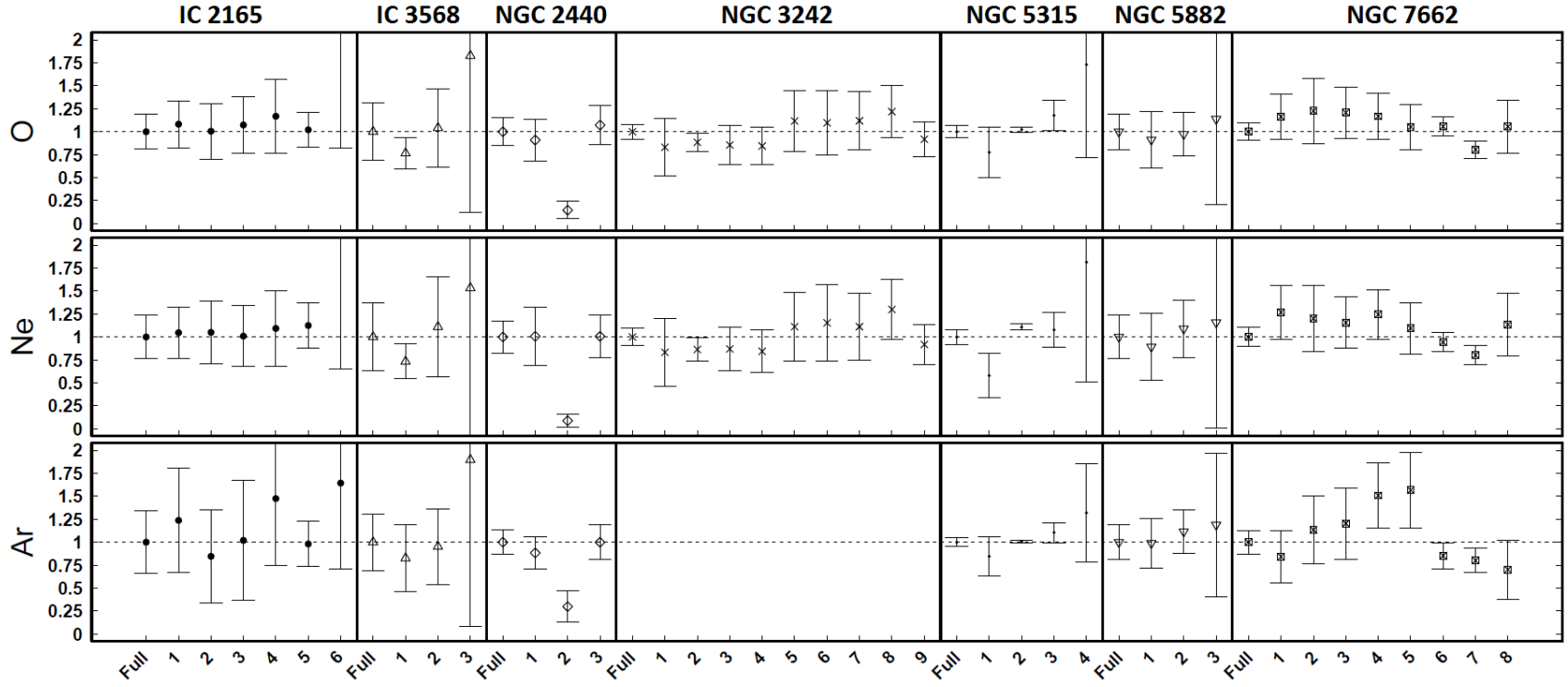

Fig. 3.3.— Top panel: Same as Figure 3.1 but for sulfur. Middle and bottom panels show the [O III] electron temperature and C III] electron density listed in Table 2.2 for each region in a PN.

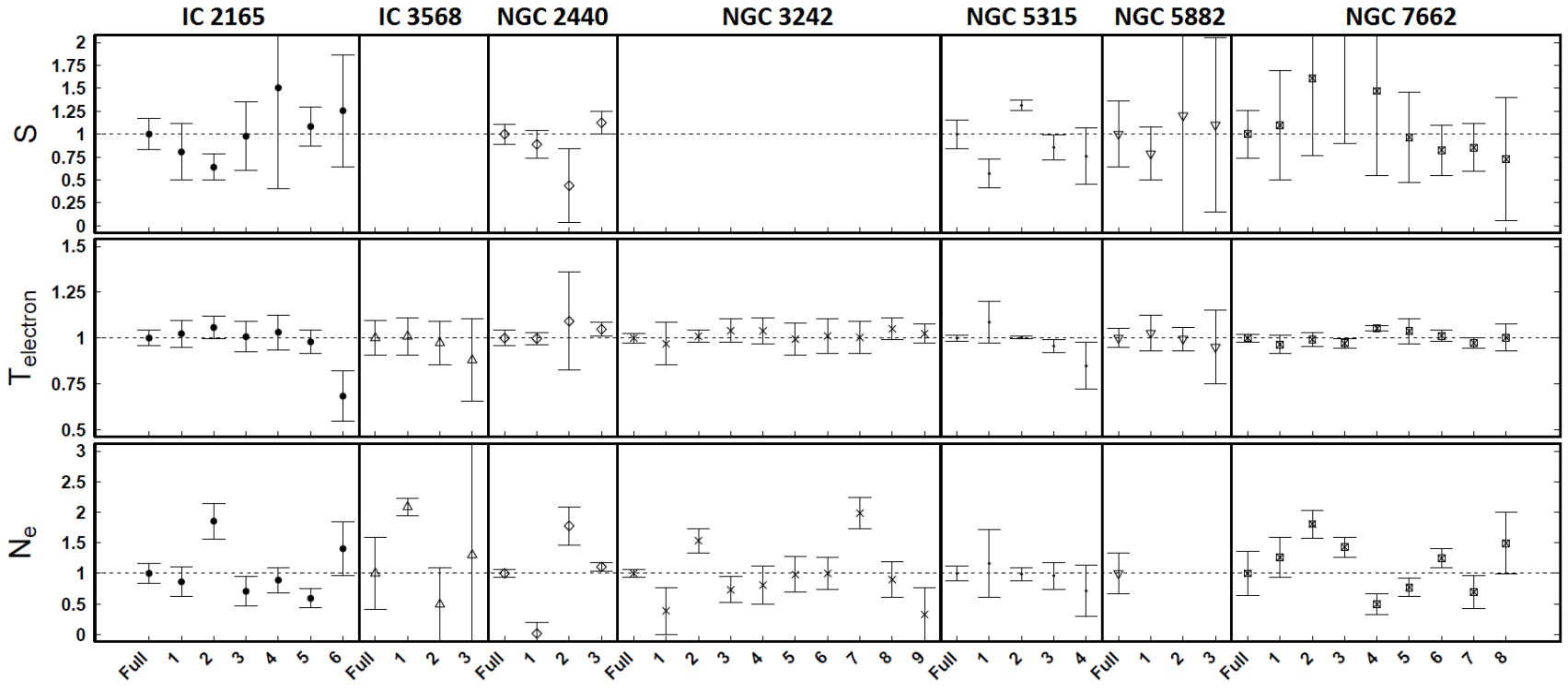

A literature search over the last twenty years shows that only NGC 2440, NGC 3242, and NGC 5882 from this sample have been investigated previously for abundance variations. Perinotto & Corradi [45] presented results on the abundances of helium, oxygen, nitrogen, neon, argon, and sulfur for NGC 2440. They made long-slit observations from 3600-9600 Å along the major axis using the Boller & Chivens spectrograph and the 1.52m ESO telescope at La Silla, Chile. The observations were divided into seven regions spanning the slit length and width of 76.1″ and 2″, respectively. There were no observed spatial variations between the seven regions within their uncertainties for every element. Monteiro et al. [41] addressed the idea of chemical inhomogeneity in NGC 3242. They observed the nebula between 3900-7000 Å using 6400 fibers onboard the instrument VIMOS-IFU, covering an area of 54″x54″. They measured accurate oxygen and helium abundances from the most abundant ionic species in this range. For other elements in the study, i.e., nitrogen, sulfur and chlorine, only less abundant ionic species were observable, resulting in large (as high as 6x) discrepancies in the total abundances measured at different locations in the nebula. Monteiro et al. [41] concluded that helium and oxygen were homogeneous throughout NGC 3242. NGC 5882 was observed by Guerrero & Manchado [16] over the wavelength range 3400-10,300 Å using the same instrument as the one employed by Perinotto & Corradi [45]. They compared the outermost halo to the inner two shells as a whole. They found the abundances of helium, oxygen, and neon to be consistent within errors between the halo and shells.

Table 3.1 compares the full region abundances for each planetary nebula with other values in the literature. Each PN has two comparison values from either authors with quoted uncertainties or average values with standard deviations from multiple authors. The majority of the abundances match within 1σ and nearly all are consistent within 2σ with the other authors. The largest discrepancy is seen

in the nitrogen abundance of NGC 2440 when compared to the value of Kwitter et al. [32]. This is most likely caused by the fact that the nitrogen abundance of Kwitter et al. [32] was calculated using the ICF method (ICF value of 9.71) whereas this value is the sum of the observed ionic species, which includes the most populated ionic states.

Table 3.1. Comparison: Total Elemental Abundances

Comparison: Total Elemental Abundances						
	IC 2165 Full			IC 3568 Full		
Element	This Work	Kwitter et al. [32]	BH[a]	This Work	Henry et al. [19]	Kwitter & Henry [30]
He/H (10^{-2})	$11.30^{+1.65}_{-1.65}$	$9.00^{+3.00}_{-3.00}$	$10.83^{+0.66}_{-0.66}$	$9.53^{+1.36}_{-1.36}$	$12.00^{+4.00}_{-4.00}$	$11.00^{+1.65}_{-1.65}$
C/H (10^{-4})	$4.14^{+0.87}_{-0.87}$	···	$6.54^{+1.76}_{-1.76}$	$4.66^{+2.71}_{-2.71}$	···	$0.97^{+0.49}_{-0.49}$
N/H (10^{-4})	$1.18^{+0.29}_{-0.29}$	$1.33^{+0.19}_{-0.19}$	$1.20^{+0.32}_{-0.32}$	···	···	···
O/H (10^{-4})	$3.39^{+0.64}_{-0.64}$	$3.11^{+0.44}_{-0.44}$	$2.28^{+0.31}_{-0.31}$	$4.06^{+1.26}_{-1.26}$	$3.77^{+0.53}_{-0.53}$	$3.14^{+0.47}_{-0.47}$
Ne/H (10^{-5})	$5.36^{+1.26}_{-1.26}$	$6.90^{+0.93}_{-0.93}$	$5.66^{+2.23}_{-2.23}$	$8.15^{+1.26}_{-1.26}$	$7.16^{+1.13}_{-1.13}$	$4.08^{+0.61}_{-0.61}$
S/H (10^{-6})	$1.80^{+0.31}_{-0.31}$	$2.70^{+0.31}_{-0.31}$	$3.62^{+1.29}_{-1.29}$	···	···	···
Ar/H (10^{-7})	$10.10^{+3.42}_{-3.42}$	$16.00^{+2.18}_{-2.18}$	$13.23^{+4.57}_{-4.57}$	$12.70^{+3.91}_{-3.91}$	$10.56^{+3.39}_{-3.39}$	···
	NGC 2440 Full			NGC 3242 Full		
Element	This Work	Kwitter et al. [32]	Hyung & Aller [25]	This Work	Henry et al. [18]	Milingo et al. [40]
He/H (10^{-2})	$12.60^{+0.84}_{-0.84}$	$10.00^{+3.00}_{-3.00}$	$12.00^{+1.20}_{-1.20}$	$10.60^{+0.45}_{-0.45}$	$8.00^{+1.00}_{-1.00}$	$11.00^{+3.30}_{-3.30}$
C/H (10^{-4})	$2.18^{+0.44}_{-0.44}$	···	$4.00^{+2.00}_{-2.00}$	$2.35^{+0.36}_{-0.36}$	$4.12^{+1.66}_{-1.66}$	···
N/H (10^{-4})	$4.62^{+0.77}_{-0.77}$	$10.67^{+1.51}_{-1.51}$	$9.50^{+2.38}_{-2.38}$	···	···	···
O/H (10^{-4})	$4.30^{+0.65}_{-0.65}$	$5.19^{+0.73}_{-0.73}$	$4.40^{+0.70}_{-0.70}$	$4.44^{+0.36}_{-0.36}$	$3.38^{+0.51}_{-0.51}$	$4.37^{+1.31}_{-1.31}$
Ne/H (10^{-5})	$7.03^{+1.24}_{-1.24}$	$10.70^{+1.56}_{-1.56}$	$9.00^{+1.35}_{-1.35}$	$9.62^{+0.91}_{-0.91}$	$8.10^{+1.35}_{-1.35}$	$9.00^{+2.70}_{-2.70}$
S/H (10^{-6})	$1.52^{+0.16}_{-0.16}$	$2.80^{+0.52}_{-0.52}$	$2.00^{+0.60}_{-0.60}$	···	···	···
Ar/H (10^{-7})	$48.00^{+6.47}_{-6.47}$	$40.60^{+5.71}_{-5.71}$	$21.00^{+4.20}_{-4.20}$	···	···	···
	NGC 5315 Full			NGC 5882 Full		
Element	This Work	Peimbert et al. [43]	TKSDT[b]	This Work	Kwitter et al. [32]	Guerrero & Manchado [16]
He/H (10^{-2})	$11.90^{+0.17}_{-0.17}$	$11.75^{+0.11}_{-0.11}$	$10.71^{+1.20}_{-1.20}$	$11.50^{+0.73}_{-0.73}$	$12.00^{+4.00}_{-4.00}$	$11.10^{+0.70}_{-0.70}$
C/H (10^{-4})	$5.20^{+0.65}_{-0.65}$	$7.08^{+1.47}_{-1.47}$	$5.96^{+5.40}_{-5.40}$	$2.72^{+1.09}_{-1.09}$	···	···
N/H (10^{-4})	$7.86^{+1.01}_{-1.01}$	$6.92^{+2.39}_{-2.39}$	$3.61^{+1.75}_{-1.75}$	$2.34^{+0.83}_{-0.83}$	$1.80^{+0.27}_{-0.27}$	$1.40^{+0.40}_{-0.40}$
O/H (10^{-4})	$5.04^{+0.33}_{-0.33}$	$7.41^{+0.51}_{-0.51}$	$6.02^{+1.55}_{-1.55}$	$7.63^{+1.49}_{-1.49}$	$5.48^{+0.77}_{-0.77}$	$4.93^{+0.45}_{-0.45}$
Ne/H (10^{-5})	$12.90^{+1.01}_{-1.01}$	$20.41^{+4.70}_{-4.70}$	$16.66^{+4.95}_{-4.95}$	$17.80^{+4.21}_{-4.21}$	$14.80^{+2.19}_{-2.19}$	$8.40^{+1.20}_{-1.20}$
S/H (10^{-6})	$20.70^{+3.23}_{-3.23}$	$32.35^{+8.94}_{-8.94}$	$17.87^{+3.31}_{-3.31}$	$11.90^{+4.29}_{-4.29}$	$7.20^{+1.10}_{-1.10}$	$7.00^{+0.70}_{-0.70}$
Ar/H (10^{-7})	$37.80^{+1.70}_{-1.70}$	$56.21^{+10.35}_{-10.35}$	$49.58^{+14.20}_{-14.21}$	$28.50^{+5.34}_{-5.34}$	$27.90^{+3.84}_{-3.84}$	$31.50^{+1.08}_{-1.08}$

Table 3.1—Continued

Comparison: Total Elemental Abundances			
	NGC 7662 Full		
Element	This Work	Kwitter et al. [32]	LHBA[c]
He/H (10^{-2})	$10.00^{+0.76}_{-0.76}$	$10.00^{+3.00}_{-3.00}$	$10.05^{+1.15}_{-1.15}$
C/H (10^{-4})	$4.08^{+0.43}_{-0.43}$	···	$6.27^{+2.48}_{-2.48}$
N/H (10^{-4})	$0.77^{+0.11}_{-0.11}$	$0.74^{+0.13}_{-0.13}$	$1.00^{+0.42}_{-0.42}$
O/H (10^{-4})	$4.47^{+0.42}_{-0.42}$	$4.19^{+0.59}_{-0.59}$	$4.59^{+1.70}_{-1.70}$
Ne/H (10^{-5})	$8.99^{+0.92}_{-0.92}$	$7.10^{+0.84}_{-0.84}$	$7.58^{+1.80}_{-1.80}$
S/H (10^{-6})	$2.59^{+0.68}_{-0.68}$	$4.30^{+0.42}_{-0.42}$	$5.71^{+1.52}_{-1.52}$
Ar/H (10^{-7})	$17.10^{+2.16}_{-2.16}$	$24.60^{+3.35}_{-3.35}$	$14.80^{+4.46}_{-4.46}$

[a]Values and uncertainties are averages and standard deviations, respectively, from Bohigas et al. [7] and Hyung [23].

[b]Values and uncertainties are averages and standard deviations, respectively, from Tsamis et al. [60], Kingsburgh & Barlow [28], Samland et al. [53], de Freitas Pacheco et al. [11], and Torres-Peimbert & Pena [59].

[c]Values and uncertainties are averages and standard deviations, respectively, from Liu et al. [34], Hyung & Aller [24], Barker [6], and Aller & Czyzak [2].

Looking at the temperatures of each region, only region 6 of IC 2165 is significantly lower than its full region temperature. This region probes the middle shell of IC 2165, as opposed to the other regions that probe the innermost shell. Therefore, this may indeed be cooler gas since it is farther from the central star and may be optically thick such that the effect of heating by radiation hardening[a] doesn't occur. Lastly, most of the density variations appear to coincide with brighter areas of each PN for the higher densities, and dimmer areas for the lower densities. This is consistent with the assumption that the brightness is proportional to the density squared and may be the result of clumps of ejected material that form prior/during the formation of the planetary nebula. The only regions with densities that are unusual are Regions 2, 1 and 7 of IC 2165, IC 3568 and NGC 3242, respectively. A plausible explanation is that there is a small knot of enhanced density in each region that is emitting the observed light, though a literature search turns up no corroboration.

To summarize, first, dereddened emission line intensities for various regions across each planetary nebula were presented. Next, these emission lines were used to calculate nebular properties of temperature and density as well as ionic abundances. Last, total abundances for He, C, N, O, Ne, S and Ar were calculated from the ionic abundances for each region. *The major result is that each of the seven planetary nebulae appears to exhibit a chemically homogeneous distribution of these elements.* This is the first time these planetary nebulae have been shown to be chemically homogeneous at sub-arcsecond, effective spatial resolution. This abundance homogeneity for each PN supports current planetary nebula formation theory. During the asymptotic giant branch stage of a star's evolution, convection processes will mix recent nuclear fusion products like carbon, nitrogen, and helium

[a]Radiation hardening refers to optically thin gas exterior to optically thick gas being illuminated by preferentially higher-energy photons since the optically thick gas absorbed the photons near the hydrogen series limit.

into the surface layers which are eventually ejected during the formation of the PN. The relevant timescales are those of nuclear fusion and envelope convection. The nuclear timescale is of the order 10^5-10^6 years whereas the convection process is model dependent and the timescale is calculated by the taking the size of the envelope divided by the velocity of the convective atmospheric elements (Renzini & Voli [48]). Models by Buell [8] (private communication) imply a convection timescale on the order of a year. Therefore, the mixing and subsequent ejection of matter, such as ^{12}C, ^{13}C and ^{14}N, to form the planetary nebula is much shorter than the nuclear timescales, and each ejection should be homogeneous.

Chapter 4

Properties of Planetary Nebula Central Stars and Their Progenitors

In order to constrain the central star's temperature and luminosity of each planetary nebula, Cloudy version 13.03 (Ferland et al. [14]) was used to generate photoionization models of each PN. For a given set of input parameters, Cloudy simultaneously solves energy and ionization equilibrium equations at specific radial points in the PN model. Three iterations for each model were carried out to ensure that each model had converged to a solution. The assumed spectral energy distribution (SED) of the central star was taken to be either the Rauch H-Ni (example shown in Figure 4.1) or the Rauch pg1159 (example shown in Figure 4.2) atmospheric simulations (Rauch [47]), depending on the known atmospheric properties of the central stars. Rauch H-Ni includes line blanketing for lines from hydrogen to nickel, whereas for Rauch pg1159, the line blanketing effects only include lines of helium, carbon, nitrogen, and oxygen. NGC 5315 was the only PN for which the Rauch pg1159 SED was employed, since its central star was observed to be hydrogen deficient by Mendez & Niemela [37]. Assumptions for each model were a spherically symmetric and static geometry without shock heating of the gas. The stellar parameters for the initial model were chosen to be the average of the most reliable values found in the literature (Shaw & Kaler [57], Shaw & Kaler [58], Zhang & Kwok [65], Corradi et al. [10], and Frew [15]) but were allowed to vary in subsequent models. Fixed angular radii for the models were measured from archival HST WFPC2 images and the values are as follows; IC 2165 r=2.67″, IC 3568 r=3.54″, NGC 2440 r=6.51″, NGC 3242 r=9.30″, NGC

5315 r=1.50″, NGC 5882 r=3.21″, and NGC 7662 r=10.71″. These fixed angular radii ensured that a change in the outer radius of each model resulted in a change in the assumed distance to the nebula. Lastly, the nebular properties initially were set to the values discussed in §2 (densities in Table 2.1 and total abundances in Table 2.3) but also left variable.

Fig. 4.1.— The Rauch H-Ni SED used in the case of NGC 3242. The r_o refers to the inner radius of the nebula from the model.

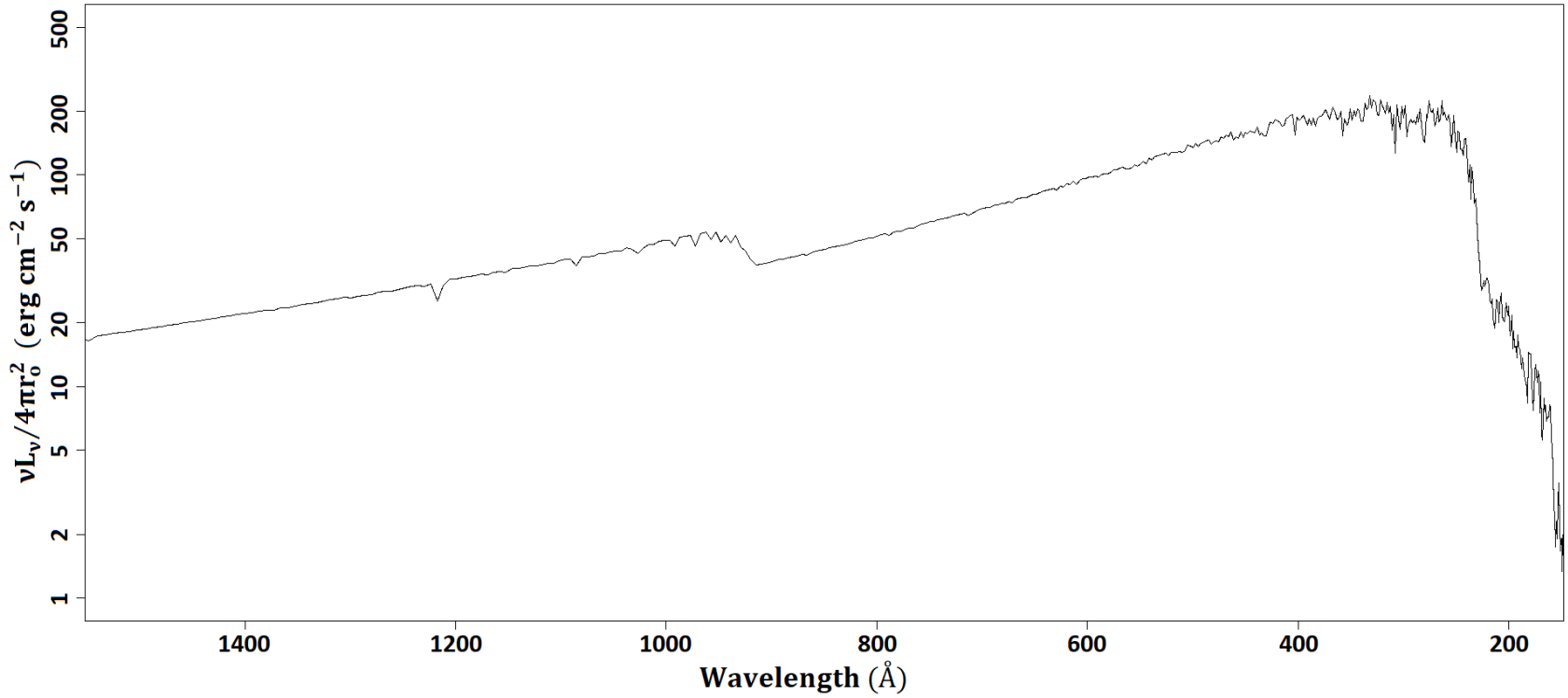

Fig. 4.2.— The Rauch pg1159 SED used in the case of NGC 5315. The r_o refers to the inner radius of the nebula from the model.

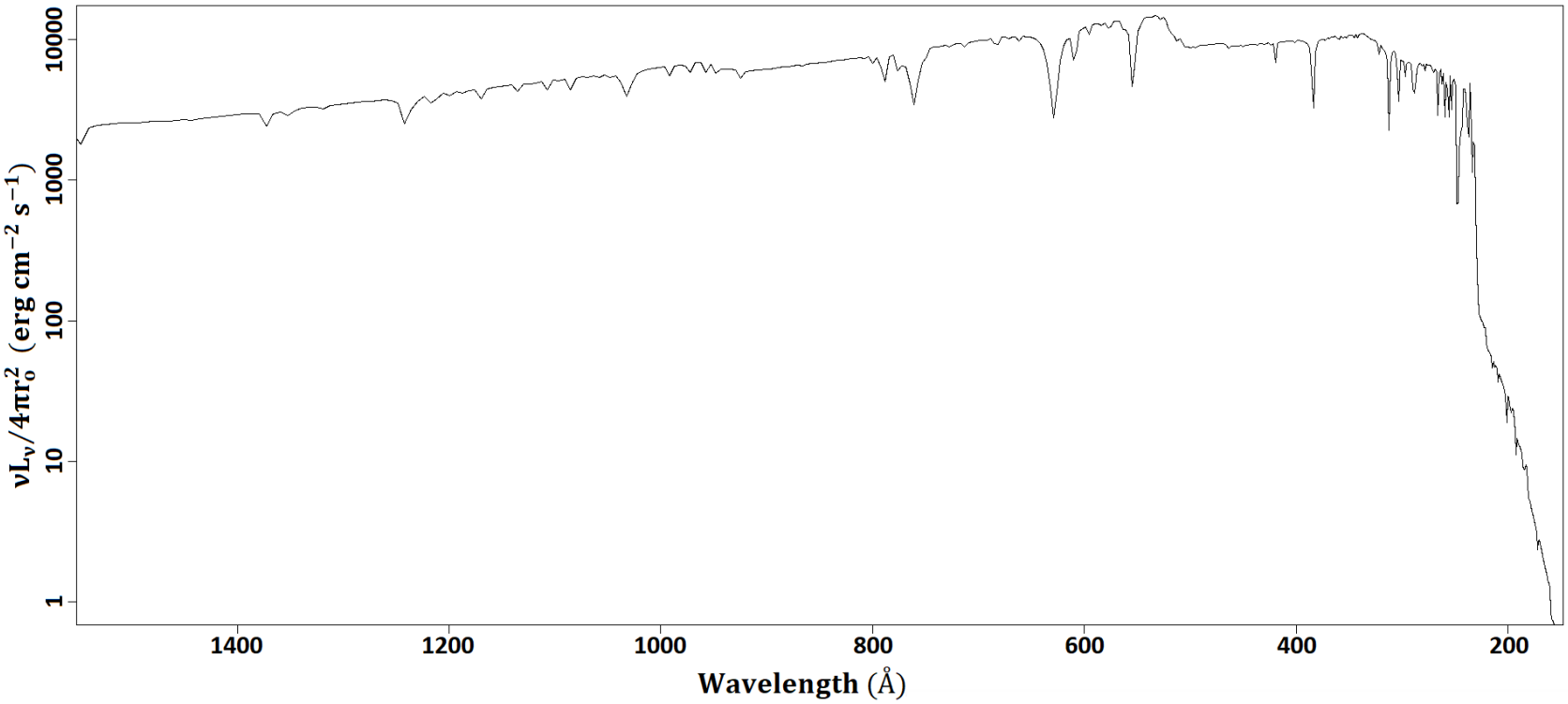

The calculations for converting the internal model gas properties into model emission line strengths were made with the self-written C++ program PANIC (PlAnetary Nebula Intensity Calculator). To summarize the process, volume emissivity values as a function of radius from each Cloudy model are read into PANIC, which then calculates the model line intensities based on the geometry and other properties of the modeled gas. Specifically, PANIC calculates the volume of gas in each region's line-of-sight for each radial distance from the model, multiplies this volume by the appropriate emissivity, and adds up each contribution to determine the maximum emission strength for a particular line. Finally, this maximum emission strength is scaled by the filling factor (the ratio of the volume of gas to the total, physical volume) to get the total emission line strength.

To weight the emission lines equally, only one[a] emission line per ion from the observations was used in the comparison to the models and only for lines having a S/N > 3. A total rms value was calculated for each model from the expression $\sqrt{\frac{1}{N}\sum_1^N (1-\frac{model}{observed})^2}$, where N is the total number of lines and diagnostics, *model* is the value of each line or diagnostic predicted by the model, and *observed* is the observed value. A similar rms value for the observations was calculated using the line's uncertainty by replacing $1-\frac{model}{observed}$ in the above expression with $\frac{uncertainty}{observed}$. This observed rms value was later used in the calculation of the uncertainties in the parameters from each model. The model that yielded the lowest rms value was chosen to be the best model.

Degeneracies between models with similar rms values were broken by employing five common diagnostics. The first, $\frac{[O\ III]\ \lambda5007+\lambda4959+[O\ II]\ \lambda3727}{H\beta}$, is used to gauge the metallicity of the nebula since oxygen is often the most abundant metal. The next two, $\frac{[O\ II]\ \lambda3727}{[O\ III]\ \lambda5007}$ and $\frac{He\ II\ \lambda4686}{He\ I\ \lambda5876}$, are sensitive to the ionization state of the nebula. The temperature of the nebular gas is probed with the fourth

[a]Additional lines from some ions were used in diagnostic line ratios only.

diagnostic, $[O\ III]\ \frac{\lambda 4363}{\lambda 5007}$. The final diagnostic, $\frac{C\ III]\ \lambda 1909}{C\ [III]\ \lambda 1907}$, is used to determine the density of the nebula.

To test the validity of the described rms method for assessing the best model, the method of Morisset & Georgiev [42] was used for NGC 3242. In their method, a quality factor, Q, is calculated by the expression $\frac{log(\frac{model}{observed})}{log(1+RelativeError)}$ where *RelativeError* is $\frac{uncertainty}{observed}$. Minimizing this Q value instead of the rms resulted in a small difference in the best fit stellar temperature and luminosity of only 200 K and 0.011 dex, respectively.

Next, the sensitivity of the final stellar parameters on the choice of nebular density profiles was explored by testing three profiles. The first had a constant density throughout the entire gas region (constant density profile). The brightest portions of each nebula are primarily from one shell, so a constant density profile is a sensible first choice. However, the sharp cutoff of the gas at the boundaries is unphysical in nature. Therefore, the second profile replaces the constant density with a Gaussian shaped density profile (Gaussian density profile), allowing for a smoother transition to low density areas. The Gaussian density profile, however, does not take into account the less luminous, exterior shells of gas seen in most of the objects. To represent these outer shells in the third profile, a radially decreasing power-law is appended to the Gaussian density profile (Gaussian with a power-law density profile). Figures 4.3 & 4.4 shows the different profiles for each planetary nebula's Full Region.

Since each model assumes a specific value for each stellar and nebular parameter, locating the global minimum (in parameter space) or best value for each stellar parameter is critical. Two methods were used to find these minima. The first method employed a suite of constant density models spanning a wide range of stellar and nebular parameters, using resources from the OU Supercomputing

Fig. 4.3.— The three different density profiles used for the full regions of IC 2165, IC 3568, NGC 2440 and NGC 3242 are shown here. The solid red lines are the constant density profiles. The blue dash lines are the Gaussian density profile. The combination of the blue dash lines and green dot-dash lines are the Gaussian with a power-law density profiles.

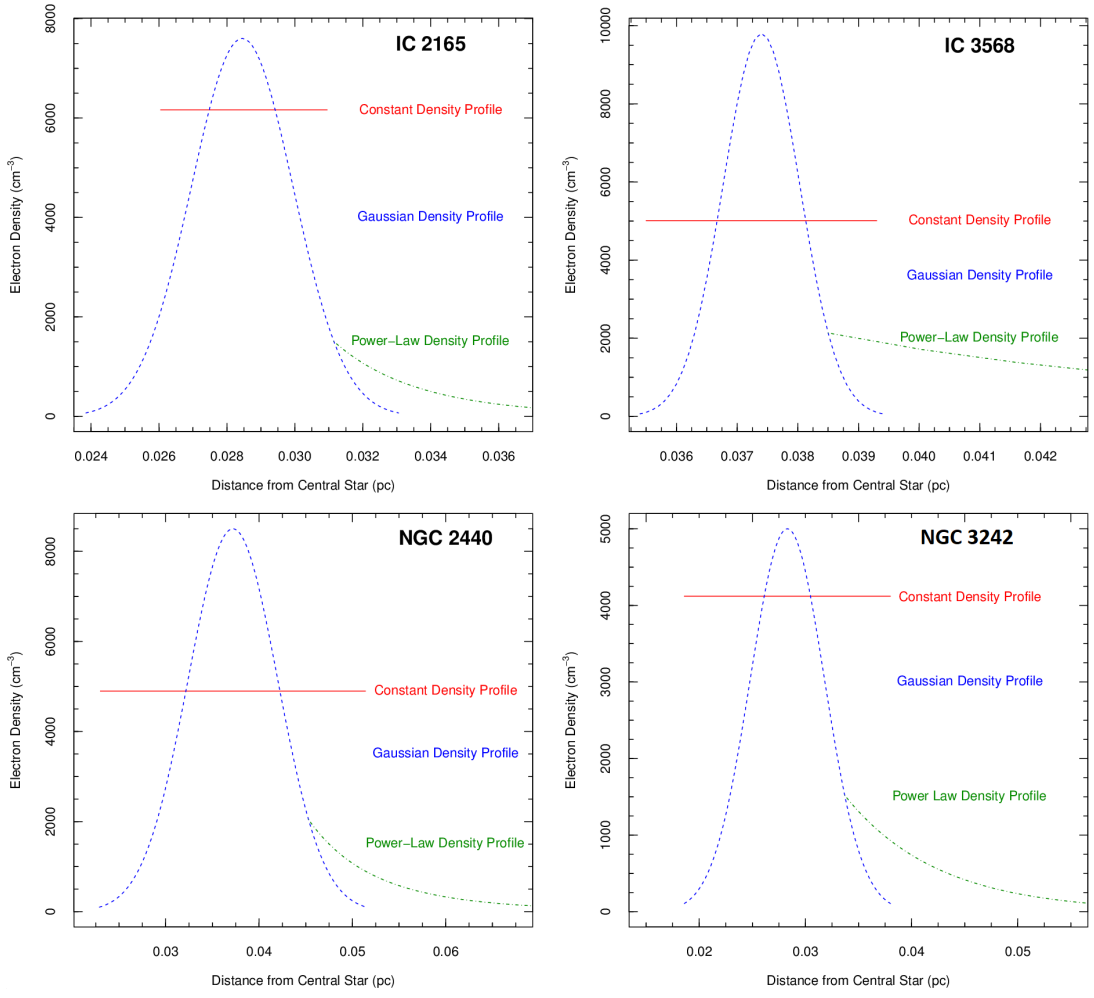

Fig. 4.4.— The same as Figure 4.3 but for NGC 5315, NGC 5882, and NGC 7662.

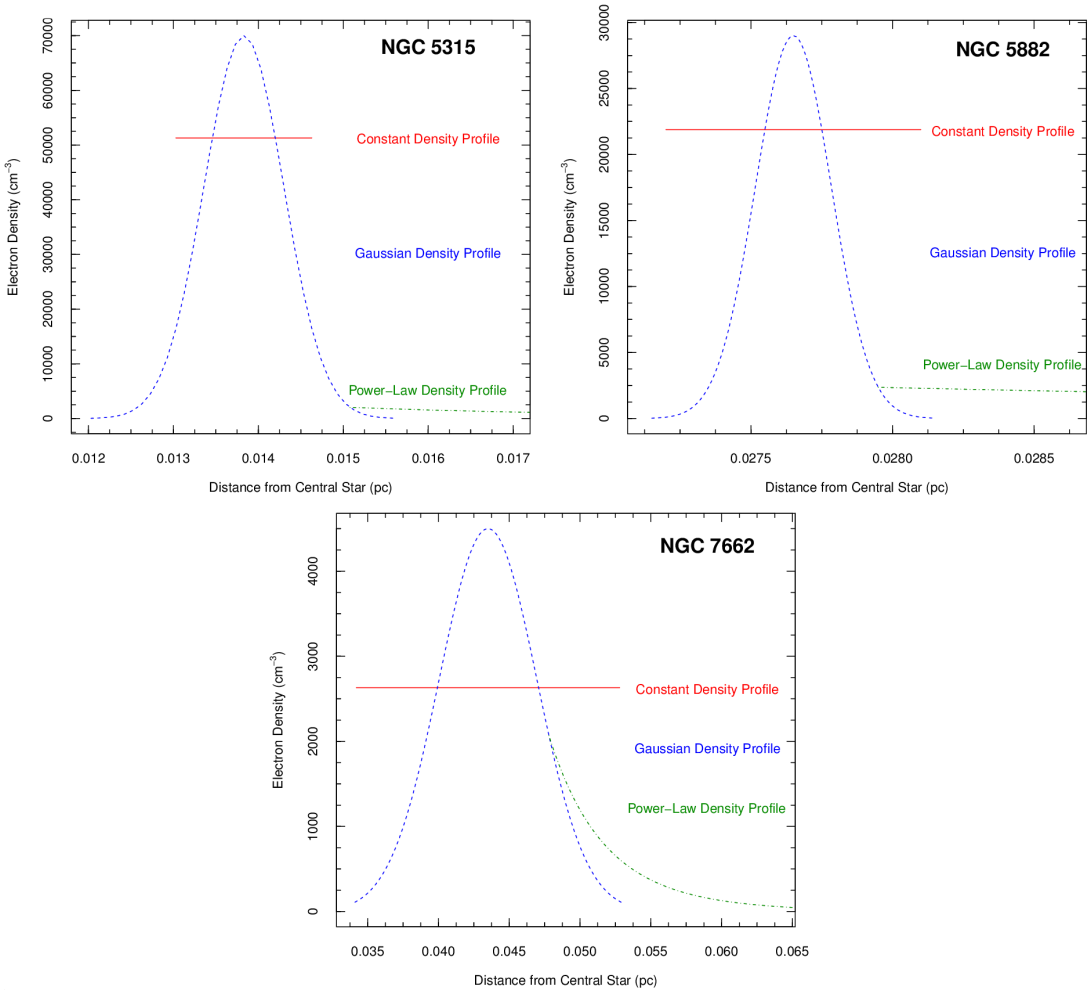

Center for Education and Research at the University of Oklahoma. The benefit of this method is that local minima can be easily identified and avoided. The downside is the sheer number of models required to adequately probe each parameter. The second method determined the rms after each model run and kept parameters that reduced the rms value. This way drastically reduces the number of models required to be run but can be susceptible to stopping in local minima. Both methods were tested on NGC 3242 with negligible differences in the final stellar parameters found. Also, it was observed by inspecting the rms values from the large suite of models that local minima were not a major concern for the stellar parameters. Therefore, only the second method was used for the other six planetary nebulae.

Describing the first method in detail, a primary grid of 81,000 constant density models was produced for NGC 3242 by varying the stellar temperature and luminosity, the inner and outer radii, and the filling factor of the gas while holding the abundances of He, C, Ne, and O constant. The range of the stellar temperature and luminosity was between 50,000-100,000K ($\triangle$T = 1000K) and ($\log[L/L_{\odot}]$)=3.0-5.0 ($\triangle$dex = 0.1), respectively. These ranges cover all published values of these stellar parameters. The filling factor was varied between 0.01 and 0.5, a range which encompasses typical values of planetary nebulae, in steps of 0.01. The inner/outer radii were varied from 0.039pc/0.0415pc to 0.041pc/0.0437pc with a step size of 10^{-3}pc/10^{-4}pc, covering values that are reasonable for the assumed distance. The nebular composition was chosen to be the full region's values from Table 2.3, since all regions had elemental abundances within error of the full region's values. Grains were chosen to be the *planetary nebula* set internal to Cloudy with a fixed scaling factor of 1.0. The density was chosen to be the full region's value of 4500 cm^{-3} except for Regions 1, 2, 7, and 9.

Next, the set of observed emission line strengths for NGC 3242 were used to reduce the primary grid to a smaller group of models which were the most successful at reproducing the observations, as determined by the previously discussed rms analysis. Finally, within the refined boundaries of the previously discussed parameters, the abundances were varied within the observed errors to produce a secondary grid of over 10 million models to further reduce the model rms (9 parameters total with 6 steps in each parameter). Ultimately, the best values were found by starting with the best model from the grid, and manually adjusting each input parameter and keeping the values that lowered the model rms. An estimation of the error for each parameter was carried out by starting with the best (lowest rms) model and varying each parameter one at a time (the stellar temperature and luminosity were varied together) until the model rms was larger than the sum of the best fit model rms and observed rms[a], e.g. model rms > 0.21 (0.06+0.15) for Region Full of NGC 3242. This estimation process was used only for the constant density models, due to constraints imposed by computational time requirements.

For the second method, the nebular and stellar parameters described above were used as starting values and other parameters such as the grain properties and filling factor were set to typical PN values. The constant density profile was again chosen. The density was adjusted until the carbon density diagnostic, (C III] λ1909/[C III] λ1907), was within roughly 1% of the observed value. Next, the radius and overall thickness of the gas was adjusted until the line strength of Hβ was within 10% of the observed value. Finally, all other parameters (abundances, stellar properties, etc.) were adjusted as needed to get the rms down around 0.3, ensuring an average error for all lines and diagnostics near 10%. From there, the

[a]Admittedly, each parameter is not fully independent. However, varying the stellar parameters together takes into account more of the covariance.

best parameters set so far were entered into a script that varied each parameter one at a time, calculated the rms after each model run by calling PANIC, compared the new rms to the previous values, and retained the sets that resulted in a smaller rms. It continuously looped through all parameters until it failed to produce a lower rms value. To minimize convergence times, the step size for each parameter began at relatively large values (e.g. $\triangle$T=500K, log[L/L$_{\odot}$] $\triangle$dex=0.1, abundance $\triangle$dex=0.1), but then was reduced to smaller values (e.g. $\triangle$T=100K, log[L/L$_{\odot}$] $\triangle$dex=0.01, abundance $\triangle$dex=0.01) to yield the smallest rms and subsequent best parameters.

The Gaussian and Gaussian with a power-law density profiles initially assumed the best fit constant density parameters as the initial values with the inner and outer radii held fixed. Since there is less gas contained within a Gaussian profile of equal height and width relative to a constant profile, the density peak of the Gaussian profile was increased by trial and error to compensate for the decrease in the Hβ line strength. However, for NGC 5315, the increase was found to be too large to keep the carbon density diagnostic within reasonable error, so the inner and outer radii were increased while keeping the peak of the Gaussian distribution located at the midpoint of the best constant density model. The slope of the power-law was chosen such that the Gaussian side of the profile was around 2000 cm^{-3} and decreased to about 10 cm^{-3} at the location of the outermost known shell/halo of each planetary nebula. The error estimation process was the same as what was described above in the first method.

Table 4.1 contains the ratios of the model-predicted strengths to their observed counterparts of important emission lines for each nebular region. The wavelength of each emission line is in the first column followed by the identification of the ion that produces it in the second column. The remaining columns contain the individual region's model/observed ratios. The majority of modeled lines for each

full region fall within the respective errors shown in Table 2.1. Region Full of NGC 3242 has the most lines that are outside the errors listed in Tables 2.1. This is probably due to the modeling assumptions becoming less valid compared to the smaller regions and the smaller uncertainties in the line strengths. Table 4.2 provides the same type of comparison as Table 4.1 but for the other two density profiles and only for the full regions. IC 2165 and NGC 2440 have the largest increase in the number of lines falling outside of the observed errors for the two non-constant density profiles compared to the constant density profile. This suggests that these PN are better represented by the constant density profile.

Table 4.1. Constant Density Model Emission Lines Compared to Observations

Constant Density Model Emission Lines Compared to Observations						
Wave (Å)	ID	IC2165 Full Model/Observed	IC2165 1 Model/Observed	IC2165 2 Model/Observed	IC2165 3 Model/Observed	IC2165 4 Model/Observed
1485	N IV]	1.00±0.11	1.00±0.15	1.00±0.15	1.00±0.13	1.01±0.13
1907	[C III]	1.01±0.11	0.96±0.13	1.05±0.15	1.03±0.13	1.06±0.13
1909[b]	C III]	1.00±0.11	0.97±0.13	1.04±0.15	1.03±0.13	1.06±0.13
3869	[Ne III]	1.00±0.07	1.00±0.07	1.00±0.11	1.00±0.12	1.01±0.11
4363[b]	[O III]	1.01±0.11	0.87±0.18	1.11±0.14	1.04±0.20	1.10±0.22
4686	He II	1.00±0.05	1.09±0.06[a]	0.81±0.06[a]	0.97±0.06	0.85±0.05[a]
4861	Hβ	0.98±0.03	1.00±0.04	0.95±0.05	0.94±0.04[a]	0.84±0.04[a]
4959[b]	[O III]	1.03±0.03	0.99±0.03	1.04±0.04	1.01±0.03	1.11±0.03
5007	[O III]	1.01±0.02	0.95±0.03[a]	1.04±0.03[a]	1.03±0.03	1.08±0.03[a]
5876	He I	1.00±0.14	1.06±0.28	0.95±0.41	0.98±0.32	0.93±0.37
7136	[Ar III]	1.00±0.14	1.00±0.15	1.00±0.30	1.00±0.15	1.00±0.22
9532	[S III]	1.00±0.06	1.00±0.12	1.00±0.10	1.00±0.12	1.00±0.14

		IC2165 5 Model/Observed	IC2165 6 Model/Observed	IC3568 Full Model/Observed	IC3568 1 Model/Observed	IC3568 2 Model/Observed
1485	N IV]	1.00±0.16	0.97±0.56	···	···	···
1549	C IV	···	···	1.00±0.13	1.00±0.19	1.02±0.17
1907	[C III]	0.92±0.14	0.91±0.33	1.00±0.10	1.02±0.14	0.99±0.16
1909[b]	C III]	0.92±0.14	0.91±0.34	1.01±0.11	1.01±0.18	1.03±0.17
3869	[Ne III]	0.99±0.08	0.99±0.18	1.00±0.06	1.00±0.19	1.01±0.06
4363[b]	[O III]	0.81±0.16[a]	0.96±0.73	0.99±0.31	1.01±0.21	0.97±0.41
4686	He II	1.00±0.08	···	···	···	···
4861	Hβ	1.10±0.04[a]	1.21±0.10[a]	0.94±0.03[a]	0.87±0.04[a]	0.96±0.04
4959[b]	[O III]	0.87±0.03[a]	0.99±0.07	1.12±0.02[a]	1.18±0.03[a]	1.13±0.03[a]
5007	[O III]	0.89±0.03[a]	0.87±0.07[a]	1.00±0.02	1.07±0.03[a]	1.01±0.03
5876	He I	1.03±0.14	1.01±0.28	1.00±0.14	0.99±0.24	1.00±0.29
7136	[Ar III]	1.01±0.13	1.00±0.24	1.00±0.21	1.01±0.32	1.00±0.31
9532	[S III]	0.99±0.07	1.00±0.18	···	···	···

Table 4.1—Continued

Constant Density Model Emission Lines Compared to Observations						
Wave		IC3568 3	NGC2440 Full	NGC2440 1	NGC2440 2	NGC2440 3
(Å)	ID	Model/Observed	Model/Observed	Model/Observed	Model/Observed	Model/Observed
1485	N IV]	···	0.98±0.12	0.97±0.11	0.79±0.21	0.85±0.11[a]
1907	[C III]	1.00±0.47	0.99±0.12	0.95±0.10	0.99±0.21	0.92±0.11
1909[b]	C III]	1.00±0.47	0.97±0.12	1.01±0.11	0.96±0.21	0.91±0.11
3727	[O II]	···	0.98±0.06	0.93±0.06[a]	1.11±0.87	0.93±0.08
3869	[Ne III]	1.00±0.29	1.00±0.05	0.98±0.06	1.01±0.27	0.98±0.06
4363[b]	[O III]	0.98±0.96	1.00±0.10	0.70±0.08[a]	1.05±0.52	0.97±0.09
4686	He II	···	1.03±0.04	1.14±0.04[a]	0.89±0.07[a]	1.06±0.04[a]
4861	Hβ	1.02±0.14	0.98±0.04	0.84±0.03[a]	1.01±0.07	1.14±0.04[a]
4959[b]	[O III]	1.13±0.09[a]	1.01±0.02	0.84±0.02[a]	1.05±0.05	1.02±0.02
5007	[O III]	0.98±0.09	0.99±0.02	0.84±0.02[a]	0.94±0.04[a]	1.04±0.02[a]
5876	He I	1.00±0.74	1.01±0.10	1.09±0.16	···	1.05±0.17
6584	[N II]	···	1.02±0.00[a]	0.97±0.00[a]	1.14±0.02[a]	1.05±0.00[a]
7136	[Ar III]	1.00±0.70	1.00±0.04	1.00±0.06	1.01±0.19	1.01±0.04
9532	[S III]	···	1.00±0.04	0.99±0.09	1.00±0.27	1.00±0.06

		NGC3242 Full	NGC3242 1	NGC3242 2	NGC3242 3	NGC3242 4
		Model/Observed	Model/Observed	Model/Observed	Model/Observed	Model/Observed
1485	N IV]	1.00±0.09	1.00±0.35	1.00±0.17	1.00±0.15	1.00±0.19
1907	[C III]	1.05±0.03[a]	1.01±0.20	1.01±0.09	1.01±0.10	1.01±0.13
1909[b]	C III]	1.05±0.04[a]	1.01±0.20	1.01±0.08	1.02±0.11	1.00±0.14
3727	[O II]	0.95±0.40	···	···	···	···
3869	[Ne III]	1.04±0.02[a]	1.01±0.08	1.00±0.07	1.00±0.06	1.01±0.06
4363[b]	[O III]	1.08±0.07[a]	0.99±0.35	0.97±0.09	0.93±0.17	0.95±0.19
4686	He II	0.94±0.02[a]	1.00±0.21	0.90±0.07[a]	0.90±0.04[a]	0.99±0.11
4861	Hβ	0.91±0.01[a]	0.93±0.06[a]	0.96±0.03[a]	0.94±0.03[a]	0.98±0.04
4959[b]	[O III]	1.07±0.01[a]	1.02±0.04	1.01±0.02	1.00±0.02	0.99±0.03
5007	[O III]	1.08±0.01[a]	1.03±0.04	1.02±0.02	1.01±0.02	1.01±0.03
5876	He I	0.96±0.07	1.00±0.23	0.95±0.19	0.98±0.38	1.00±0.38

Table 4.1—Continued

Constant Density Model Emission Lines Compared to Observations						
Wave (Å)	ID	NGC3242 Full Model/Observed	NGC3242 1 Model/Observed	NGC3242 2 Model/Observed	NGC3242 3 Model/Observed	NGC3242 4 Model/Observed
7136	[Ar III]	1.00±0.11	···	···	···	···
9532	[S III]	1.01±0.20	···	···	···	···

		NGC3242 5 Model/Observed	NGC3242 6 Model/Observed	NGC3242 7 Model/Observed	NGC3242 8 Model/Observed	NGC3242 9 Model/Observed
1485	N IV]	1.01±0.20	1.00±0.20	1.00±0.15	1.00±0.14	1.00±0.31
1907	[C III]	1.02±0.12	1.01±0.12	1.02±0.13	1.00±0.11	0.99±0.14
1909[b]	C III]	1.03±0.13	1.01±0.11	1.03±0.12	1.00±0.11	1.00±0.14
3869	[Ne III]	1.01±0.06	1.00±0.06	1.01±0.06	1.00±0.05	1.00±0.06
4363[b]	[O III]	1.07±0.25	1.01±0.27	1.10±0.25	0.93±0.15	0.99±0.14
4686	He II	1.00±0.07	0.99±0.09	0.99±0.08	0.73±0.04[a]	0.96±0.10
4861	Hβ	0.89±0.04[a]	0.95±0.03[a]	0.97±0.04	0.96±0.03[a]	0.98±0.04
4959[b]	[O III]	1.07±0.02[a]	1.02±0.02	1.07±0.03[a]	0.99±0.02	1.02±0.03
5007	[O III]	1.08±0.02[a]	1.03±0.02[a]	1.08±0.02[a]	1.01±0.02	1.03±0.03
5876	He I	0.99±0.31	1.00±0.34	0.98±0.27	0.89±0.27	0.99±0.35

		NGC5315 Full Model/Observed	NGC5315 1 Model/Observed	NGC5315 2 Model/Observed	NGC5315 3 Model/Observed	NGC5315 4 Model/Observed
1549	C IV	0.99±0.04	0.99±0.11	0.99±0.06	1.04±0.06	0.99±0.18
1907	[C III]	1.00±0.07	1.00±0.23	1.01±0.06	0.97±0.12	0.98±0.30
1909[b]	C III]	1.01±0.05	1.00±0.25	1.04±0.03[a]	1.02±0.09	0.98±0.25
3869	[Ne III]	0.99±0.01	1.00±0.08	1.00±0.01	1.01±0.02	1.01±0.09
4363[b]	[O III]	0.99±0.06	1.02±0.36	1.03±0.02[a]	1.14±0.14	1.09±0.66
4861	Hβ	1.06±0.01[a]	1.00±0.03	0.90±0.01[a]	0.89±0.01[a]	0.91±0.04[a]
4959[b]	[O III]	0.98±0.01[a]	1.28±0.03[a]	0.99±0.01	1.13±0.01[a]	1.25±0.03[a]
5007	[O III]	0.98±0.00[a]	0.99±0.02	1.02±0.00[a]	1.06±0.01[a]	1.04±0.03[a]
5876	He I	1.01±0.01	0.99±0.13	1.00±0.01	0.96±0.01[a]	0.97±0.05
7136	[Ar III]	0.99±0.00[a]	1.00±0.02	1.00±0.00	1.01±0.01	1.01±0.04

Table 4.1—Continued

Constant Density Model Emission Lines Compared to Observations						
Wave		NGC5315 Full	NGC5315 1	NGC5315 2	NGC5315 3	NGC5315 4
(Å)	ID	Model/Observed	Model/Observed	Model/Observed	Model/Observed	Model/Observed
9532	[S III]	0.96±0.01[a]	1.02±0.02	1.02±0.00[a]	1.08±0.01[a]	1.08±0.03[a]
		NGC5882 Full	NGC5882 1	NGC5882 2	NGC5882 3	
		Model/Observed	Model/Observed	Model/Observed	Model/Observed	
1549	C IV	1.00±0.24	0.91±0.35	0.91±0.19	1.08±1.10	
1907	[C III]	1.00±0.14	···	···	···	
1909[b]	C III]	0.99±0.11	1.03±0.26[c]	1.07±0.15[c]	0.89±0.26[c]	
3869	[Ne III]	1.02±0.04	1.02±0.05	1.04±0.03[a]	1.02±0.09	
4363[b]	[O III]	1.13±0.20	1.22±0.35	1.00±0.23	0.94±0.86	
4686	He II	0.98±0.24	0.92±0.22	0.84±0.18	···	
4861	Hβ	0.81±0.02[a]	0.84±0.03[a]	0.77±0.01[a]	0.82±0.04[a]	
4959[b]	[O III]	1.33±0.02[a]	1.40±0.02[a]	1.25±0.01[a]	1.27±0.03[a]	
5007	[O III]	1.12±0.02[a]	1.19±0.02[a]	1.07±0.01[a]	1.06±0.03[a]	
5876	He I	0.98±0.05	0.95±0.12	0.94±0.05[a]	1.01±0.09	
6584	[N II]	1.00±0.03	1.00±0.02	1.01±0.04	1.01±0.05	
7136	[Ar III]	1.00±0.05	0.99±0.07	1.03±0.03	1.01±0.09	
9532	[S III]	1.02±0.03	1.00±0.04	1.02±0.03	1.01±0.07	
		NGC7662 Full	NGC7662 1	NGC7662 2	NGC7662 3	NGC7662 4
		Model/Observed	Model/Observed	Model/Observed	Model/Observed	Model/Observed
1485	N IV]	1.07±0.06[a]	1.01±0.19	1.03±0.10	1.00±0.14	0.97±0.10
1549	C IV	1.00±0.04	0.96±0.09	0.82±0.05[a]	0.94±0.10	0.97±0.07
1750	N III]	0.90±0.24	···	···	···	···
1907	[C III]	0.96±0.04	1.01±0.09	1.12±0.05[a]	1.05±0.11	0.95±0.07
1909[b]	C III]	0.95±0.05	1.00±0.10	1.12±0.05[a]	1.04±0.11	0.96±0.07
3727	[O II]	1.02±0.30	···	···	···	···
3869	[Ne III]	0.98±0.03	0.99±0.05	1.01±0.04	1.00±0.06	0.99±0.03
4363[b]	[O III]	0.83±0.06[a]	0.93±0.14	1.10±0.10	1.08±0.08	0.93±0.04[a]

Table 4.1—Continued

Constant Density Model Emission Lines Compared to Observations

Wave (Å)	ID	NGC7662 Full Model/Observed	NGC7662 1 Model/Observed	NGC7662 2 Model/Observed	NGC7662 3 Model/Observed	NGC7662 4 Model/Observed
4686	He II	1.02±0.02[a]	1.06±0.05[a]	0.93±0.02[a]	0.99±0.04	0.47±0.02[a]
4861	Hβ	0.99±0.01	1.04±0.03[a]	0.89±0.02[a]	0.88±0.03[a]	1.08±0.02[a]
4959[b]	[O III]	1.02±0.01[a]	1.02±0.02	1.07±0.01[a]	1.19±0.02[a]	1.02±0.02
5007	[O III]	0.93±0.01[a]	0.93±0.02[a]	1.01±0.01	1.02±0.02	0.93±0.02[a]
5876	He I	1.02±0.14	···	0.97±0.48	···	0.99±0.31
7136	[Ar III]	1.00±0.12	1.00±0.14	1.04±0.12	1.00±0.09	0.94±0.12
9532	[S III]	0.99±0.09	1.00±0.16	1.04±0.16	1.01±0.19	0.93±0.15

Wave (Å)	ID	NGC7662 5 Model/Observed	NGC7662 6 Model/Observed	NGC7662 7 Model/Observed	NGC7662 8 Model/Observed
1485	N IV]	1.07±0.11	1.00±0.10	0.97±0.12	1.01±0.17
1549	C IV	1.00±0.05	1.01±0.04	0.96±0.08	0.86±0.08[a]
1750	N III]	0.91±0.29	···	···	···
1907	[C III]	0.98±0.05	0.97±0.04	0.98±0.08	0.98±0.08
1909[b]	C III]	0.97±0.06	0.97±0.04	0.99±0.08	0.93±0.09
3727	[O II]	···	···	1.06±0.30	···
3869	[Ne III]	0.96±0.03[a]	0.99±0.02	1.00±0.04	0.97±0.04
4363[b]	[O III]	0.91±0.17	0.90±0.08[a]	0.86±0.08[a]	0.80±0.19[a]
4686	He II	0.56±0.02[a]	0.95±0.02[a]	1.11±0.04[a]	1.13±0.06[a]
4861	Hβ	1.07±0.02[a]	1.08±0.01[a]	0.91±0.03[a]	1.20±0.03[a]
4959[b]	[O III]	0.98±0.01[a]	1.01±0.01	1.00±0.02	0.73±0.01[a]
5007	[O III]	0.93±0.01[a]	0.92±0.01[a]	0.87±0.02[a]	0.72±0.01[a]
5876	He I	0.95±0.25	0.99±0.11	1.03±0.23	···
7136	[Ar III]	0.97±0.18	0.99±0.17	0.97±0.11	···
9532	[S III]	0.97±0.14	1.00±0.13	0.98±0.17	···

[a]Modeled emission line intensity outside observed error bar.

[b]This line was only included in a diagnostic for the rms calculation for reasons discussed in the text.

[c]Blended 1907 and 1909.

Table 4.2. Non-constant Density Model Emission Lines Compared to Observations For Full Regions

Non-constant Density Model Emission Lines Compared to Observations For Full Regions							
		IC2165 Full		IC3568 Full		NGC2440 Full	
Wave		Gaussian	Gaussian With power-law	Gaussian	Gaussian With power-law	Gaussian	Gaussian With power-law
(Å)	ID	Model/Observed	Model/Observed	Model/Observed	Model/Observed	Model/Observed	Model/Observed
1485	N IV]	1.00±0.11	1.00±0.11	···	···	0.77±0.12[a]	0.77±0.12[a]
1549	C IV	···	···	1.01±0.13	1.01±0.13	···	···
1907	[C III]	1.04±0.11	1.06±0.11	0.99±0.10	0.99±0.10	1.02±0.12	1.00±0.12
1909[b]	C III]	1.12±0.11[a]	1.14±0.11[a]	1.08±0.11	1.06±0.11	1.04±0.12	1.02±0.12
3727	[O II]	···	···	···	···	0.83±0.06[a]	0.83±[a] 0.06
3869	[Ne III]	1.00±0.07	1.00±0.07	0.99±0.06	0.99±0.06	0.99±0.05	1.02±0.05
4363[b]	[O III]	1.13±0.11[a]	1.15±0.11[a]	1.05±0.31	0.99±0.31	1.06±0.10	1.04±0.10
4686	He II	0.99±0.05	1.00±0.05	···	···	1.12±0.04[a]	1.10±0.04[a]
4861	Hβ	0.97±0.03	0.98±0.03	0.99±0.03	1.02±0.03	1.03±0.04	1.02±0.04
4959[b]	[O III]	1.08±0.03[a]	1.09±0.03[a]	1.19±0.02[a]	1.12±0.02[a]	1.10±0.02[a]	1.07±0.02[a]
5007	[O III]	1.06±0.02[a]	1.07±0.02[a]	1.06±0.02[a]	1.00±0.02	1.08±0.02[a]	1.06±0.02[a]
5876	He I	0.98±0.14	0.99±0.14	0.99±0.14	1.00±0.14	1.03±0.10	1.02±0.10
6584	[N II]	···	···	···	···	1.16±0.00[a]	1.16±0.00[a]
7136	[Ar III]	1.00±0.14	0.99±0.14	0.99±0.21	1.00±0.21	1.08±0.04[a]	1.07±0.04[a]
9532	[S III]	1.00±0.06	0.99±0.06	···	···	1.05±0.04[a]	1.04±0.04

Table 4.2—Continued

Non-constant Density Model Emission Lines Compared to Observations For Full Regions							
		NGC5315 Full		NGC5882 Full		NGC3242 Full	
Wave		Gaussian	Gaussian With power-law	Gaussian	Gaussian With power-law	Gaussian	Gaussian With power-law
(Å)	ID	Model/Observed	Model/Observed	Model/Observed	Model/Observed	Model/Observed	Model/Observed
1485	N IV]	···	···	···	···	1.00±0.09	1.00±0.09
1549	C IV	1.00±0.04	0.99±0.04	1.00±0.24	1.16±0.24	···	···
1907	[C III]	0.99±0.07	0.99±0.07	1.00±0.14	1.00±0.14	1.10±0.03[a]	1.11±0.03[a]
1909[b]	C III]	1.07±0.05[a]	1.07±0.05[a]	1.00±0.11	0.99±0.11	1.10±0.04[a]	1.11±0.04[a]
3727	[O II]	···	···	···	···	0.95±0.40	0.90±0.40
3869	[Ne III]	1.00±0.01	0.99±0.01	1.03±0.04	1.07±0.04[a]	1.05±0.02[a]	1.02±0.02
4363[b]	[O III]	1.05±0.06	1.02±0.06	1.12±0.20	1.14±0.20	1.13±0.07[a]	1.18±0.07[a]
4686	He II	···	···	0.99±0.24	0.96±0.24	0.90±0.02[a]	0.93±0.02[a]
4861	Hβ	1.03±0.01[a]	1.04±0.01[a]	0.81±0.02[a]	0.86±0.02[a]	0.92±0.01[a]	0.94±0.01[a]
4959[b]	[O III]	1.01±0.01	1.00±0.01	1.32±0.02[a]	1.37±0.02[a]	1.09±0.01[a]	1.12±0.01[a]
5007	[O III]	0.99±0.00[a]	0.98±0.00[a]	1.11±0.02[a]	1.16±0.02[a]	1.11±0.01[a]	1.13±0.01[a]
5876	He I	1.01±0.01	1.00±0.01	0.99±0.05	1.05±0.05	0.92±0.07[a]	0.95±0.07
6584	[N II]	···	···	1.00±0.03	0.98±0.03	···	···
7136	[Ar III]	0.98±0.00[a]	1.00±0.00	1.00±0.05	0.99±0.05	1.00±0.11	1.03±0.11
9532	[S III]	0.95±0.01[a]	0.95±0.01[a]	1.01±0.03	1.01±0.03	1.02±0.20	1.03±0.20

Table 4.2—Continued

Non-constant Density Model Emission Lines Compared to Observations For Full Regions			
		NGC7662 Full	
		Gaussian	Gaussian With power-law
Wave (Å)	ID	Model/Observed	Model/Observed
1485	N IV]	1.02±0.06	1.02±0.06
1549	C IV	0.93±0.04[a]	0.91±0.04[a]
1750	N III]	1.00±0.24	0.99±0.24
1907	[C III]	1.04±0.04	1.04±0.04
1909[b]	C III]	1.06±0.05[a]	1.07±0.05[a]
3727	[O II]	0.90±0.30	0.90±0.30
3869	[Ne III]	1.00±0.03	1.01±0.03
4363[b]	[O III]	0.91±0.06[a]	0.92±0.06[a]
4686	He II	1.04±0.02[a]	1.03±0.02[a]
4861	Hβ	0.97±0.01[a]	0.99±0.01
4959[b]	[O III]	1.07±0.01[a]	1.09±0.01[a]
5007	[O III]	0.98±0.01[a]	0.99±0.01
5876	He I	1.03±0.14	1.02±0.14
7136	[Ar III]	1.00±0.12	1.00±0.12
9532	[S III]	1.00±0.09	1.01±0.09

[a]Modeled emission line intensity outside observed error bar.

[b]This line was only included in a diagnostic for the rms calculation for reasons discussed in the text.

Table 4.3 contains the best parameter values and associated errors for the constant density models. Names of the stellar and nebular parameters that were used in the modeling are in the first column along with the values for each region in the subsequent columns. Below the modeling parameters are the nebular temperatures, densities, ionization correction factors, and rms values for each region. For most of the regions, the model rms is below the observed rms, implying a good fit. The smallest model rms of 0.0063 from the full region of IC 2165 shows that the assumed model represented that region's structure quite well. In most cases, the modeled temperatures and densities of the gas are within the observed errors. Also, the model abundances for the regions agree within error with the observed abundances in most cases. The asymmetry in the errors is due to the $1 - \frac{model}{observed}$ term in the equation for the rms having a lower bound of 1. The errors in stellar temperature and luminosity and nebular abundances are inversely related to overall signal strength in the emission lines, where the larger error corresponds to overall weaker signal strength.

Table 4.3. Constant Density Models

Constant Density Models					
Parameter	IC2165 Full	IC2165 1	IC2165 2	IC2165 3	IC2165 4
T_{star} (kK)	$110.0^{+7.0}_{-17.0}$	110.0	110.0	110.0	110.0
L_{star} (log[L/$L_{\odot}$])	$3.17^{+0.20}_{-0.14}$	3.17	3.17	3.17	3.17
Distance (kpc)	$2.39^{+0.36}_{-0.33}$	2.39	2.39	2.39	2.39
H_{den} (log[$H_{density}$])	$3.79^{+0.02}_{-0.03}$	$3.75^{+0.04}_{-0.04}$	$4.06^{+0.05}_{-0.07}$	$3.70^{+0.04}_{-0.04}$	$3.75^{+0.04}_{-0.05}$
Inner Radius (10^{-2}pc)	$2.60^{+0.06}_{-0.06}$	$2.56^{+0.11}_{-0.15}$	$2.60^{+0.05}_{-0.04}$	$2.38^{+0.15}_{-0.16}$	$2.47^{+0.13}_{-0.13}$
Outer Radius (10^{-2}pc)	$3.09^{+0.05}_{-0.05}$	$3.09^{+0.08}_{-0.07}$	$2.73^{+0.04}_{-0.05}$	$3.11^{+0.12}_{-0.11}$	$2.96^{+0.12}_{-0.12}$
Filling Factor (10^{-1})	$9.89^{+0.11}_{-0.99}$	$10.00^{+0.00}_{-0.16}$	$9.49^{+0.51}_{-2.97}$	$10.00^{+0.00}_{-0.17}$	$10.0^{+0.00}_{-0.25}$
He/H (10^{-2})	$10.28^{+1.41}_{-1.29}$	$11.07^{+2.58}_{-2.03}$	$10.26^{+4.20}_{-5.03}$	$10.33^{+2.55}_{-2.01}$	$10.47^{+3.33}_{-3.23}$
C/H (10^{-4})	$4.57^{+2.41}_{-1.59}$	$4.75^{+5.55}_{-2.63}$	$2.86^{+5.15}_{-2.16}$	$4.35^{+4.78}_{-2.30}$	$3.80^{+5.97}_{-2.45}$
N/H (10^{-4})	$1.10^{+0.43}_{-0.43}$	$0.78^{+0.56}_{-0.55}$	$1.38^{+1.52}_{-1.35}$	$0.94^{+0.34}_{-0.66}$	$0.95^{+0.91}_{-0.87}$
O/H (10^{-4})	$2.69^{+0.91}_{-0.80}$	$2.89^{+1.95}_{-1.49}$	$1.75^{+1.80}_{-1.38}$	$2.68^{+1.89}_{-1.42}$	$2.82^{+2.43}_{-1.84}$
Ne/H (10^{-5})	$3.39^{+1.32}_{-1.31}$	$3.70^{+2.70}_{-2.63}$	$2.10^{+2.14}_{-2.06}$	$2.98^{+2.15}_{-2.07}$	$2.90^{+2.72}_{-2.65}$
S/H (10^{-6})	$3.73^{+1.42}_{-1.44}$	$3.56^{+2.53}_{-2.50}$	$2.15^{+2.11}_{-2.11}$	$5.19^{+3.72}_{-3.57}$	$4.44^{+4.08}_{-4.02}$
Ar/H (10^{-7})	$20.09^{+7.58}_{-7.76}$	$24.89^{+17.77}_{-17.48}$	$9.86^{+9.86}_{-9.68}$	$26.06^{+17.6}_{-18.12}$	$24.66^{+22.65}_{-22.47}$
[O III] T_e (K)	13500	13900	14800	13700	14100
[S II] N$_e$(cm^{-3})	7900	...	...	...	...
C III] N_e (cm^{-3})	7200	6600	14000	5800	6700
icf (O)	1.55	1.54	1.53	1.82	1.92
icf (Ar)	1.30	1.30	1.25	1.36	1.37
icf (Ne)	1.22	1.21	1.18	1.38	1.41
icf (S)	4.30	4.43	3.30	6.07	5.98
Model RMS (10^{-2})	0.63	4.00	7.00	2.13	6.86
Observed RMS (10^{-2})	9.35	14.53	19.35	15.8	17.69

Table 4.3—Continued

Constant Density Models					
Parameter	IC2165 5	IC2165 6	IC3568 Full	IC3568 1	IC3568 2
T_{star} (kK)	110.0	110.0	$69.6^{+15.0}_{-18.3}$	69.6	69.6
L_{star} (log[L/$L_{\odot}$])	3.17	3.17	$3.52^{+0.74}_{-0.38}$	3.52	3.52
Distance (kpc)	2.39	2.39	$2.29^{+1.26}_{-0.67}$	2.29	2.29
H_{den} (log[$H_{density}$])	$3.62^{+0.03}_{-0.03}$	$3.99^{+0.09}_{-0.18}$	$3.70^{+0.05}_{-0.05}$	$3.76^{+0.06}_{-0.08}$	$3.59^{+0.06}_{-0.08}$
Inner Radius (10^{-2}pc)	$1.80^{+0.24}_{-0.37}$	$3.15^{+0.23}_{-0.91}$	$3.55^{+0.08}_{-0.09}$	$3.44^{+0.09}_{-0.09}$	$3.97^{+0.21}_{-0.20}$
Outer Radius (10^{-2}pc)	$3.32^{+0.12}_{-0.11}$	$3.57^{+0.06}_{-0.07}$	$3.93^{+0.09}_{-0.08}$	$3.74^{+0.10}_{-0.10}$	$4.66^{+0.24}_{-0.23}$
Filling Factor (10^{-1})	$9.92^{+0.08}_{-1.32}$	$9.64^{+0.36}_{-5.54}$	$10.00^{+0.00}_{-2.20}$	$9.88^{+0.12}_{-3.03}$	$9.96^{+0.04}_{-3.16}$
He/H (10^{-2})	$9.18^{+1.78}_{-1.42}$	$7.59^{+9.40}_{-7.59}$	$9.71^{+4.42}_{-4.46}$	$10.89^{+6.89}_{-7.34}$	$8.53^{+5.59}_{-5.58}$
C/H (10^{-4})	$5.85^{+5.63}_{-2.83}$	$38.73^{+212.46}_{-28.25}$	$5.47^{+2.85}_{-2.38}$	$2.85^{+2.05}_{-1.73}$	$7.08^{+5.51}_{-4.13}$
N/H (10^{-4})	$0.81^{+0.54}_{-0.50}$	$0.89^{+105.96}_{-0.89}$	...	...	...
O/H (10^{-4})	$2.54^{+1.54}_{-1.19}$	$5.31^{+12.47}_{-4.71}$	$4.72^{+1.30}_{-0.92}$	$4.25^{+1.78}_{-1.01}$	$5.02^{+2.23}_{-1.21}$
Ne/H (10^{-5})	$4.27^{+2.81}_{-2.64}$	$10.94^{+20.68}_{-10.94}$	$8.05^{+4.83}_{-4.34}$	$2.02^{+1.69}_{-1.57}$	$9.14^{+8.24}_{-6.90}$
S/H (10^{-6})	$5.05^{+3.27}_{-3.10}$	$2.30^{+3.73}_{-2.30}$	...	...	...
Ar/H (10^{-7})	$20.84^{+6.07}_{-12.72}$	$12.25^{+20.11}_{-12.25}$	$17.22^{+9.39}_{-9.46}$	$16.33^{+13.18}_{-12.70}$	$15.89^{+12.95}_{-12.50}$
[O III] T_e (K)	12800	9500	10000	10800	9600
C III] N_e (cm^{-3})	4600	11100	5600	6500	4200
icf (O)	1.31	1.02	1.07	1.08	1.07
icf (Ar)	1.28	1.05	1.28	1.25	1.28
icf (Ne)	1.10	0.91	0.94	0.94	0.93
icf (S)	4.41	1.52	...	...	...
Model RMS (10^{-2})	5.09	7.93	1.70	4.42	2.04
Observed RMS (10^{-2})	11.40	32.67	13.39	17.49	19.79

Table 4.3—Continued

Constant Density Models					
Parameter	IC3568 3	NGC2440 Full	NGC2440 1	NGC2440 2	NGC2440 3
T_{star} (kK)	69.6	$169.8^{+20.2}_{-17.7}$	169.8	169.8	169.8
L_{star} (log[L/$L_{\odot}$])	3.52	$2.74^{+0.04}_{-0.04}$	2.74	2.74	2.74
Distance (kpc)	2.29	$1.63^{+0.14}_{-0.13}$	1.63	1.63	1.63
H_{den} (log[$H_{density}$])	$3.77^{+0.11}_{-0.25}$	$3.69^{+0.02}_{-0.02}$	$3.40^{+0.03}_{-0.03}$	$3.95^{+0.08}_{-0.15}$	$3.80^{+0.03}_{-0.03}$
Inner Radius (10^{-2}pc)	$3.83^{+0.14}_{-3.83}$	$2.30^{+0.70}_{-1.20}$	$3.86^{+0.94}_{-1.06}$	$2.46^{+0.36}_{-0.86}$	$2.28^{+0.58}_{-0.78}$
Outer Radius (10^{-2}pc)	$4.01^{+0.10}_{-0.12}$	$5.14^{+0.12}_{-0.14}$	$7.54^{+0.50}_{-0.45}$	$2.93^{+0.12}_{-0.15}$	$4.13^{+0.16}_{-0.18}$
Filling Factor (10^{-1})	$10.00^{+0.00}_{-7.00}$	$1.76^{+0.14}_{-0.16}$	$3.01^{+0.48}_{-0.44}$	$2.42^{+1.25}_{-1.40}$	$2.09^{+0.26}_{-0.30}$
He/H (10^{-2})	$9.73^{+12.15}_{-9.73}$	$12.27^{+1.85}_{-2.04}$	$14.93^{+3.44}_{-3.34}$	$12.25^{+19.38}_{-5.94}$	$11.40^{+2.72}_{-2.69}$
C/H (10^{-4})	$24.89^{+56.39}_{-24.89}$	$2.54^{+1.26}_{-1.06}$	$3.56^{+3.36}_{-2.33}$	$1.08^{+2.90}_{-1.08}$	$2.45^{+2.33}_{-1.62}$
N/H (10^{-4})	···	$6.71^{+2.00}_{-1.93}$	$8.71^{+4.78}_{-3.81}$	$3.41^{+4.91}_{-3.41}$	$6.34^{+3.43}_{-2.95}$
O/H (10^{-4})	$7.96^{+31.85}_{-4.65}$	$2.90^{+0.77}_{-0.72}$	$4.06^{+2.10}_{-1.49}$	$1.07^{+1.22}_{-1.07}$	$2.53^{+1.10}_{-0.98}$
Ne/H (10^{-5})	$11.53^{+25.62}_{-11.53}$	$4.02^{+1.61}_{-1.62}$	$7.50^{+5.38}_{-4.87}$	$0.92^{+1.71}_{-0.92}$	$3.16^{+2.09}_{-1.98}$
S/H (10^{-6})	···	$1.64^{+0.65}_{-0.64}$	$2.09^{+1.38}_{-1.33}$	$0.59^{+1.07}_{-0.59}$	$1.37^{+0.86}_{-0.85}$
Ar/H (10^{-7})	$24.38^{+41.69}_{-24.38}$	$14.96^{+6.17}_{-5.84}$	$23.44^{+15.46}_{-14.93}$	$7.59^{+13.79}_{-7.59}$	$12.79^{+8.10}_{-8.01}$
O III] T_e (K)	8800	14400	13300	16900	14600
[S II] $N_e(cm^{-3})$	···	6400	3400	···	8200
C III] N_e (cm^{-3})	6700	5800	2800	11300	7600
icf (O)	1.08	1.60	1.46	2.05	1.54
icf (Ar)	1.26	1.21	1.24	1.39	1.20
icf (Ne)	0.95	1.46	1.45	0.17	1.39
icf (S)	···	1.83	1.66	2.53	1.80
Model RMS (10^{-2})	1.00	1.49	8.45	9.20	6.97
Observed RMS (10^{-2})	49.97	7.44	8.35	35.57	8.75

Table 4.3—Continued

Constant Density Models					
	NGC3242 Full	NGC3242 1	NGC3242 2	NGC3242 3	NGC3242 4
T_{star} (kK)	$89.7^{+7.3}_{-4.7}$	89.7	89.7	89.7	89.7
L_{star} (log[L/$L_{\odot}$])	$3.36^{+0.28}_{-0.22}$	3.36	3.36	3.36	3.36
Distance (kpc)	$0.84^{+0.15}_{-0.32}$	0.84	0.84	0.84	0.84
H_{den} (log[$H_{density}$])	$3.62^{+0.04}_{-0.06}$	$3.25^{+0.06}_{-0.06}$	$3.77^{+0.04}_{-0.03}$	$3.50^{+0.06}_{-0.07}$	$3.50^{+0.06}_{-0.07}$
Inner Radius (10^{-2}pc)	$1.86^{+0.74}_{-1.86}$	$2.04^{+1.36}_{-2.04}$	$3.33^{+0.12}_{-0.16}$	$2.52^{+0.48}_{-0.82}$	$1.96^{+0.74}_{-1.96}$
Outer Radius (10^{-2}pc)	$3.80^{+0.30}_{-0.30}$	$10.50^{+2.90}_{-2.40}$	$3.90^{+0.13}_{-0.09}$	$4.59^{+0.81}_{-0.59}$	$10.20^{+2.60}_{-2.10}$
Filling Factor (10^{-1})	$4.36^{+1.14}_{-1.06}$	$4.39^{+1.31}_{-1.19}$	$4.80^{+1.00}_{-0.90}$	$5.93^{+1.77}_{-1.63}$	$1.56^{+0.54}_{-0.46}$
He/H (10^{-2})	$10.45^{+4.34}_{-3.03}$	$11.53^{+4.34}_{-3.38}$	$11.02^{+3.11}_{-2.31}$	$10.30^{+4.15}_{-3.39}$	$9.57^{+4.23}_{-3.95}$
C/H (10^{-4})	$5.97^{+7.52}_{-3.73}$	$4.85^{+4.92}_{-3.50}$	$3.67^{+2.35}_{-1.89}$	$5.01^{+5.46}_{-3.19}$	$4.10^{+4.03}_{-2.32}$
O/H (10^{-4})	$4.70^{+2.71}_{-1.81}$	$4.26^{+2.35}_{-1.30}$	$3.76^{+1.25}_{-0.94}$	$3.76^{+2.41}_{-1.57}$	$4.21^{+2.55}_{-1.58}$
Ne/H (10^{-5})	$7.40^{+6.73}_{-6.24}$	$7.78^{+7.36}_{-6.37}$	$6.40^{+3.60}_{-3.24}$	$6.19^{+5.03}_{-4.72}$	$6.90^{+5.40}_{-5.04}$
[O III] T_e (K)	11800	11100	11600	11800	11800
C III] N_e (cm^{-3})	4600	1500	6800	3500	3600
icf (O)	1.57	1.13	1.22	1.56	1.51
icf (Ne)	1.24	1.00	1.03	1.18	1.18
Model RMS (10^{-2})	6.26	2.40	3.75	4.46	1.63
Observed RMS (10^{-2})	15.02	20.91	10.68	17.06	18.57

Table 4.3—Continued

Constant Density Models					
Parameter	NGC3242 5	NGC3242 6	NGC3242 7	NGC3242 8	NGC3242 9
T_{star} (kK)	89.7	89.7	89.7	89.7	89.7
L_{star} (log[L/$L_{\odot}$])	3.36	3.36	3.36	3.36	3.36
Distance (kpc)	0.84	0.84	0.84	0.84	0.84
H_{den} (log[$H_{density}$])	$3.60^{+0.05}_{-0.06}$	$3.60^{+0.05}_{-0.06}$	$3.90^{+0.04}_{-0.04}$	$3.55^{+0.05}_{-0.06}$	$3.25^{+0.06}_{-0.07}$
Inner Radius (10^{-2}pc)	$2.52^{+0.48}_{-0.32}$	$1.88^{+0.52}_{-1.88}$	$2.02^{+0.08}_{-0.12}$	$2.98^{+0.22}_{-0.28}$	$3.56^{+0.84}_{-3.56}$
Outer Radius (10^{-2}pc)	$4.21^{+0.69}_{-0.41}$	$6.49^{+1.31}_{-0.96}$	$2.52^{+0.08}_{-0.12}$	$3.72^{+0.28}_{-0.22}$	$8.40^{+1.90}_{-1.50}$
Filling Factor (10^{-1})	$3.77^{+1.03}_{-0.97}$	$1.52^{+0.48}_{-0.42}$	$4.53^{+0.87}_{-0.83}$	$1.00^{+0.00}_{-0.27}$	$4.34^{+1.36}_{-1.34}$
He/H (10^{-2})	$10.12^{+3.69}_{-2.87}$	$9.20^{+3.68}_{-3.32}$	$9.29^{+2.19}_{-1.88}$	$7.69^{+2.78}_{-2.56}$	$10.50^{+4.64}_{-4.04}$
C/H (10^{-4})	$6.30^{+6.29}_{-2.39}$	$5.60^{+5.12}_{-3.09}$	$4.47^{+4.04}_{-2.65}$	$3.51^{+3.91}_{-2.36}$	$4.81^{+5.19}_{-3.15}$
O/H (10^{-4})	$5.30^{+2.65}_{-1.75}$	$5.08^{+2.68}_{-1.84}$	$3.77^{+1.60}_{-1.14}$	$3.30^{+1.94}_{-1.35}$	$4.54^{+2.38}_{-1.59}$
Ne/H (10^{-5})	$7.93^{+6.20}_{-5.74}$	$8.07^{+6.38}_{-5.67}$	$5.85^{+3.92}_{-3.71}$	$5.48^{+4.52}_{-4.10}$	$7.38^{+6.42}_{-5.72}$
[O III] T_e (K)	11500	11700	11700	11900	11500
C III] N_e (cm^{-3})	4500	4400	9200	3900	1600
icf (O)	1.54	1.74	1.35	1.46	1.46
icf (Ne)	1.19	1.30	1.09	1.07	1.16
Model RMS (10^{-2})	4.03	1.67	2.63	9.90	3.22
Observed RMS (10^{-2})	16.46	17.63	15.16	13.12	18.50

Table 4.3—Continued

Constant Density Models					
Parameter	NGC5315 Full	NGC5315 1	NGC5315 2	NGC5315 3	NGC5315 4
T_{star} (kK)	$69.9^{+6.5}_{-2.1}$	69.9	69.9	69.9	69.9
L_{star} (log[L/$L_{\odot}$])	$4.89^{+0.16}_{-0.15}$	4.89	4.89	4.89	4.89
Distance (kpc)	$2.02^{+0.07}_{-0.08}$	2.02	2.02	2.02	2.02
H_{den} (log[$H_{density}$])	$4.71^{+0.02}_{-0.02}$	$4.76^{+0.04}_{-0.05}$	$4.72^{+0.02}_{-0.02}$	$4.71^{+0.03}_{-0.03}$	$4.53^{+0.06}_{-0.09}$
Inner Radius (10^{-2}pc)	$1.31^{+0.01}_{-0.01}$	$1.56^{+0.03}_{-0.04}$	$1.88^{+0.01}_{-0.01}$	$2.13^{+0.01}_{-0.01}$	$1.89^{+0.25}_{-0.72}$
Outer Radius (10^{-2}pc)	$1.46^{+0.01}_{-0.01}$	$1.63^{+0.02}_{-0.02}$	$1.98^{+0.01}_{-0.01}$	$2.15^{+0.01}_{-0.01}$	$2.33^{+0.09}_{-0.11}$
Filling Factor (10^{-1})	$9.59^{+0.41}_{-0.71}$	$2.39^{+0.58}_{-0.60}$	$9.43^{+0.57}_{-0.63}$	$8.77^{+1.23}_{-1.41}$	$0.45^{+0.18}_{-0.18}$
He/H (10^{-2})	$11.40^{+1.78}_{-2.07}$	$11.99^{+5.38}_{-5.98}$	$13.21^{+2.28}_{-2.25}$	$16.29^{+4.60}_{-4.81}$	$16.48^{+10.43}_{-11.80}$
C/H (10^{-4})	$16.44^{+3.51}_{-2.64}$	$19.82^{+11.09}_{-10.04}$	$9.77^{+1.71}_{-1.64}$	$14.49^{+5.01}_{-4.72}$	$100.69^{+50.66}_{-63.54}$
O/H (10^{-4})	$6.31^{+1.10}_{-0.81}$	$6.81^{+3.91}_{-2.24}$	$7.46^{+1.05}_{-0.86}$	$9.93^{+2.95}_{-1.80}$	$15.31^{+14.89}_{-6.40}$
Ne/H (10^{-5})	$14.59^{+3.61}_{-3.37}$	$10.79^{+7.83}_{-7.07}$	$18.24^{+4.67}_{-4.11}$	$18.97^{+9.22}_{-8.25}$	$3.33^{+4.44}_{-3.04}$
S/H (10^{-6})	$421.70^{+35.39}_{-32.65}$	$287.08^{+101.97}_{-82.90}$	$248.89^{+26.54}_{-25.01}$	$245.47^{+56.52}_{-41.30}$	$314.05^{+132.63}_{-95.27}$
Ar/H (10^{-7})	$954.99^{+219.90}_{-196.42}$	$743.02^{+487.25}_{-447.90}$	$603.95^{+137.36}_{-136.21}$	$623.73^{+267.52}_{-252.20}$	$961.61^{+1033.65}_{-936.49}$
[O III] T_e (K)	8800	9600	8900	8600	7500
[S II] N$_e$(cm^{-3})	20000[a]	20000[a]	···	20000[a]	20000[a]
C III] N_e (cm^{-3})	64000	73400	66300	67200	45400
icf (O)	1.36	1.70	1.31	1.50	1.55
icf (Ar)	1.96	2.23	1.85	2.03	1.52
icf (Ne)	1.21	1.46	1.18	1.34	1.35
icf (S)	47.27	38.16	21.26	20.11	29.07
Model RMS (10^{-2})	2.23	0.93	3.16	5.19	3.80
Observed RMS (10^{-2})	3.90	16.53	3.53	7.06	23.73

Table 4.3—Continued

Constant Density Models				
Parameter	NGC5882 Full	NGC5882 1	NGC5882 2	NGC5882 3
T_{star} (kK)	$78.7^{+3.3}_{-7.0}$	78.7	78.7	78.7
L_{star} (log[L/$L_{\odot}$])	$3.45^{+0.20}_{-0.14}$	3.45	3.45	3.45
Distance (kpc)	$1.81^{+0.60}_{-0.82}$	1.81	1.81	1.81
H_{den} (log[$H_{density}$])	$4.34^{+0.05}_{-0.06}$	$4.35^{+0.05}_{-0.07}$	$4.35^{+0.04}_{-0.06}$	$4.35^{+0.06}_{-0.15}$
Inner Radius (10^{-2}pc)	$2.72^{+0.03}_{-0.03}$	$2.75^{+0.03}_{-0.03}$	$2.71^{+0.03}_{-0.03}$	$2.25^{+0.63}_{-0.76}$
Outer Radius (10^{-2}pc)	$2.81^{+0.03}_{-0.03}$	$2.83^{+0.03}_{-0.03}$	$2.80^{+0.03}_{-0.03}$	$2.96^{+0.08}_{-0.10}$
Filling Factor (10^{-1})	$3.47^{+0.94}_{-0.87}$	$2.47^{+0.76}_{-0.72}$	$3.14^{+0.78}_{-0.76}$	$2.91^{+0.95}_{-1.49}$
He/H (10^{-2})	$12.59^{+6.71}_{-5.39}$	$12.19^{+7.76}_{-6.02}$	$12.97^{+6.53}_{-5.39}$	$11.35^{+13.77}_{-11.35}$
C/H (10^{-4})	$4.19^{+3.72}_{-3.34}$	$2.37^{+1.90}_{-1.73}$	$6.30^{+3.70}_{-3.66}$	$9.33^{+16.37}_{-9.33}$
N/H (10^{-4})	$2.89^{+2.76}_{-2.78}$	$4.28^{+3.67}_{-3.65}$	$1.43^{+0.97}_{-1.01}$	$1.48^{+2.41}_{-1.48}$
O/H (10^{-4})	$12.82^{+6.13}_{-3.15}$	$11.86^{+6.34}_{-2.95}$	$13.77^{+5.28}_{-2.81}$	$16.14^{+31.72}_{-5.18}$
Ne/H (10^{-5})	$23.23^{+24.78}_{-19.43}$	$19.05^{+19.85}_{-15.16}$	$29.04^{+22.25}_{-18.08}$	$3.08^{+7.16}_{-3.08}$
S/H (10^{-6})	$7.85^{+6.94}_{-5.82}$	$8.30^{+7.55}_{-6.92}$	$7.33^{+4.97}_{-5.09}$	$7.36^{+12.14}_{-7.36}$
Ar/H (10^{-7})	$38.90^{+35.19}_{-35.04}$	$36.81^{+33.98}_{-31.32}$	$40.46^{+27.15}_{-28.71}$	$40.64^{+65.51}_{-40.64}$
[O III] T_e (K)	8400	8600	8200	7700
[S II] N$_e$(cm^{-3})	20000[a]	20000[a]	20000[a]	20000[a]
C III] N_e (cm^{-3})	26700	...	...	...
icf (O)	1.12	1.12	1.13	1.10
icf (Ar)	1.18	1.17	1.19	1.10
icf (Ne)	0.98	0.99	0.99	0.97
icf (S)	1.89	1.86	1.88	1.58
Model RMS (10^{-2})	5.58	7.60	9.20	7.50
Observed RMS (10^{-2})	14.20	16.48	11.56	41.36

Table 4.3—Continued

Constant Density Models					
Parameter	NGC7662 Full	NGC7662 1	NGC7662 2	NGC7662 3	NGC7662 4
T_{star} (kK)	$109.9^{+9.1}_{-5.9}$	109.9	109.9	109.9	109.9
L_{star} (log[L/$L_{\odot}$])	$3.24^{+0.18}_{-0.14}$	3.24	3.24	3.24	3.24
Distance (kpc)	$1.02^{+0.15}_{-0.22}$	1.02	1.02	1.02	1.02
H_{den} (log[$H_{density}$])	$3.42^{+0.04}_{-0.04}$	$3.54^{+0.04}_{-0.04}$	$3.70^{+0.05}_{-0.08}$	$3.60^{+0.04}_{-0.04}$	$3.32^{+0.06}_{-0.08}$
Inner Radius (10^{-2}pc)	$3.42^{+0.36}_{-0.63}$	$4.69^{+0.11}_{-0.09}$	$4.24^{+0.10}_{-0.08}$	$3.81^{+0.06}_{-0.09}$	$3.34^{+0.54}_{-3.34}$
Outer Radius (10^{-2}pc)	$5.28^{+0.36}_{-0.34}$	$5.47^{+0.19}_{-0.18}$	$4.55^{+0.13}_{-0.12}$	$4.37^{+0.16}_{-0.15}$	$8.49^{+1.61}_{-1.69}$
Filling Factor (10^{-1})	$10.00^{+0.00}_{-1.80}$	$9.40^{+0.60}_{-1.80}$	$10.00^{+0.00}_{-3.38}$	$10.00^{+0.00}_{-1.87}$	$10.00^{+0.00}_{-3.1}$
He/H (10^{-2})	$9.53^{+2.77}_{-2.61}$	$9.10^{+8.28}_{-4.83}$	$10.35^{+4.78}_{-4.98}$	$8.32^{+5.49}_{-3.75}$	$5.02^{+3.29}_{-3.54}$
C/H (10^{-4})	$5.94^{+5.81}_{-2.99}$	$4.86^{+2.90}_{-2.05}$	$3.66^{+5.25}_{-2.79}$	$4.89^{+3.15}_{-3.55}$	$3.19^{+5.13}_{-2.12}$
N/H (10^{-4})	$0.77^{+0.44}_{-0.41}$	$0.75^{+0.40}_{-0.39}$	$0.77^{+0.82}_{-0.77}$	$0.85^{+0.50}_{-0.46}$	$0.38^{+0.45}_{-0.38}$
O/H (10^{-4})	$4.11^{+1.78}_{-1.48}$	$4.10^{+1.15}_{-0.94}$	$3.62^{+2.69}_{-1.80}$	$4.63^{+1.39}_{-1.17}$	$2.70^{+2.67}_{-1.83}$
Ne/H (10^{-5})	$6.85^{+5.73}_{-5.16}$	$7.52^{+3.97}_{-3.80}$	$5.42^{+6.33}_{-5.42}$	$6.17^{+3.38}_{-3.28}$	$4.60^{+5.17}_{-4.60}$
S/H (10^{-6})	$3.54^{+2.77}_{-2.69}$	$2.29^{+1.18}_{-1.17}$	$3.56^{+3.67}_{-3.56}$	$3.46^{+1.79}_{-1.87}$	$1.81^{+2.17}_{-1.81}$
Ar/H (10^{-7})	$25.18^{+19.49}_{-19.15}$	$16.94^{+8.76}_{-8.63}$	$18.58^{+19.44}_{-18.58}$	$28.64^{+15.10}_{-15.46}$	$10.47^{+12.44}_{-10.47}$
[O III] T_e (K)	12200	12300	13100	12600	13400
C III] N_e (cm^{-3})	2800	3800	5800	4400	1900
icf (O)	1.62	1.39	1.43	1.78	1.74
icf (Ar)	1.36	1.27	1.26	1.38	1.29
icf (Ne)	1.27	1.11	1.12	1.31	1.35
icf (S)	4.83	3.03	3.01	4.28	3.48
Model RMS (10^{-2})	4.67	3.17	10.99	4.95	18.65
Observed RMS (10^{-2})	12.42	10.17	17.98	9.55	12.60

Table 4.3—Continued

Constant Density Models				
Parameter	NGC7662 5	NGC7662 6	NGC7662 7	NGC7662 8
T_{star} (kK)	109.9	109.9	109.9	109.9
L_{star} (log[L/$L_{\odot}$])	3.24	3.24	3.24	3.24
Distance (kpc)	1.02	1.02	1.02	1.02
H_{den} (log[$H_{density}$])	$3.34^{+0.05}_{-0.07}$	$3.54^{+0.03}_{-0.03}$	$3.37^{+0.04}_{-0.04}$	$3.42^{+0.05}_{-0.07}$
Inner Radius (10^{-2}pc)	$3.05^{+0.64}_{-3.05}$	$3.33^{+0.10}_{-0.08}$	$1.84^{+0.76}_{-1.84}$	$3.70^{+0.25}_{-0.17}$
Outer Radius (10^{-2}pc)	$7.53^{+1.11}_{-1.34}$	$4.86^{+0.22}_{-0.21}$	$5.45^{+0.55}_{-0.61}$	$5.22^{+0.56}_{-0.45}$
Filling Factor (10^{-1})	$10.00^{+0.00}_{-2.94}$	$10.00^{+0.00}_{-1.25}$	$10.00^{+0.00}_{-1.80}$	$10.00^{+0.00}_{-2.59}$
He/H (10^{-2})	$6.46^{+4.01}_{-3.83}$	$8.83^{+1.88}_{-1.75}$	$12.05^{+3.44}_{-2.72}$	$4.89^{+4.23}_{-2.54}$
C/H (10^{-4})	$3.77^{+5.35}_{-2.25}$	$4.56^{+2.36}_{-1.61}$	$5.48^{+6.82}_{-3.19}$	$4.28^{+3.85}_{-2.04}$
N/H (10^{-4})	$0.51^{+0.38}_{-0.37}$	$0.55^{+0.25}_{-0.24}$	$0.56^{+0.54}_{-0.27}$	$0.55^{+0.37}_{-0.33}$
O/H (10^{-4})	$2.82^{+2.42}_{-1.62}$	$3.56^{+1.11}_{-0.93}$	$3.44^{+1.93}_{-1.53}$	$3.18^{+1.60}_{-1.18}$
Ne/H (10^{-5})	$4.70^{+5.53}_{-4.70}$	$5.25^{+2.51}_{-2.30}$	$6.34^{+3.48}_{-5.31}$	$6.27^{+4.45}_{-4.03}$
S/H (10^{-6})	$2.32^{+2.58}_{-2.32}$	$2.54^{+1.18}_{-1.12}$	$3.12^{+2.91}_{-2.72}$	2.05
Ar/H (10^{-7})	$13.87^{+14.97}_{-13.87}$	$18.11^{+8.19}_{-7.88}$	$23.50^{+22.21}_{-20.68}$	14.72
[O III] T_e (K)	13100	12800	12400	13300
C III] N_e (cm^{-3})	2100	3700	2500	2600
icf (O)	1.72	1.62	1.35	1.67
icf (Ar)	1.30	1.32	1.33	1.47
icf (Ne)	1.34	1.26	1.10	1.59
icf (S)	3.96	4.46	5.21	5.51
Model RMS (10^{-2})	14.78	3.41	7.16	11.80
Observed RMS (10^{-2})	13.29	7.61	13.83	9.35

[a]High Density Limit Default.

As stated in the previous chapter, ionization correction factors account for the unseen ionization states when calculating elemental abundances. Therefore, it is important to have accurate ICFs whenever they are used. From the models, an exact ICF can be determined since the elemental abundance is an input parameter. This allows for a check on the accuracy of the observed ICFs based off the model. The oxygen and argon model ionization correction factors for IC 3568, NGC 5315, and NGC 5882 are larger than their observed counterparts, while the same ICFs are smaller for IC 2165, NGC 2440, NGC 3242, and NGC 7662. Also, IC 3568, NGC 5315, and NGC 5882 have lower stellar temperatures than IC 2165, NGC 2440, NGC 3242, and NGC 7662. Therefore, the ICF equations employed by ELSA could be under-correcting for PN with lower stellar temperatures and over-correcting for those with higher stellar temperatures. The ICF equations for argon and oxygen are $\frac{1}{1-(N^+/N)} * \frac{He^+ + He^{+2}}{He^+}$ and $\frac{He^+ + He^{+2}}{He^+}$, respectively. For lower stellar temperatures, the He^+ ionic state will be populated more than in the case of a higher stellar temperature, reducing the ratio and subsequent ICF value. The neon model ICFs are smaller in all PNe except for NGC 5315, and upon inspection of the ICF equation, $\frac{O^+ + O^{+2}}{O^{+2}} * \frac{He^+ + He^{+2}}{He^+}$, no clear reason can be found to explain the differences. Calculating the average observed Ne/O for this sample and comparing to the average modeled Ne/O shows a discrepancy of about 10%, 0.20 ± 0.02 and 0.18 for the observed and modeled ratio, respectively. Thus, on average, the systematic error introduced by using ICFs seems to be minor in this case. Interestingly for neon, many regions have ICFs less than 1, which may point to a problem in the neon abundance calculations. Specifically, the atomic constants such as the collision strengths or Einstein A values may be slightly off from their true values, resulting in an ionic abundance of neon that is too large. Alternatively, it could be minor numerical errors introduced in the calculations, i.e. rounding. Lastly, all PN except NGC 5882 have model ICFs of sulphur larger

than their observed ICFs with the largest discrepancy seen in NGC 5315. There is a well-known sulfur anomaly where the calculated abundances of sulfur for PNe are systematically lower than those of H II regions of the same metallicity (Henry et al. [19]). It has been shown by Henry et al. [20] that this may be the result of the sulfur ICF calculated from observations failing to account for populated ionization stages above S^{+2}. This looks to be the case here as well since all of the model sulfur abundances are larger than the observed sulfur abundance by nearly the same factor that the model ICF is larger than the observed counterpart.

To further investigate the ICFs of oxygen, argon and neon, a suite of over 400 Cloudy models provided by Gary Ferland was used. This suite covers a large range of stellar temperatures (50-500 kK, $\triangle = 0.1$ dex), metallicities ($10^{-0.6}$-$10^{0.4}$ times solar, $\triangle = 0.2$ dex), and nebular densities (10^2-10^5 cm^{-3}, $\triangle = 0.5$ dex). Each model uses the Rauch H-Ca atmospheric simulation and typical planetary nebula values for all other input parameters. For each model, the ICFs for O, Ar, and Ne from the equations used by ELSA and the value from the model are compared in Figure 4.5. The stellar temperature is limited to include only up to 200 kK, as none of the stars in this sample are above this value. The models increase in stellar metallicity first (repeats every 6th model), then nebular density (repeats every 36th model), and finally stellar temperature for each successive model number. For the majority of models, the oxygen ICF from the ELSA equation is smaller than the model ICF and vice versa for neon. This is what is seen for the PN in this sample, albeit at different stellar temperatures and smaller percent differences. Also, all of the model argon ICFs are smaller than the ELSA equation counterparts, which is not observed in this PN sample. These discrepancies may be the result of the boundaries of the nebular gas and the stellar atmosphere model being different (Rauch H-Ca vs. Rauch H-Ni) and warrants further investigation.

Fig. 4.5.— Relative percent error of the oxygen, argon, and neon ICFs calculated with the equations in ELSA with respect to the ICF from each model. The models increase in stellar metallicity first (repeats every 6th model), then nebular density (repeats every 36th model), and finally stellar temperature for each successive model number.

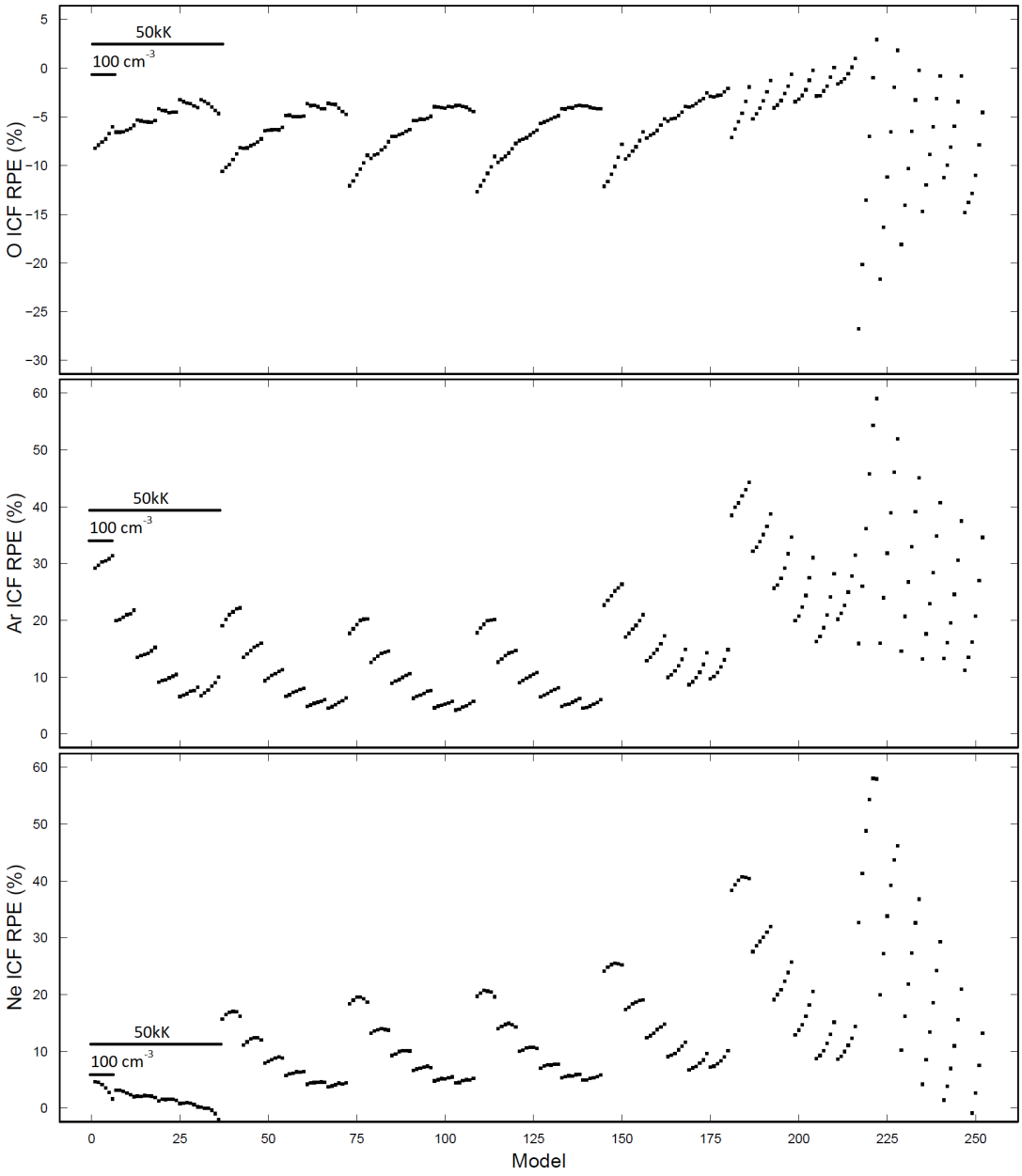

The parameters for the best fit models for the Gaussian and Gaussian with a power-law density profiles are in Table 4.4. This table has the same format as Table 4.3 but only contains the full regions. The difference between these stellar parameters and the constant density models is small in most cases. Only IC 3568 had a somewhat large change in the luminosity of 0.16 dex. However, this is small compared to the errors estimated for the best fit constant density model. Therefore, the choice of density structure only has a minor effect on the final stellar temperature and luminosity and the adoption of the stellar parameters from the constant density models is reasonable. The Gaussian and Gaussian with a power-law density profiles also generate similar electron temperatures but higher electron densities when compared with the constant density profile. This makes sense, since these two profiles have peak density values significantly above the constant density profile (see Figures 4.3 & 4.4). The ionization correction factors are either slightly larger or smaller than the constant density ICFs as well. This could be an indication that the choice of density structure affects the ICFs but is fairly negligible. Lastly, the rms values for the non-constant density profiles of IC 2165 and NGC 2440 are considerably larger than their constant density counterparts while the rms of the Gaussian profile for NGC 5882 is smaller than the constant density rms value. This indicates that IC 2165 and NGC 2440 are better represented using a constant density model while a Gaussian density profile appears more suitable in the case of NGC 5882.

Table 4.4. Non-constant Density Models

Non-constant Density Models						
	IC2165 Full		IC3568 Full		NGC2440 Full	
Parameter	Gaussian	Gaussian With power-law	Gaussian	Gaussian With power-law	Gaussian	Gaussian With power-law
T_{star} (kK)	110.0	110.0	69.2	66.6	171.8	171.9
L_{star} (log[L/$L_{\odot}$])	3.19	3.19	3.67	3.68	2.74	2.73
Filling Factor (10^{-1})	9.51	9.45	9.70	8.67	1.76	1.71
He/H (10^{-2})	10.19	10.14	9.27	9.04	12.27	12.27
C/H (10^{-4})	3.84	3.92	5.35	5.24	2.54	2.54
N/H (10^{-4})	1.18	1.15	0.15	0.17	0.74	0.74
O/H (10^{-4})	2.54	2.54	4.83	4.45	2.71	2.69
Ne/H (10^{-5})	3.04	3.00	7.69	7.57	3.42	3.58
S/H (10^{-6})	2.80	2.82	12.08	13.30	1.49	1.49
Ar/H (10^{-7})	14.26	14.35	15.35	16.11	13.03	13.00
O III] T_e (K)	13700	13700	10000	10000	14200	14200
[S II] N$_e$(cm^{-3})	12600	12500	···	···	8700	8500
C III] N_e (cm^{-3})	11800	11700	9100	8500	8300	8100
icf (O)	1.45	1.45	1.09	1.08	1.44	1.43
icf(Ar)	1.26	1.26	1.27	1.32	1.16	1.16
icf (Ne)	1.14	1.15	0.94	0.95	1.26	1.27
icf(S)	3.29	3.36	···	···	1.64	1.62
RMS (10^{-2})	3.40	3.60	3.13	2.31	10.25	9.97

Table 4.4—Continued

Non-constant Density Models						
	NGC5315 Full		NGC5882 Full		NGC3242 Full	
Parameter	Gaussian	Gaussian With power-law	Gaussian	Gaussian With power-law	Gaussian	Gaussian With power-law
T_{star} (kK)	69.9	69.9	79.2	78.7	91.6	91.2
L_{star} (log[L/$L_{\odot}$])	4.92	4.94	3.42	3.42	3.26	3.29
Filling Factor (10^{-1})	9.68	9.75	8.30	8.26	9.77	9.83
He/H (10^{-2})	11.94	11.80	12.62	12.59	9.84	9.93
C/H (10^{-4})	16.87	17.82	4.29	4.29	5.28	5.21
N/H (10^{-4})	0.57	0.57	2.41	0.24	···	···
O/H (10^{-4})	6.59	6.52	12.88	12.88	4.54	4.46
Ne/H (10^{-5})	14.89	14.83	23.66	23.66	7.11	6.61
S/H (10^{-6})	431.52	454.99	7.66	7.69	···	···
Ar/H (10^{-7})	959.40	1016.25	38.11	38.46	···	···
O III] T_e (K)	8900	8900	8400	8300	11900	12000
[S II] $N_e(cm^{-3})$	20000[a]	20000[a]	20000[a]	20000[a]	···	···
C III] N_e (cm^{-3})	72100	72200	27400	26700	4700	4700
icf (O)	1.39	1.40	1.12	1.12	1.52	1.53
icf(Ar)	1.98	1.99	1.17	1.22	···	···
icf (Ne)	1.23	1.24	0.99	0.99	1.22	1.23
icf(S)	47.57	50.88	1.84	1.96	···	···
RMS (10^{-2})	3.32	3.45	5.52	7.97	7.88	8.61

Table 4.4—Continued

Non-constant Density Models		
	NGC7662 Full	
Parameter	Gaussian	Gaussian With power-law
T_{star} (kK)	108.8	108.8
L_{star} (log[L/$L_{\odot}$])	3.36	3.36
Filling Factor (10^{-1})	10.00	10.00
He/H (10^{-2})	9.84	9.59
C/H (10^{-4})	5.81	5.78
N/H (10^{-4})	0.75	0.74
O/H (10^{-4})	3.94	3.94
Ne/H (10^{-5})	6.44	6.35
S/H (10^{-6})	3.43	3.48
Ar/H (10^{-7})	24.89	25.23
O III] T_e (K)	12400	12400
C III] N_e (cm^{-3})	4300	4200
icf (O)	1.51	1.51
icf(Ar)	1.36	1.36
icf (Ne)	1.19	1.19
icf(S)	2.22	4.75
RMS (10^{-2})	4.87	5.50

[a]High Density Limit Default.

Stellar parameters determined by various authors over the last three decades are compared to the best-fit constant density values in Table 4.5 and Figure 4.6. The first column in Table 4.5 gives the name of each sample PN followed in subsequent columns by the luminosities [in $\log(L/L_{\odot})$] and temperatures (in kK) for each source. As can be seen in Figure 4.6, the stellar parameters for IC 2165 agree within the 1σ uncertainties with those from Paper II and the temperature agrees with that of Zhang & Kwok [65]. The stellar parameters for IC 3568 are consistent with the other authors, except for the temperature of Paper II (300 K smaller than the lower limit). The luminosity for NGC 2440 is significantly lower than the other published values, although the temperature matches (given the uncertainties) with that of Zhang & Kwok [65]. NGC 3242's temperature and luminosity are consistent with all authors except for Zhang & Kwok [65] and Corradi et al. [10], respectively. For NGC 5315, the luminosity is significantly higher compared to the values from the other authors, except for the upper bound determined by Shaw & Kaler [58]. The temperatures for NGC 5315 and NGC 5882 are consistent with Paper II and Zhang & Kwok [65], respectively. The luminosities for NGC 5882 and NGC 7662 match with the values of Frew [15] and Paper II, within uncertainties. Lastly, Shaw & Kaler [57] and Frew [15] have temperatures consistent with the value for NGC 7662.

Table 4.5. Comparison: Stellar Parameters

Object	Model	SK85/89[a]	ZK93[b]	CSSP03[c]	F08[d]	Paper II[e]
Luminosity ($\log[L/L_\odot]$)						
IC 2165	3.17	3.76	3.95	3.51	···	3.16
IC 3568	3.52	4.12	3.78	3.73	···	3.88
NGC 2440	2.74	3.88	3.51	···	3.32	3.10
NGC 3242	3.36	3.59	3.40	3.88	3.54	3.64
NGC 5315	4.89	<5.25	3.95	···	···	3.50
NGC 5882	3.45	3.72	3.80	···	3.52	3.45
NGC 7662	3.24	3.89	3.76	3.99	3.42	3.42
Effective Temperature (kK)						
IC 2165	110.0	118.0	112.1	154.9	···	110.0
IC 3568	69.6	52.0	51.3	55.0	···	51.0
NGC 2440	169.8	112.0	178.8	···	208.0	198.0
NGC 3242	89.7	90.0	75.0	89.0	89.0	89.0
NGC 5315	69.9	61.0	59.9	···	···	70.0
NGC 5882	78.7	70.0	73.0	···	68.0	70.0
NGC 7662	109.9	113.0	96.8	100.0	111.0	95.0

[a]Shaw & Kaler [57] and Shaw & Kaler [58], Observation.

[b]Zhang & Kwok [65], Observation.

[c]Corradi et al. [10], Observation.

[d]Frew [15], Observation.

[e]Henry et al. [21], Model.

Fig. 4.6.— Comparison of the best fit constant density stellar temperature and luminosity for each planetary nebula to other values in the literature.

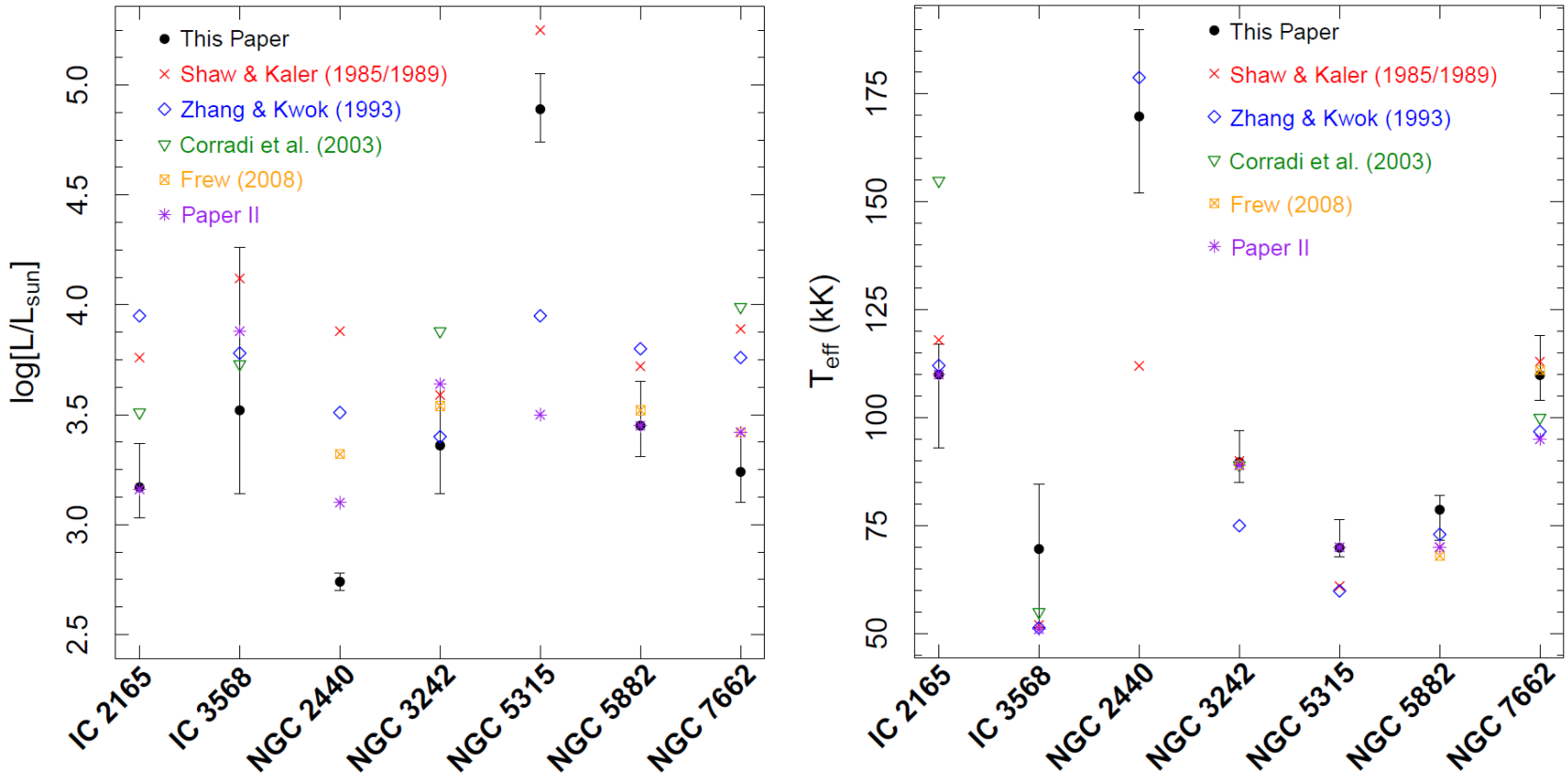

Values of the final mass and radius as well as the main sequence lifespan, ZAMS mass, radius, luminosity, temperature, and spectral type can be estimated from the model-derived T and L values for each planetary nebula. Each of these derived properties is shown in Table 4.6. The final and ZAMS masses are estimated by interpolating between theoretical post-AGB evolutionary tracks on the H-R diagram shown in Figure 4.7. For NGC 5315, the mass estimates are from extrapolation since there are no post-AGB evolutionary tracks that have been successfully modeled with luminosities that high. Each track is from either Vassiliadis & Wood [61] (VW 1994, red solid lines), Schoenberner [54] (S 1983, blue dash lines), or Miller Bertolami [39] (MB 2016, green dash and purple dash-dot lines). Beneath each author on the plot is the ZAMS/final mass in solar masses following each evolutionary track from top to bottom. The ZAMS/final masses from different interpolations were averaged together when overlapping occurred, since a single set of models was insufficient for all calculations. The final masses for five of the PNe match with the white dwarf mass peak, $0.565 M_{\odot}$, from Liebert et al. [33]. The current radius was calculated using the Stefan-Boltzmann law. Mass-luminosity and mass-radius relations from Demircan & Kahraman [12] (appropriate for a given mass) were used to calculate the ZAMS luminosity and radius, respectively. The Stefan-Boltzmann law was also employed to calculate the ZAMS temperature. The main sequence lifespan was based on the approximate lifespan of the Sun, $\tau_{\odot} \approx \mathrm{M}_{\odot}/\mathrm{L}_{\odot} = 9.5$ Gyr, and the age of the Milky Way Galaxy, 13.2 Gyr, was used as a hard upper limit. Lastly, the ZAMS spectral type was determined from the ZAMS luminosity with the spectral type range within the brackets being based on the uncertainties in the luminosity.

Table 4.6. Derived Stellar Parameters.

Stellar Property	IC 2165	IC 3568	NGC 2440	NGC 3242	NGC 5315	NGC 5882	NGC 7662
Final Mass ($M_\odot$)	$0.56^{+0.02}_{-0.01}$	$0.55^{+0.26}_{-0.01}$	$0.66^{+0.08}_{-0.06}$	$0.56^{+0.01}_{-0.01}$	$1.17^{+0.09}_{-0.09}$	$0.56^{+0.03}_{-0.01}$	$0.56^{+0.02}_{-0.01}$
Current Radius ($R_\odot$)	$0.11^{+0.08}_{-0.03}$	$0.16^{+0.36}_{-0.07}$	$0.03^{+0.01}_{-0.01}$	$0.20^{+0.10}_{-0.07}$	$1.90^{+0.53}_{-0.55}$	$0.29^{+0.15}_{-0.06}$	$0.12^{+0.04}_{-0.03}$
Main Sequence Lifespan (Gyr)	$9.5^{+3.7}_{-4.3}$	$8.3^{+4.9}_{-8.1}$	$0.5^{+0.8}_{-0.2}$	$10.7^{+2.5}_{-6.4}$	$0.04^{+0.01}_{-0.01}$	$8.9^{+3.5}_{-4.4}$	$8.7^{+3.4}_{-4.0}$
ZAMS Mass ($M_\odot$)	$0.99^{+0.22}_{-0.15}$	$1.04^{+3.02}_{-0.23}$	$2.81^{+0.66}_{-0.81}$	$0.95^{+0.35}_{-0.09}$	$6.55^{+0.66}_{-0.65}$	$1.02^{+0.27}_{-0.11}$	$1.02^{+0.24}_{-0.11}$
ZAMS Radius ($R_\odot$)	$1.05^{+0.22}_{-0.15}$	$1.10^{+1.79}_{-0.23}$	$2.36^{+0.29}_{-0.40}$	$1.01^{+0.34}_{-0.09}$	$3.78^{+0.21}_{-0.21}$	$1.08^{+0.27}_{-0.11}$	$1.08^{+0.24}_{-0.11}$
ZAMS L_{star} ($L_\odot$)	$0.99^{+1.21}_{-0.47}$	$1.20^{+247.43}_{-0.75}$	$58.65^{+75.32}_{-43.09}$	$0.84^{+1.98}_{-0.27}$	$1618.68^{+734.07}_{-546.60}$	$1.09^{+1.68}_{-0.39}$	$1.12^{+1.47}_{-0.40}$
ZAMS Temperature (kK)	$5.6^{+6.0}_{-4.0}$	$5.8^{+7.7}_{-0.7}$	$10.4^{+1.7}_{-2.2}$	$5.5^{+0.9}_{-0.3}$	$18.9^{+1.3}_{-1.3}$	$5.7^{+0.7}_{-0.3}$	$5.7^{+0.6}_{-0.3}$
ZAMS Spectral Type	G2 [F6-G8]	G0 [B6-K3]	B8 [B7-A3]	G4 [G7-F5]	B2 [B2-B3]	G1 [F5-G5]	G1 [F5-G5]

Amnuel [3] suggested that an increase in progenitor mass would increase the probability of low mass companions, which would determine the axisymmetric morphology of the planetary nebula. As can be seen in Table 4.6, the central stars of IC 2165, IC 3568, NGC 3242, NGC 5882, and NGC 7662 are each solar-like while those of NGC 2440 and NGC 5315 are super-solar. NGC 5882, NGC 2440, and NGC 5315 are the only PN in this sample to exhibit very asymmetric structures (Figures 1.2 & 1.3), in support of the claim made by Amnuel [3] that increasing the progenitor mass would increase the probability of a companion, assuming each does indeed have a companion.

Fig. 4.7.— Log L/L_{sun} vs. log T_{eff} for the entire planetary nebula sample. Post-AGB model tracks from Vassiliadis & Wood [61] (VW 1994, solid red lines, Z=0.016), Schoenberner [54] (S 1983, blue dashed lines, Z=0.016) and Miller Bertolami [39] (MB 2016, purple dash-dot lines, Z=0.02 and green dash lines, Z=0.01) are overlaid. Beneath each author on the plot is the ZAMS/final mass in solar masses following each evolutionary track from top to bottom.

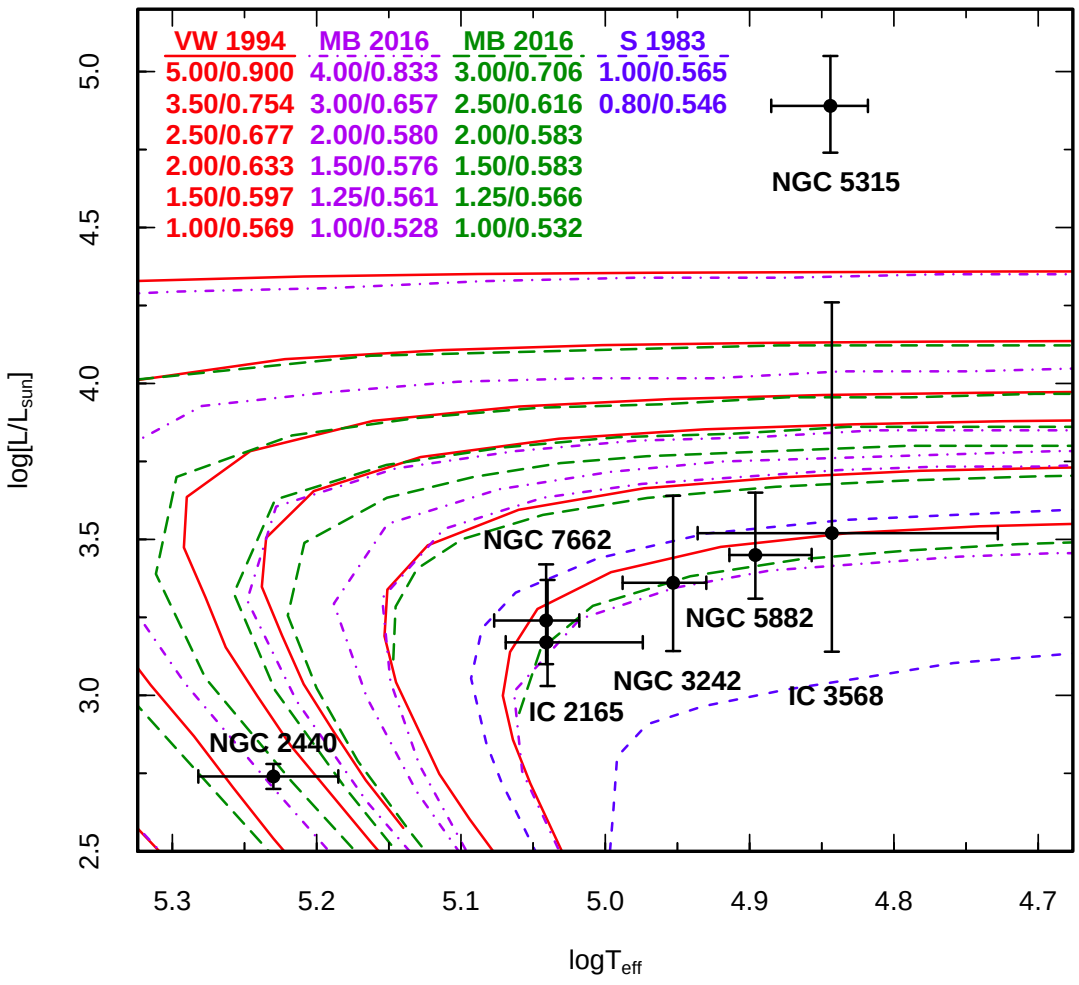

Chapter 5

Summary and Conclusions

The level of homogeneity of elements distributed in a small set of PN was investigated. Also, each PN was modeled to constrain the stellar luminosity and temperature. To test the homogeneity, the co-spatial observations described in Paper I were divided into different spatial regions and spectra were extracted. Individual line strengths were measured and these measurements were used to calculate the nebular temperatures, densities, and abundances. Comparisons of the nebular properties among regions of each PN were then made.

Next, model of each PN were generated in order to determine the stellar properties using observational constraints. An rms value determined the effectiveness of each model to match each observation, and the rms value was used to choose the best parameters and estimate errors. Finally, three different density profiles (constant density, Gaussian density, and Gaussian with a power-law density profile) were used to see the effects each has on the best stellar parameters.

The conclusions from this work are as follows.

- The planetary nebulae in this sample are chemically homogeneous, which implies the shells of material that were ejected from their respective stars were well-mixed and the resulting nebula is as well. This is in line with current theoretical work on the formation of planetary nebulae. Specifically, the mixing timescale is much shorter than the nuclear timescale in the central star. The homogeneity also means that observations can be taken anywhere across the PN and the resulting abundance will accurately represent the nebula as a whole.

- The constant density models can constrain the stellar parameters quite well

depending on the planetary nebula. Also, the choice of density structure has only a small effect on the final stellar properties. This is advantageous since the model calculation time for non-constant density profiles is considerably higher than for constant density profiles.

- The progenitor (ZAMS) masses for the majority of this sample were around 1 $M_{\odot}$. This is expected since the observed distribution of white dwarf masses peaks at a progenitor mass around 1 $M_{\odot}$. The largest mass at 6.55 $M_{\odot}$ for NGC 5315 is somewhat questionable given the need to extrapolate from the post-AGB evolutionary models. This can only be improved with more high mass models being calculated.

Chapter 6

Improvements and Future Work

Given that the sample size is only seven planetary nebulae, including more PNe would better explore the homogeneity of planetary nebulae. This would allow for a wider range of morphological types and progenitor masses to be tested. Also, probing the fainter outer structures would either corroborate the claims made here or show any discrepancies that would need explanations. A dedicated observing program would be required in most cases since few spatial studies have been made. Since HST time is quite competitive, a ground based program is being pursued. Lastly, it would be prudent to redo the observations for NGC 2440 to definitively decide on its homogeneity.

The modeling method employed in this work is a basic gradient descent type approach for finding the minima of the parameters. By design, this method doesn't give a sense of errors in each parameter nor insurance that the global minimum is found. A better approach (to be implemented for future work) would be to use a method called Goodman and Weare's Affine Invariant Markov Chain Monte Carlo Ensemble sampling. This method utilizes a random sampling technique in a user defined number of chains. First, the starting points of each chain are randomly chosen from a distribution of possible parameters defined by the user. Next, a change in a parameter is proposed by sampling a normal distribution about the parameter with a user-defined standard deviation. Then, the likelihood of the current position and proposed change are calculated and compared. If the likelihood of the change is higher, it's accepted outright and accepted part of the time if it is lower. The acceptance for lower likelihoods is determined by first calculating the relative probabilities of the change to the original position (always

< 1), picking a random number between 0 and 1 to compare with, and keeping the change if the relative probability value is greater than the random number. In this way, the posterior probability distribution is sampled along each chain. From the various chains, the posterior probability distribution for a parameter can be sampled well enough to give highly probable values for that parameter. The best possible values can be determined quite efficiently using this method and using multiple starting locations help ensure that the global minimum is found.

Keeping with the theme of spatial variations, another project is currently underway looking at chemical differences between H II regions in six nearly face-on, nearby spiral galaxies (M 51, M 83, M 100, M 101, NGC 2403, and NGC 2997). H II regions are the birthplace of stars and tracers of the current chemical composition in spiral galaxies. Studying H II regions across a galaxy will map out the chemical distribution, which is an important constraint for determining mixing rates, infall rates, and star formation efficiencies.

The main goal is to test the assumption that galaxies are chemically homogeneous around the galaxy for a fixed distance from the center. Secondary goals include calculating radial abundance gradients and star formation rates as well as improving the abundance measurements of carbon and neon for metal rich H II regions. These goals are attainable since the galaxies were observed at the McDonald Observatory using the VIRUS-P (Visible Integra-field Replicable Unit Spectrograph-Prototype, Hill et al. [22]) instrument. This instrument has 246 fibers, each with a 4.16″ diameter on the sky, spaced such that a 100″x102″ area near the center of the galaxy can be covered in three exposures as seen for NGC 2403 in Figure 6.1. These observations cover a full 360° around the galaxy centers and include metal rich H II regions. The full wavelength range is in the optical (3480-6900 Å) and emission line measurements are being carried out using the

program ROBOSPECT (Waters & Hollek [63]), which automates the measurements. Currently, calculations for the abundances of oxygen and nitrogen have been made for NGC 2403 using the ONS (Strong Line) empirical relation of Pilyugin & Grebel [46]. There is a clear radial and inconclusive azimuthal abundance gradient for both elements. More analysis is underway for NGC 2403 as well as the other galaxies with completion expected in August.

Fig. 6.1.— The three exposures from VIRUS-P covering a 100″x102″ area of the central region of NGC 2403.

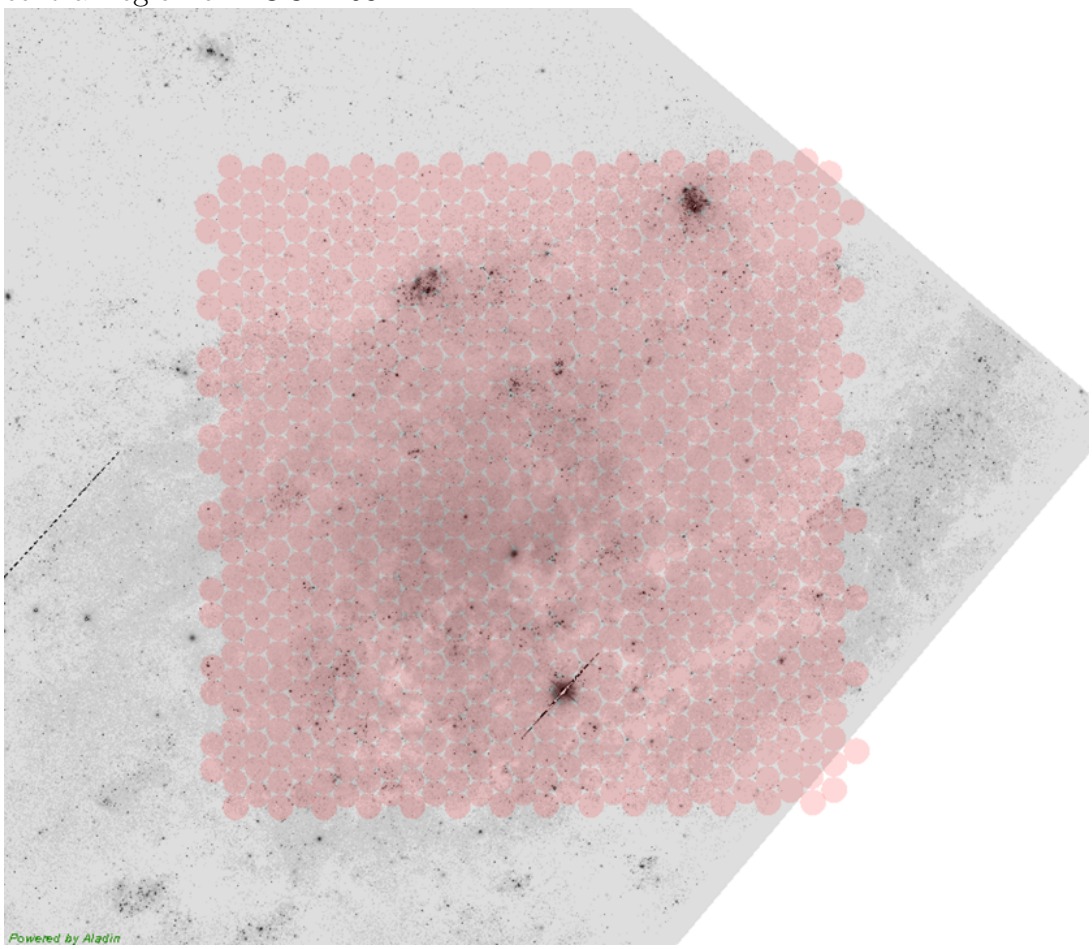

References

[1] Acker, A., Marcout, J., Ochsenbein, F., et al. 1992, The Strasbourg-ESO Catalogue of Galactic Planetary Nebulae. Parts I, II., by Acker, A.; Marcout, J.; Ochsenbein, F.; Stenholm, B.; Tylenda, R.; Schohn, C.. European Southern Observatory, Garching (Germany), 1992, 1047 p., ISBN 3-923524-41-2

[2] Aller, L. H., & Czyzak, S. J. 1983, ApJS, 51, 211

[3] Amnuel, P. 1995, Ap&SS, 225, 275

[4] Asplund, M., Grevesse, N., Sauval, A. J. & Scott, P. 2009, The Chemical Composition of the Sun, Annual Review of Astronomy and Astrophysics, 47(1):481-522

[5] Balick, B., Gonzalez, G., Frank, A., & Jacoby, G. 1992, ApJ, 392, 582

[6] Barker, T. 1986, ApJ, 308, 314

[7] Bohigas, J., Rodríguez, M., & Dufour, R. J. 2013, Rev. Mexicana Astron. Astrofis., 49, 227

[8] Buell, J. F. 1997, Ph.D. Thesis

[9] Corradi, R. L. M., Gonçalves, D. R., Villaver, E., Mampaso, A., & Perinotto, M. 2000, ApJ, 542, 861

[10] Corradi, R. L. M., Schönberner, D., Steffen, M., & Perinotto, M. 2003, MNRAS, 340, 417

[11] de Freitas Pacheco, J. A., Maciel, W. J., Costa, R. D. D., & Barbuy, B. 1991, A&A, 250, 159

[12] Demircan, O., & Kahraman, G. 1991, Ap&SS, 181, 313

[13] Dufour, R. J., Kwitter, K. B., Shaw, R. A., et al. 2015, ApJ, 813, 121 (Paper I)

[14] Ferland, G. J., Porter, R. L., van Hoof, P. A. M., et al. 2013, Rev. Mexicana Astron. Astrofis., 49, 137

[15] Frew, D. J. 2008, Ph.D. Thesis

[16] Guerrero, M. A., & Manchado, A. 1999, ApJ, 522, 378

[17] Guerrero, M. A., Jaxon, E. G., & Chu, Y.-H. 2004, AJ, 128, 1705

[18] Henry, R. B. C., Kwitter, K. B., & Bates, J. A. 2000, ApJ, 531, 928

[19] Henry, R. B. C., Kwitter, K. B., & Balick, B. 2004, AJ, 127, 2284

[20] Henry, R. B. C., Speck, A., Karakas, A. I., Ferland, G. J., & Maguire, M. 2012, ApJ, 749, 61

[21] Henry, R. B. C., Balick, B., Dufour, R. J., et al. 2015, ApJ, 813, 121 (Paper II)

[22] Hill, G. J., MacQueen, P. J., Smith, M. P., et al. 2008, Proc. SPIE, 7014, 701470

[23] Hyung, S. 1994, ApJS, 90, 119

[24] Hyung, S., & Aller, L. H. 1997, ApJ, 491, 242

[25] Hyung, S., & Aller, L. H. 1998, PASP, 110, 466

[26] Johnson, M. D., Levitt, J. S., Henry, R. B. C., & Kwitter, K. B. 2006, Planetary Nebulae in our Galaxy and Beyond, 234, 439

[27] Karakas, A. I., & Lattanzio, J. C. 2014, PASA, 31, e030

[28] Kingsburgh, R. L., & Barlow, M. J. 1994, MNRAS, 271, 257

[29] Krabbe, A. C., & Copetti, M. V. F. 2006, A&A, 450, 159

[30] Kwitter, K. B., & Henry, R. B. C. 1998, ApJ, 493, 247

[31] Kwitter, K. B., & Henry, R. B. C. 2001, ApJ, 562, 804

[32] Kwitter, K. B., Henry, R. B. C., & Milingo, J. B. 2003, PASP, 115, 80

[33] Liebert, J., Bergeron, P., & Holberg, J. B. 2005, ApJS, 156, 47

[34] Liu, Y., Liu, X.-W., Barlow, M. J., & Luo, S.-G. 2004, MNRAS, 353, 1251

[35] López, J. A., Meaburn, J., Bryce, M., & Holloway, A. J. 1998, ApJ, 493, 803

[36] Marigo, P., Bressan, A., Nanni, A., Girardi, L., & Pumo, M. L. 2013, MNRAS, 434, 488

[37] Mendez, R. H., & Niemela, V. S. 1982, Wolf-Rayet Stars: Observations, Physics, Evolution, 99, 457

[38] Miller, T. R., Henry, R. B. C., Balick, B., et al. 2016, ApJ, 830, 9

[39] Miller Bertolami, M. M. 2016, A&A, 588, A25

[40] Milingo, J. B., Henry, R. B. C., & Kwitter, K. B. 2002, ApJS, 138, 285

[41] Monteiro, H., Gonçalves, D. R., Leal-Ferreira, M. L., & Corradi, R. L. M. 2013, A&A, 560, A102

[42] Morisset, C., & Georgiev, L. 2009, A&A, 507, 1517

[43] Peimbert, M., Peimbert, A., Ruiz, M. T., & Esteban, C. 2004, ApJS, 150, 431

[44] Perinotto, M. 1991, ApJS, 76, 687

[45] Perinotto, M., & Corradi, R. L. M. 1998, A&A, 332, 721

[46] Pilyugin, L. S., & Grebel, E. K. 2016, MNRAS, 457, 3678

[47] Rauch, T. 2003, A&A, 403, 709

[48] Renzini, A., & Voli, M. 1981, A&A, 94, 175

[49] Ruiz, N., Guerrero, M. A., Chu, Y.-H., & Gruendl, R. A. 2011, AJ, 142, 91

[50] Savage, B. D., & Mathis, J. S. 1979, ARA&A, 17, 73

[51] Richer, M. G., McCall, M. L., & Martin, P. G. 1991, ApJ, 377, 210

[52] Salaris, Maurizio & Cassisi, Santi. 2005, Evolution of stars and stellar populations, John Wiley and Sons, pp. 119121, ISBN 0-470-09220-3

[53] Samland, M., Koeppen, J., Acker, A., & Stenholm, B. 1992, A&A, 264, 184

[54] Schoenberner, D. 1983, ApJ, 272, 708

[55] Schröder, K.-P., & Cuntz, M. 2005, ApJ, 630, L73

[56] Seaton, M. J. 1979, MNRAS, 187, 73P

[57] Shaw, R. A., & Kaler, J. B. 1985, ApJ, 295, 537

[58] Shaw, R. A., & Kaler, J. B. 1989, ApJS, 69, 495

[59] Torres-Peimbert, S., & Pena, M. 1981, Rev. Mexicana Astron. Astrofis., 6, 301

[60] Tsamis, Y. G., Barlow, M. J., Liu, X.-W., Danziger, I. J., & Storey, P. J. 2003, MNRAS, 345, 186

[61] Vassiliadis, E., & Wood, P. R. 1994, ApJS, 92, 125

[62] Villaver, E., García-Segura, G., & Manchado, A. 2002, ApJ, 571, 880

[63] Waters, C. Z., & Hollek, J. K. 2013, PASP, 125, 1164

[64] Weller, W. G., & Heathcote, S. R. 1987, in Late Stages of Stellar Evolution, ed. S. Kwok & S. R. Pottasch (Dordrecht: Reidel), 409

[65] Zhang, C. Y., & Kwok, S. 1993, ApJS, 88, 137